LIGAND EFFECTS ON BIOINSPIRED IRON COMPLEXES

A Dissertation

by

MA. DEL ROSARIO MEJIA RODRIGUEZ

Submitted to the Office of Graduate Studies of
Texas A&M University
in partial fulfillment of the requirements for the degree of

DOCTOR OF PHILOSOPHY

May 2004

Major Subject: Chemistry

LIGAND EFFECTS ON BIOINSPIRED IRON COMPLEXES

A Dissertation

by

MA. DEL ROSARIO MEJIA RODRIGUEZ

Submitted to Texas A&M University
in partial fulfillment of the requirements
for the degree of

DOCTOR OF PHILOSOPHY

Approved as to style and content by:

M. Y. Darensbourg (Chair of Committee)	P. A. Lindahl (Member)
M. B. Hall (Member)	J. W. Morse (Member)
	E. A. Schweikert (Head of Department)

May 2004

Major Subject: Chemistry

ABSTRACT

Ligand Effects on Bioinspired Iron Complexes. (May 2004)

Ma. del Rosario Mejía Rodríguez, B.S., Universidad Autónoma de Querétaro;

M.S., Western Illinois University

Chair of Advisory Committee: Dr. Marcetta Y. Darensbourg

The synthesis of diiron thiolate complexes was carried out using two ligands that were expected to furnish improved catalytic activity, solubility in water, and stability to the metal complexes. The water-soluble phosphine 1,3,5-triaza-7-phosphaadamantane, PTA, coordinates to the Fe centers forming the disubstituted complex (μ-pdt)$[Fe(CO)_2PTA]_2$, which presents one PTA in each iron in a *transoid* arrangement. Substitution of one CO ligand in the (μ-pdt)$[Fe(CO)_3]_2$ parent complex forms the asymmetric (μ-pdt)$[Fe(CO)_3][Fe(CO)_2PTA]$. Enhanced water solubility was achieved through reactions with electrophiles, H^+ and CH_3^+, which reacted with the N on the PTA ligand forming the protonated and methylated derivatives, respectively.

The 1,3-bis(2,4,6-trimethylphenyl)imidazol-2-ylidene), IMes, was reacted with (μ-pdt)$[Fe(CO)_3]_2$ yielding the asymmetric (μ-pdt)$[Fe(CO)_3][Fe(CO)_2IMes]$, an electron rich, air stable complex that does not show reactivity with H^+.

Electrocatalytic production of hydrogen was studied for the all-CO, bis-PMe_3, mono- and di-PTA Fe^IFe^I complexes, as well as the PTA-protonated and -methylated derivatives. The all-CO species produce H_2, in the presence of the weak HOAc, at

their second reduction event, $Fe^{I}Fe^{0} \rightarrow Fe^{0}Fe^{0}$, that occurs at ca. –1.9 V, through an EECC mechanism. The mono- and di-substituted phosphine complexes present electrocatalytic production of H_2 from the $Fe^{0}Fe^{I}$ redox state; this reduction takes place at –1.54 V for (μ-pdt)[Fe(CO)$_3$][Fe(CO)$_2$PTA], and at ca. –1.8 for the disubstituted PMe_3 and PTA derivatives. A positive charge on the starting complex does not have an effect on the production of H_2. It was found that the protonated and methylated derivatives are not the catalytic species for H_2 production. At their first reduction event the neutral precursor forms, and catalysis occurs from the $Fe^{I}Fe^{I}$ complex in all cases.

The possibility of enhanced catalytic activity in the presence of H_2O was explored by conducting electrochemical experiments in the mixed CH_3CN:H_2O solvent system for the PTA-substituted complexes. The reduction potential of the catalytic peak is shifted to more positive values by the presence of H_2O. The cyclic voltammogram of $\{(\mu\text{-pdt})[Fe(CO)_2(PTA\cdot H)]_2\}^{2+}$ in CH_3CN:H_2O 3:1 shows the reduction of a more easily reduced species in the return scan. This curve-crossing event provides evidence for the $(\eta^2\text{-}H_2)Fe^{II}$ intermediate proposed in the ECCE mechanism.

DEDICATION

This dissertation is dedicated to the memory of my parents, and my sister Ma. Luisa, who gave me the possibility to get an education. To my husband Humberto, and my children Sandra Pamela, Carlos Humberto, and Ana Cristina for their love and endless support. To my sisters and brothers for their continuous encouragement.

ACKNOWLEDGEMENTS

First of all, I wish to thank my advisor Prof. Marcetta Y. Darensbourg for helping me so much to get through graduate school. Having a family and being older than most graduate students made this endeavor more challenging, not only for me but for my advisor, too. Prof. Marcetta Darensbourg's commitment to students is a clear example of what mentorship is about. For her it is not only about chemistry and research, a field where she excels at and sets the example to follow, but also about the person inside each student. She gives us the opportunity to do science and learn from her, while she is also helping us to grow as individuals. My most sincere thanks for her patience, encouragement, guidance, and support during these years at Texas A&M.

I would like to thank the members of my committee Dr. Michael B. Hall, Dr. Paul A. Lindahl, and Dr. John W. Morse for their time and effort to serve in my committee. Their advice was very valuable and appreciated.

I would like to acknowledge Dr. Daesung Chong for the electrochemical work we did in collaboration. I am thankful for his willingness to share his knowledge of electrochemistry, and working with me. Also, I thank Dr. Manuel Soriaga for his advice in Electrochemistry, and Jean Sanabria-Chinchilla, from the Soriaga's research group, for his help.

I want to thank Dr. Don Darensbourg for always having an open door to discuss chemistry, and the friendly atmosphere we have in these research groups. I wish to

thank Dr. Matt Miller and Dr. Joseph Reibenspies for the X-ray crystal structure determinations, and Dr. K. P. Sarathy for his help with the NMR facilities.

I would like to thank Dr. Irene Georgakaki with whom I worked very closely, for her friendship, and for all the things I learned from her about iron hydrogenases, and the work in this research project. Thank you to current and former group members for always taking the time to help, and for being so friendly: Dr. Xuan Zhao, Dr. Erica Lyon, Dr. Missy Golden, Marilyn Rampersad, Chiao-Yi (Joey) Chiang, Jesse Tye, and Steve Jeffery. Also, I want to thank students in Dr. Don Darensbourg's research group, especially Dr. Cesar Ortiz for providing PTA ligand; Dr. Sam Lewis and Ryan Mackiewicz, for their continuous help with computer-related problems. I thank Ms. Sue Winters for all her help.

I am thankful to the Autonomus University of Queretaro and to the Secretary of Public Education in Mexico (program SEP-PROMEP) for providing financial support. I express my thanks to Q. M. José Merced Esparza García for all his support.

I am grateful to my sisters and brothers, and to the rest of my family for all the encouragement and support they have always showed. To my friends in Queretaro, Macomb, IL, and here (College Station, TX), thanks.

Especially, I want to express my most sincere thanks to my husband, Humberto. He has always been my support, but especially throughout this time. Without him I would not be here.

Thanks to God for giving me life and strength, and the means to reach this milestone.

TABLE OF CONTENTS

CHAPTER Page

LIST OF TABLES

TABLE Page

LIST OF FIGURES

FIGURE Page

FIGURE Page

FIGURE Page

CHAPTER I

INTRODUCTION

Out of the total number of metallic elements known to man, Nature has chosen only a few of them to be present in living systems. Proteins incorporate some of those to perform specific functions; for instance, metals found in the active centers of enzymes are generally responsible for the catalytic activity. Metalloenzymes can contain one (mononuclear), two (dinuclear), or multiple (polynuclear) metals in their active sites. Most dinuclear enzymes contain two atoms of the same metal, for example hemocyanin (2 Cu), hemerythrin (2 Fe), ribonucleotide reductase (2 Fe), alkaline phosphatase (2 Zn), urease (2 Ni), and Fe-only hydrogenase (2 Fe), among others. Heterobinuclear metalloenzymes are less common, but are found in some organisms, one example being Ni-Fe hydrogenase.[1]

Hydrogenases are enzymes that catalyze the reversible oxidation of molecular dihydrogen to protons and electrons according to Equation 1.[2]

$$H_2 \rightleftharpoons 2\,H^+ + 2\,e^- \qquad \text{(I-1)}$$

The metal-containing hydrogenases are comprised of the [Ni-Fe]- and [Fe-only]-hydrogenase, [Ni-Fe]H_2ase and [Fe]H_2ase hereafter, while a reported metal-free

---

This dissertation follows the style and format of *Inorganic Chemistry*.

hydrogenase has not been completely characterized. Even though the reaction catalyzed by hydrogenases is presented as a reversible reaction, it will proceed in one way or the other depending on the role of the hydrogenase present in that particular organism. The [Ni-Fe]H_2ases are enzymes designed primarily for H_2 consumption, while [Fe]H_2ases principally reduce protons to produce H_2. The so-called metal-free hydrogenase activates an organic substrate (N^5,N^{10}-methenyl tetrahydromethanopterin) which then binds and heterolytically splits H_2.[3]

The protein crystal structures of the [Fe]H_2ases from *Clostridium pasteurianum* (CpI) and *Desulfuvibrio desulfuricans* (DdH) were solved and published by Peters *et al.*,[4] and Fontecilla-Camps *et al.*,[5] respectively. These crystallographic studies showed that the active center of the enzyme (the site at which catalytic activity occurs) is deeply buried in the protein. A hydrophobic channel that travels from the protein surface to the active site facilitates the diffusion of gases (H_2 and CO). A series of [4Fe4S] clusters provide a path for electrons to enter or exit from the active center. The active center, termed H-cluster, Figure I-1, is comprised of a [4Fe4S] cluster that is bridged through a cysteinyl sulfur to a [2Fe2S] cluster. The latter is arranged forming a butterfly core with the two sulfurs bridged by a three light atoms chain. As

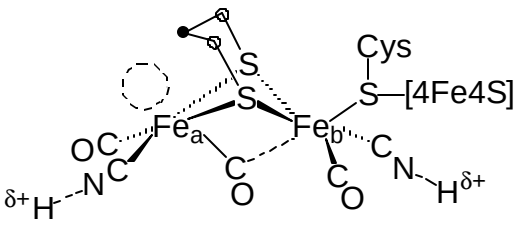

Figure I-1. The H-cluster and the binuclear active center of [Fe]H_2ase.

crystallographic studies cannot make a distinction between carbon, oxygen, and nitrogen, the three light atoms were originally assigned as carbons, yielding the propanedithiolate bridge.[5a] Later studies and theoretical calculations suggest nitrogen as the middle atom in the three light atoms chain is a more favored assignment because it explains the close contact between this middle atom and Cys 178.[5b,6] Furthermore, the di-(thiomethyl)-amine (dtn) bridge, -S-CH_2-NH-CH_2-S-, provides a basic site that would assist the heterolytic splitting of H_2 into H^+ and H, the accepted mechanism for hydrogenase activity.

Spectroscopic studies showed that diatomic ligands, CO and CN^-, complete the coordination sphere of the two Fe atoms. The ligands on each of the two Fe atoms, Fe_a and Fe_b in Figure I-1, or the distal and proximal Fe, respectively, are arranged forming a square pyramid, where the pyramid on Fe_a is inverted with respect to the one on Fe_b. Dependent on the oxidation state of the iron atoms, the CO underneath Fe_a switches from a terminal position to semibridging to bridging. These changes are evidenced by FTIR studies in the CO region of the spectrum.[5b] Surprisingly, there is only one covalent attachment point of the H-cluster to the protein, the cysteine S, and hydrogen-bonding through the N on the CN^- ligand.

Infrared spectroscopy studies performed in the [Fe]H_2ase from D. desulfuricans found three different oxidation levels based on the stretching frequencies of CO and CN^-.[5b] The as-isolated enzyme presents two bands that correspond to CN^- stretching frequencies, 2107 and 2087 cm^{-1}, two bands from terminal CO, 2007 and 1983 cm^{-1}, and one for a semibridging CO, 1847 cm^{-1}. After reduction at –535 mV the IR

spectrum shows a more complicated pattern, with the 1847 peak shifting to 1894 cm^{-1}, a value that indicates the CO is terminally bound. The reduced form of the enzyme, the active form, has an apparent open site, as presented in Figure I-1, where H_2 or H^+ can bind. This is also the place where CO binds in the CO-inhibited form.

Aiming to mimic the active center of [Fe]H_2ase, Figure I-1, chemists recognized the close similarity of this moiety with classical organometallic complexes, and used the well-known $(\mu\text{-SR})_2Fe_2(CO)_6$ as the parent compound to synthesize three generations of model complexes, Figure I-2.[7]

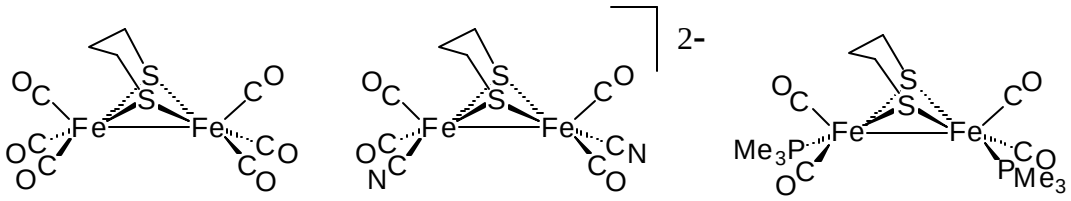

Figure I-2. Model complexes for the dinuclear active center of [Fe]-H_2ase; first, second and third generation models.

Studies performed with these model complexes yielded valuable information: (1) The Fe^IFe^I systems have Fe-Fe distances slightly shorter than the ones found in enzyme crystal structures (2.6 Å). (2) The Fe-Fe bond density in the first generation, all-CO-derivative, model complexes is not sufficiently basic to react with H^+.[7e] (3) The second generation model has two possible sites for protonation, the Fe-Fe bond and the N on the cyanide ligand, making it not ideal for further studies.[7e] (4) There is

regioselectivity in CO/CN^- substitution, one CN^- going on each iron center.[7a] (5) Using PMe_3 instead of CN^- renders a disubstituted complex with very similar electronic features and makes it viable for metal-metal bond protonation to afford the $Fe^{II}(\mu\text{-}H)Fe^{II}$ species exclusively.[7e] Photolysis of the Fe^{II} binuclear complex creates an open site for H_2 binding and catalyzes H/D exchange in H_2/D_2 mixtures,[8] an assay reaction that is used by biochemists to monitor hydrogenase activity.

This research group has explored the fundamental properties of the well-known dinuclear iron thiolate compounds. Soon after the crystal structure of the enzyme was determined, a major effort was mounted to expand the knowledge on such metal complexes, aiming to have a better understanding of the chemistry that occurs at active center of the enzyme. Our work has focused on the CO and PMe_3 derivatives in studies of the effect of the ligand, the dithiolate bridge, and the S-to-S linker on electrocatalysis. From the conclusions reached in the previous studies cited above, our research efforts, as well as that of other groups, are now focused in the improvement of these diiron catalysts to have a more accurate mimic of the function of [Fe]H_2ase.

The rational design of model complexes for the active site of [Fe]H_2ase takes into consideration not only the structural features of the active site, but also the function of the enzyme. In order to design a complex that replicates both structural and functional features, classical organometallic reactivity and theoretical computations are considered together to identify the components which could fulfill such requirements.

Pickett and coworkers modified the propanedithiolate ligand to obtain a ligand that contains three sulfurs, $MeC(CH_2SH)_2CH_2SH$, two of which are thiolate sulfurs and

one thioether. This novel ligand was reacted with $Fe_3(CO)_{12}$ to form the diiron all-CO complex shown in Figure I-3 a.[9] This complex models the actual [2Fe-3S] cluster in the active center where catalysis takes place. Previous model complexes contained a [2Fe-2S] motif. Also, by incorporating a third sulfur in the coordination sphere of this dinuclear complex, asymmetry has been included as the two iron centers are distinct. This compound reacts readily with two equivalents of cyanide in CH_3CN to form a dicyanide substituted species, in which the thioether is dissociated, and a molecule of CO takes this coordination site.[9] Figure I-3 b shows an intermediate in the CO/CN substitution reaction. This intermediate provided spectroscopic evidence in the IR spectrum for the presence of a bridging CO (ν_{CO} = 1780 cm^{-1}).[10] One electron oxidation of the dicyanide Fe^IFe^I complex yielded a mixed valent Fe^IFe^{II} species that has been spectroscopically detected by IR and EPR spectroscopies. The data collected for this species indicates that this species is a good spectroscopic model for the oxidized CO-inhibited form of [Fe]H_2ase. The significance of finding supporting evidence for low valent, organometallic-like iron compounds in biological settings presents a paradigm change for bioinorganic chemistry.

Rauchfuss and coworkers also modified the propanedithiolate ligand to include a nitrogen as the central atom in the three light atoms chain.[11] This was done to model the di-(thiomethyl)-amine moiety that bridges the two sulfur atoms, as proposed by Fontecilla-Camps and coworkers.[5b] The stick drawing for the diiron compound that contains this ligand is shown in Figure I-3 c. Rauchfuss *et al.* also reported a study on the electrocatalytic production of H_2 using [Fe]H_2ase model complexes.[12] Upon

addition of a strong acid to the asymmetric disubstituted complex {(μ-pdt)[$Fe(CO)_2PMe_3$][$Fe(CO)_2CN$]}$^-$ a neutral bridging hydride is formed. A second proton goes to the N on CN^-. A two-electron reduction process occurs at –1 V to release H_2 and regenerate the starting catalysts (CCEE mechanism).

A research group in Sweden has synthesized a model system that involves light-driven proton reduction by utilizing a photosensitizer that is attached to the diiron thiolate complexes.[13] These complexes contain a N atom as the middle atom of the S-to-S linker. Compound I-3 d is one the complexes prepared by this group; attachment of further redox active components is through the bromide on the aromatic ring.

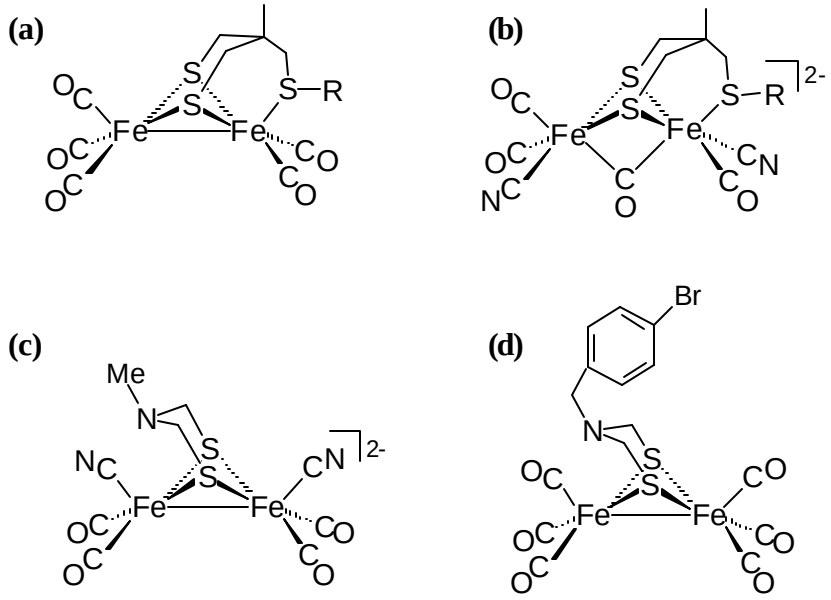

Figure I-3. Recent Fe^IFe^I model complexes for the active center of [Fe]H_2ase. a) Ref 9; b) Ref 10; c) Ref 11; d) Ref 13.

Recent work in this group in the synthesis and study of model complexes for the active center of [Fe]H_2ase is based in the analogies presented in Figure I-4. In the enzyme H_2 uptake occurs at an Fe^{II} center, where H_2 binds to be heterolytically activated to form H^+ and H^-. To study the H_2 uptake reaction dinuclear disubstituted $Fe^{II}Fe^{II}$ complexes have proved useful. Good electron donors coordinated to the (μ-SRS)$Fe^{I}Fe^{I}$ core, phosphines for instance, are required to produce the bridging hydride produced by protonation or binuclear oxidative addition, and stabilize the resulting $Fe^{II}Fe^{II}$ species.

In the reduced state of the enzyme, suggested to be $Fe^{I}Fe^{I}$, the electron density of the Fe-Fe bond is polarized, presented in Figure I-4 in the extreme case in which the electron pair resides on one of the Fe atoms making it more like an Fe^0; the other Fe could be seen more like Fe^{II}. The electron richness of Fe^0 is sufficient to undergo oxidative addition of a proton, forming a terminal hydride, the first intermediate in the H_2 production mechanism. We have approached this process with dinuclear $Fe^{I}Fe^{I}$ thiolate complexes. Ligands completing the coordination sphere in such model complexes are CO, PMe_3, and PTA (PTA = 1,3,5-triaza-7-phosphaadamantane). Studies of H_2 production using diiron complexes as catalysts will be presented in Chapter IV of this dissertation. Asymmetrically substituted complexes in which one CO ligand has been substituted from the parent hexacarbonyl complex, (μ-pdt)$[Fe(CO)_3]_2$, by electron rich donors, the phosphine PTA, and a N-heterocyclic carbene, will be presented in Chapter V. Possible effects in the dynamic properties of

the $Fe(CO)_3$ units by the presence of a good electron donor in the other iron center will be discussed.

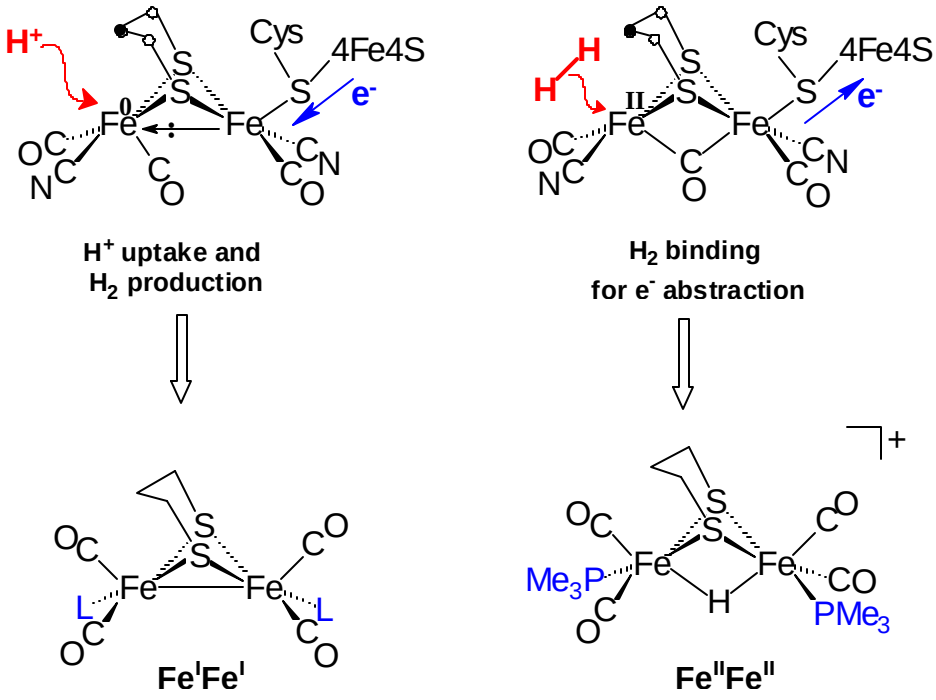

Figure I-4. Analogies between the active center of [Fe]H_2ase and model complexes that have been synthesized.

The need for energy sources alternative to fossil fuels has drawn the attention to the use of hydrogen. In Nature the production or uptake of H_2 is carefully balanced by having different types of hydrogenases performing the transformations involved in the process. In "real life" the use of H_2 as an energy source relies on the use of precious metals, platinum being the most common, to effect the conversions presented in Equation I-xx and I-xx. These reactions occur in fuel cells, devices that convert chemical energy into electricity.

$$H_2 + 2\,Pt \longrightarrow 2\,Pt\text{-}H \qquad \text{(I-2)}$$

$$2\,Pt\text{-}H \longrightarrow 2\,Pt + 2\,H^+ + 2\,e^- \qquad \text{(I-3)}$$

The hydrogenase enzymes catalyze the reversible oxidation of H_2 in the presence of suitable electron carriers, ferredoxin, cytochrome c_3, and NAD, for example. These enzymes are highly active catalysts; one molecule of the [Fe]H_2ase of *Desulfovibirio desulfuricans* can produce 9,000 molecules of per second at 30 °C. This figure is 6000 s^{-1} for the hydrogenase of *Clostridium pasteurianum*.[14] On the other hand, laboratory studies of immobilized enzyme on the surface of electrodes use methyl viologen as electron transfer mediator between the electrode and the protein.[15] Such studies have been conducted at H_2 uptake and production using modified electrodes, glassy carbon electrode modified with immobilized enzyme or whole cells, as well as with a bare carbon electrode in the presence of hydrogenase in solution. While the anodic current observed at positive overvoltage is due to hydrogen oxidation,

the cathodic current observed at negative potentials corresponds to H_2 evolution. Recent studies conducted by Armstrong and coworkers,[16] using the [Ni-Fe]H_2ase from *Allochromatium vinosum* adsorbed on a pyrolitic graphite electrode demonstrated that the active site of this enzyme can oxidize H_2 at rates comparable to electrodeposited platinum. Clearly future developments of fuel cells for mass marketing would benefit from discovery of electrodes that were more like Nature's own i.e., cheap electrodes modified with binuclear base metal catalysts.

Although third generation model complexes, showed the desirable catalytic activity it has been proven that there is only slight differences in reactivity with various thiolate bridges or phosphine ligands. Furthermore, a catalyst decomposition route involves elimination of $HPMe_3^+$. At this time it seems appropriate to explore other ligands that may form diiron complexes similar to the ones already prepared, yet with varying characteristics in order to gain stability and to further develop the chemistry of these biologically relevant and inspired catalysts.

CHAPTER II

EXPERIMENTAL

Materials and Techniques

All manipulations were performed using standard Schlenk techniques under N_2, unless stated otherwise. Solvents were of reagent grade and purified as follows: Dichlorometahane was distilled over P_2O_5 under N_2. Acetonitrile was distilled once from CaH_2, once from P_2O_5, and freshly distilled from CaH_2. Toluene, hexane, diethyl ether, and THF were distilled from sodium/benzophenone under N_2. The parent (μ-pdt)$Fe_2(CO)_6$, and 1,3,5-triaza-7-phosphaadamantane (PTA), were prepared according to literature methods.[17,18] The following materials were of reagent grade and used as received: $Fe_3(CO)_{12}$, ethanethiol, 1,3-propanedithiol, potassium *tert*-butoxide, KO^tBu, $CF_3SO_3CH_3$, conc. HCl and NH_4PF_6 (Aldrich Chemical Company), 3-bis(2,4,6-trimethylphenyl)imidazolium chloride (Strem), deuterated solvents, and ^{13}CO (Cambridge Isotope Laboratories).

Infrared spectra were recorded on a Mattson 6021 FTIR with DTGS and MCT detectors, or on an IBM IR/32 using a 0.1 mm NaCl cell. ^1H, and ^{31}P NMR (85% H_3PO_4 was used as external reference) spectra were recorded on a Unity+ 300 MHz superconducting NMR instrument operating at 299.9, and 121.43 MHz, respectively. ^{13}C NMR spectra were recorded on a Unity Inova-400 NMR instrument with a 5 mm autoswitchable probe and equipped with a variable-temperature control module operating at 100.49 MHz. ^1H and ^{13}C NMR spectra were referenced using published

solvent resonances. Elemental analyses were carried out by Canadian Microanalytical Service in Delta, British Columbia, Canada. Conductivity measurements were performed in an Orion 160 conductivity meter. Mass Spectral analyses were done at the Laboratory for Biological Mass Spectroscopy at Texas A&M University. Electrospray Ionization mass spectra were recorded using a MDS-Series QStar Pulsar with a spray voltage of 5 KeV.

X-ray structure determinations. The X-ray diffraction data were collected on a Bruker Smart 1000 CCD diffractometer and covered a hemisphere of reciprocal space by a combination of three sets of exposures. The space groups were determined based on systematic absences and intensity statistics. The structures were solved by direct methods. Anisotropic displacement parameters were determined for all non-hydrogen atoms. Hydrogen atoms were placed at idealized positions and refined with fixed isotropic displacement parameters. The following is a list of programs used: for data collection and cell refinement, SMART,[19] data reduction, SAINTPLUS,[20] structure solution, SHELXS-97 (Sheldrick),[21] structure refinement, SHELXL-97 (Sheldrick),[22] and molecular graphics and preparation of material for publication, SHELXTL-Plus, version 5.1 or later (Bruker).[23]

Experimental for Chapter III

Synthesis of [(μ-SCH_2CH_3)$Fe(CO)_3$]$_2$. The known diiron hexacarbonyl complex was prepared by following the literature procedure[17] by warming a toluene solution of $Fe_3(CO)_{12}$ (2 g, 4 mmol, in 30 mL toluene) with CH_3CH_2SH (8 mmol, 0.6 mL), under N_2, until a color change from green to red-brown was observed. Following solvent reduction to 3-4 mL, the product was purified by chromatography on successive silica columns, the first with toluene as eluent followed by pentane. Crystalline product was obtained by cooling the concentrated pentane solution at –5 °C. Yield: 3 mmol. Spectroscopic data: [(μ-SCH_2CH_3)$Fe(CO)_3$]$_2$: ^{1}H NMR (acetone-d_6): ä (ppm) 2.51(q, J_{H-H} = 7.6 Hz), 2.20 (q, J_{H-H} = 7.6 Hz), 1.40 (t, J_{H-H} = 7.6 Hz), 1.33 (t, J_{H-H} = 7.6 Hz), 1.11 (t, J_{H-H} = 7.6 Hz); IR (CH_3CN, cm^{-1}): ν(CO), 2071(m), 2035(vs), 1992(s).

Synthesis of [(μ-SCH_2CH_3)$Fe(CO)_2(PMe_3)$]$_2$. To a degassed 100-mL Schlenk flask fitted with a water condenser and containing 0.468 g (1.16 mmol) [(μ-SEt)$Fe(CO)_3$]$_2$ under a flow of N_2, 30 mL of freshly distilled hexane and 0.48 mL (4.66 mmol) of PMe_3 were added. Magnetic stirring and gentle heating (40-50 °C) was maintained overnight. Following solvent removal in vacuo, the diiron complex was obtained as a red oil. From a concentrated hexane solution stored in the freezer (-5 °C), crystalline compound was obtained. IR (hexanes, cm^{-1}): ν(CO) 1988(s), 1944(m), and 1925(s); IR (CH_3CN,cm^{-1}): ν(CO) 1977(s), 1931(m), and 1908(s); ^{1}H NMR (acetone-d^6 -C**H**$_3$, 18 H); *syn* isomer: 2.36 (q, S-C**H**$_2$, 4 H, J_{H-H} = 7.2 Hz), 1.24 (t, C-C**H**$_3$, 6H, J_{H-H} = 7.2 Hz); *anti* isomer: 2.27 (q, S-C**H**$_2$, 2 H, J_{H-H} =

7.2 Hz), 1.97 (q, S-C**H**$_2$, 2 H, J_{H-H} = 7.2 Hz), 1.25 (t, C-C**H**$_3$, 3H, J_{H-H} = 7.2 Hz), 1.1 (t, C-C**H**$_3$, 3H, J_{H-H} = 7.2 Hz). ^{31}P NMR (acetone-d^6): 9.32 (s, **P**Me$_3$).

Crystal data: **[(m-SCH$_2$CH$_3$)Fe(CO)$_2$(PMe$_3$)]$_2$**: Crystal suitable for X-ray analysis were grown in a hexane solution maintained at –5 °C within a few days. A single crystal was mounted on a glass fiber with epoxy cement at 110 K in a N_2 cold stream. $Fe_2C_{14}H_{28}O_4P_2S_2$, M = 498.1, triclinic, space group P-1, with a = 10.474(2) Å, b = 14.233(3) Å, c = 15.932(3) Å, α = 75.656(4)°, β = 89.180(4)°, γ = 86.004(3)°, and Z = 4, R1 = 0.0453 and wR2 = 0.1159 for 14722 reflections.

Synthesis of {(m-H)(m-SCH$_2$CH$_3$)$_2$[Fe(CO)$_2$(PMe$_3$)]$_2$}[PF$_6$]. The hydride was obtained by adding ~ 1 mL concentrated HCl(aq) to a methanol solution of [(μ-SEt)-Fe(CO)$_2$(PMe$_3$)]$_2$ (0.55 g) . The solution warmed up upon addition of HCl while the color changed from orange-red to yellowish orange. Addition of ~ 2 mL of a saturated aqueous solution of NH_4PF_6 precipitated the PF_6^- salt. The precipitate was filtered, washed with distilled H_2O and diethyl ether, air-dried and then stored in the glove box. ^{1}H NMR (CD_2Cl_2): ä(ppm) 1.19 (t, C-C**H**$_3$, 6 H, J_{H-H} = 7.6 Hz), 1.73 (d, P-C**H**$_3$, 18 H, J_{P-H} = 12.8 Hz), 2.05 (q, S-C**H**$_2$, 4 H, J_{H-H} = 7.6 Hz), -15.79 (t, Fe-**H**-Fe, 1 H, J_{P-H} = 3.6 Hz), small resonances at – 15.66 and –15.58 probably due to different isomers of this compound. ^{31}P NMR (acetone-d$_6$): ä(ppm) 19.2 (s, **P**Me$_3$), -142.3 (m, **P**F_6^-), small peaks at 21.6 and 23.8. Elemental Analysis for $Fe_2S_2C_{14}H_{29}O_4P_3F_6$, calculated (found) (%): C 26.1 (25.31); H 4.5 (4.52).

Crystal data: **{(m-H)(m-SCH$_2$CH$_3$)$_2$[Fe(CO)$_2$(PMe$_3$)]$_2$}[PF$_6$]**: Crystal suitable for X-ray analysis were grown from a methanol solution layered with hexanes at room

temperature. A single crystal was mounted on a glass fiber with epoxy cement at 110 K in a N_2 cold stream. $Fe_2C_{14}H_{29}F_6O_4P_3S_2$, M = 644.1, monoclinic, space group P(2)1/c, with a = 10.3731(9) Å, b = 12.5853(11) Å, c = 20.2228(17) Å, $\alpha = 90°$, $\beta = 98.0290(10)°$, $\gamma = 90°$, and Z = 4, R1 = 0.0278 and wR2 = 0.0710 for 11188 reflections.

^{13}CO-enriched [(μ-SCH$_2$CH$_3$)Fe(CO)$_3$]$_2$ sample for variable temperature ^{13}C NMR experiment. 20-30 mg of [(μ-SEt)Fe(CO)$_3$]$_2$ were placed in a 25-mL Schlenk flask. After adding 3 mL acetone-d_6 the flask was gently degassed and filled with ^{13}CO. The solution was under photolysis for 3 h using a UV lamp. An aliquot of the solution was transferred to a degassed NMR tube via syringe. At 22 °C the 13C NMR spectrum presents two resonances, at 210.1 and 209.2 ppm. The resonance at 209.2 broadens and coalesces at ~ –60 °C. The low temperature spectrum, –80 °C, shows three sharp resonances, 211.1, 210.0, and 208.4 ppm, and a broad signal at 211.8 ppm.

Experimental for Chapter IV

Preparation of (μ-pdt)[Fe(CO)$_2$PTA]$_2$. To the red solution of (μ-pdt)-[Fe(CO)$_3$] (0.602 g, 1.56 mmoles) in CH_3CN (25 mL) was added via cannula the PTA solution (0.503 g, 3.20 mmoles, dissolved in 12 mL MeOH). The reaction mixture was refluxed until IR spectroscopy indicated there was no remaining carbonyl complex starting material. After solvent removal in vacuum, the solid residue was washed twice with 15-20 mL portions of dry degassed hexanes. An orange solid was obtained in nearly quantitative yield. Crystals suitable for X-ray analysis were grown from a

layered methanol-hexanes solution. IR (í(CO) region in CH_3CN, cm^{-1}) 1986(w), 1953(s), 1907(m); ^1H NMR (ppm, acetone-d_6) 4.51 (s, 6 H), 4.13(s, 6H), 1.99 (t, 4 H, S*CH*$_2$, J = 5.9 Hz), 1.77 (q, 2 H, C*CH*$_2$C, J = 5.9 Hz); ^{31}P NMR, –17.75 ppm. Elemental analysis found (calculated) %: C 35.8 (35.4), H 4.86 (4.69), N 13.5 (13.0).

Crystal data: **(m-pdt)[Fe(CO)$_2$PTA]$_2$**: Crystal suitable for X-ray analysis were grown from a layered methanol-hexanes solution maintained at –5 °C. A single crystal was mounted on a glass fiber with epoxy cement at 110 K in a N_2 cold stream. $Fe_2C_{19}H_{30}N_6O_4P_2S_2$, M = 644.2, monoclinic, space group P2(1)/c, with a = 12.8193(10) Å, b = 24.0187(19) Å, c = 8.4330(7) Å, $\alpha = 90°$, $\beta = 105.5690(10)°$, $\gamma = 90°$, and Z = 4, R1 = 0.0555 and wR2 = 0.1303 for 15572 reflections.

Synthesis of (m-pdt)[Fe(CO)$_2$PTA][Fe(CO)$_3$]. The same procedure as described above was followed but temperature was controlled at ~ 40 °C. After 20 hr the main product (ν(CO) IR monitor) was the mono-substituted complex, as a mixture with 5-10% of the parent (μ-pdt)[$Fe(CO)_3$] complex and 5-10% disubstituted product, (μ-pdt)- [$Fe(CO)_2PTA]_2$**.** Further manipulations of this mixture were performed in air**.** Following solvent evaporation the solids were dissolved in a minimum of THF for column chromatography on a 2.5 x 30 cm silica gel column. Hexane was used to first elute the all-CO complex, followed by THF to separate the PTA products. The (μ-pdt)[$Fe(CO)_2PTA$][$Fe(CO)_3$] complex eluted first and on concentration of the THF solution, orange, needle-shaped crystals of this complex were obtained. IR (í(CO) region in CH_3CN, cm^{-1}) 2041(s), 1984(vs), 1965(s), 1926(m); ^{31}P NMR (CD_3CN) -18.4 ppm.

Crystal data: **(μ-pdt)[Fe(CO)$_2$PTA][Fe(CO)$_3$]**: Crystal suitable for X-ray analysis were grown from a concentrated THF solution maintained at –5 °C. A single crystal was mounted on a glass fiber with epoxy cement at 110 K in a N_2 cold stream. $Fe_2C_{14}H_{18}N_3O_5PS_2$, M = 515.10, monoclinic, space group P2(1)/n, with a = 11.8502(16) Å, b = 12.4174(18) Å, c = 13.1985(18) Å, $\alpha = 90°$, $\beta = 94.424(8)°$, $\gamma = 90°$, and Z = 4, R1 = 0.0657 and wR2 = 0.1346 for 10087 reflections.

Synthesis of {(μ-pdt)[Fe(CO)$_2$(PTA-H)]$_2$}(PF$_6$)$_2$. 0.143 g of (μ-pdt)-[Fe(CO)$_2$PTA]$_2$ (0.22 mmoles) were dissolved in 13 mL 0.1 M HCl, forming a reddish orange solution. An orange solid precipitated upon addition of a saturated aqueous solution of NH_4PF_6. After filtration and air-drying, 0.170 g of product (0.18 mmol, 80% yield) was obtained. IR (in CH_3CN, cm^{-1}) 2001(w), 1969(s), 1925(m); ^{1}H NMR (ppm, acetone-d_6) 5.33 (s, 6 H), 4.79(s, 6H), 2.11 (t, 4 H), 1.85 (q, 2 H); ^{31}P NMR -3.88, -142.98 ppm (PF_6^-). Λ_M 263 ohm^{-1} cm^2 $mole^{-1}$. ESI Mass spectrum: m/z = 645.0, $\{[(\mu\text{-pdt})[Fe(CO)_2(PTA\text{-}H)]\ [Fe(CO)_2PTA)]\}^+$

Synthesis of {(μ-pdt)[Fe(CO)$_2$(PTA-CH$_3$)]$_2$}(CF$_3$SO$_3$)$_2$. On addition of 70 μL (0.102 g, 0.618 mmol) $CF_3SO_3CH_3$ to a 10 mL CH_2Cl_2 solution containing 0.100 g (0.155 mmol) **1-(PTA)$_2$** a reddish-orange solid precipitated. After filtration in air the solid was washed with CH_2Cl_2 and air-dried. IR (in CH_3CN, cm^{-1}) 2003(w), 1970(s), 1927(m); ^{1}H NMR (CD_3CN) 1.77 (m, 2 H, C*CH$_2$*C), 2.06 (t, 4 H, *SCH$_2$*, J = 5.6 Hz), 2.74 (s, 6 H, N*CH$_3$*), complex set of peaks from δ3.95 to δ4.91 ppm (24 H); ^{31}P NMR 1.68 ppm. Elemental analysis found (calculated) %: C 27.9 (28.4), H 3.73 (3.73), N

8.27 (8.64). Λ_M 275 ohm^{-1} cm^2 $mole^{-1}$. m/z = 822.99, $\{[(\mu\text{-pdt})[Fe(CO)_2(PTA\text{-}CH_3)]_2(CF_3SO_3)\}^+$

Electrochemistry. Electrochemical measurements were made using a BAS 100A potentiostat. All voltammograms were obtained in a conventional and a gas-tight three-electrode cell under N_2 or CO atmosphere and room temperature. The working electrode was a glassy carbon disk (0.071 cm^2) polished with 1*m*m diamond paste and sonicated for 15 min. Supporting electrolyte was 0.1 M *n*-Bu_4NBF_4. The experimental reference electrode was Ag/Ag^+ prepared by anodizing a silver wire in an CH_3CN solution of 0.01 M $AgNO_3$/0.1 M *n*-Bu_4NBF_4. All potentials are reported relative to the normal hydrogen electrode (NHE) using Cp_2Fe/Cp_2Fe^+ as reference (the literature value for $E_{1/2}{}^{NHE}$ = 0.40 V in CH_3CN).[24] The counter electrode was platinum wire.

Bulk electrolyses for electrocatalytic reaction were carried out under N_2 atmosphere using an EG&G Model 273 Potentiostat and Galvanostat or BAS 100A Potentiostat. All electrocatalytic experiments were run for 1 h on a vitreous carbon rod (A = 3.34 cm^2) in a gas-tight, H-type electrolysis cell containing ca. 20 mL CH_3CN which was 5.0 mM in the diiron PTA derivatives and 0.1 M in *n*-Bu_4NBF_4 in the presence of HOAc (up to 100 mM).

***In situ* IR spectroscopy; spectroelectrochemistry.** *In situ* IR monitoring experiments during the course of bulk electrolysis were performed by use of a ReactIR^{TM} 1000 equipped with an MCT detector and 30 bounce SiCOMP *in situ* probe which was purchased from Applied Systems Inc. The *in situ* infrared spectroscopic measurements were made on ca. 35 mL solutions. The experimental setup is shown in

Figure IV-5. Infrared spectroelectrochemistry experiments for complex {(μ-pdt)[Fe(CO)$_2$(PTA-CH$_3$)]$_2$}(CF$_3$SO$_3$)$_2$ in CH$_3$CN/H$_2$O (3:1, v/v) mixtures were conducted on non-electrolyzed solutions.

The EPR spectrum was recorded on a Bruker X-band EPR spectrometer (model ESP 300E) with Oxford Liquid Helium/Nitrogen cryostat at 10 K, 1 mW power and 0.1 mT modulated amplitude.

Experimental for Chapter V

Preparation of (μ-pdt)[Fe(CO)$_3$][Fe(CO)$_2$IMes]. Deprotonation of 1,3-bis-(2,4,6-trimethylphenyl)imidazolium was performed according to the procedure published by Arduengo and coworkers.[25] Reaction of 0.700 g ImesH$^+$Cl$^-$ (2.05 mmoles) with KO^{t}Bu (2.16 mmoles) in THF followed by evaporation of the solvent, extraction on warm toluene, and removal of toluene under vacuum afforded 1,3-bis(2,4,6-trimethylphenyl)imidazol-2-ylidene (**IMes)** as a white solid that was used without further purification. The **IMes** ligand was dissolved in 15 mL of THF and (μ-pdt)- [Fe(CO)$_3$]$_2$, (0.779 g, 2.02 mmoles) dissolved in 4mL THF was added via cannula. The reaction mixture was heated in a water bath to ca. 50 °C until IR spectroscopy indicated the substitution reaction was complete (ca. 1.5 hr). Filtration through celite followed by solvent removal in vacuum afforded a red oil that was dissolved in diethyl ether (2 x 20 mL) which was then removed under vacuum. (μ-pdt)[Fe(CO)$_3$]- [Fe(CO)$_2$IMes] was obtained as a red solid after overnight drying in vacuum. Needle shaped crystals suitable for X-Ray analysis were grown from a

layered THF-hexanes solution. IR (í(CO) region in THF, cm^{-1}) 2035(s), 2027(sh), 1969(vs), 1947(m), 1916(w); in toluene, 2039(m), 2029(m), 1973(vs), 1949(m), 1914(w) ^{1}H NMR (ppm, acetone-d_6) 4.51 (s, 6 H), 4.13(s, 6H), 1.99 (t, 4 H, S*CH*$_2$, J = 5.9 Hz), 1.77 (q, 2 H, C*CH*$_2$C, J = 5.9 Hz). Elemental analysis found (calculated) %: C 52.1 (52.6), H 4.17 (4.56), N 4.65 (4.23).

Crystal data: **(m-pdt)[Fe(CO)$_3$][Fe(CO)$_2$IMes]**: Crystal suitable for X-ray analysis were grown from a layered THF-hexanes solution maintained at –5 °C. A single crystal was mounted on a glass fiber with epoxy cement at 110 K in a N_2 cold stream. $Fe_2C_{29}H_{30}N_2O_5S_2$, M = 662.28, monoclinic, space group I2/a, with a = 19.158(17) Å, b

$\alpha = 90°$, $\beta = 107.148(17)°$, $\gamma = 90°$, and Z = 4, R1 = 0.0720 and wR2 = 0.1426 for 13741 reflections.

^{13}CO-enriched samples for variable temperature ^{13}C NMR experiment. 20-30 mg of the diiron complex, (μ-pdt)[Fe(CO)$_3$][Fe(CO)$_2$IMes] or (μ-pdt)-[Fe(CO)$_3$][Fe(CO)$_2$PTA], were placed in a 25-mL Schlenk flask. After adding 3 mL acetone-d_6 the flask was gently degassed and filled with ^{13}CO. The solution was placed under photolysis for 3 h using a UV lamp. An aliquot of the solution was transferred to a degassed NMR tube via syringe. ^{13}C NMR spectrum for (μ-pdt)[Fe(CO)$_3$][Fe(CO)$_2$IMes]: two resonances at room temperature, 211.8 and 215.6 ppm; the resonance at 211.8 ppm coalesces at –50 °C; at –80 °C, resonances at 208.4, 212.2, and 215.2 ppm. ^{13}C NMR spectrum for (μ-pdt)[Fe(CO)$_3$][Fe(CO)$_2$PTA]: at room temperature resonances at 211.6 and 213.5 (d, J_{P-H} = 17.3 Hz) ppm; at –80 °C, resonances at 208.5, 211.2, 212.8, 213.0, and 213.5 (d) ppm.

Cyclic voltammetry of (μ-pdt)[Fe(CO)$_3$][Fe(CO)$_2$IMes]. Electrochemical experiments to determine the redox events of this monosubstituted diiron complex were carried out under the same experimental conditions as described in the Experimental for Chapter IV.

CHAPTER III

MODEL COMPLEXES OF THE ACTIVE SITE OF [Fe]HYDROGENASE. SYNTHESIS AND CHARACTERIZATION OF A BINUCLEAR DIIRON COMPLEX BRIDGED BY TWO MONODENTATE THIOLATES*

The similarity of the active site (named the H-cluster) of the all-iron hydrogenase, [Fe]H_2ase, to classical organometallic complexes has inspired chemists to synthesize model complexes that mimic the structure and function of this enzyme. Two synthetic routes have been used in the preparation of such diiron dithiolate complexes. The first synthetic approach is based in the oxidative addition of thiols to an Fe^0 source, usually $Fe_3(CO)_{12}$, Equation III-1.[17] The second involves the reduction of the long known disulfide, $(\mu\text{-}S_2)[Fe(CO)_3]_2$, followed by reaction of the dianionic disulfido complex with a dihalide, Equation III-2.[26]

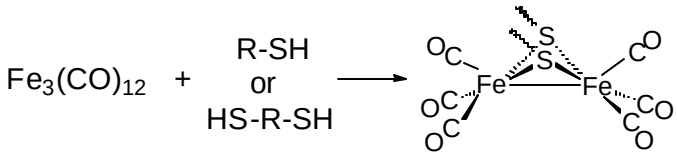

(III-1)

$$(\mu\text{-}S_2)Fe_2(CO)_6 \xrightarrow{LiBEt_3H} [(\mu\text{-}S_2)Fe_2(CO)_6]^{2-} \xrightarrow{Br\text{-}R\text{-}Br} (\mu\text{-}SRS)Fe_2(CO)_6 \qquad \text{(III-2)}$$

---

*Part of the data reported in this chapter is reprinted with permission from "Catalysis of H_2/D_2 Scrambling and Other Exchange Processes by [Fe]-Hydrogenase Model Complexes" by Zhao, X.; Georgakaki, I. P.; Miller, M. L.; Mejia-Rodriguez, R.; Chiang, C.-Y.; Darensbourg, M. Y. *Inorg. Chem.* **2002**, *41*, 3917. Copyright 2002 by the American Chemical Society.

The diiron complexes of the general formula $(\mu\text{-}SR)_2[Fe(CO)_3]_2$ have been extensively studied. In 1962, R. B. King reported the chromatographic separation of two isomers of $[(\mu\text{-}SCH_3)Fe(CO)_3]_2$.[27] The conclusion that more than one isomer had been formed was derived from ^1H NMR spectra, which indicated that the difference between the isomers was the orientation of the methyl groups attached to the sulfurs. Later that same year, King reported that no isomers were observed for a compound that presented the two iron centers bridged by a bidentate dithiolate; two carbon atoms linked the sulfurs in the $(\mu\text{-}C_2H_4S_2)Fe_2(CO)_6$ complex.[28] The presence of an S-to-S linker in the latter compound was the only difference between these two diiron complexes studied by King.

There are three possible spatial arrangements of the R groups on the sulfurs of $[(\mu\text{-}SR)Fe(CO)_3]_2$; these are presented in Chart III-1. Based on the orientation of the carbon atom next to sulfur (the alpha carbon), the *anti* isomer presents one R group in the equatorial and one in the axial position; in the *syn* orientation both R groups are in equatorial positions. The *syn'* orientation has both R groups in axial positions; this orientation has been found exclusively in linked dithiolates, SRS. To our knowledge

Chart III-1

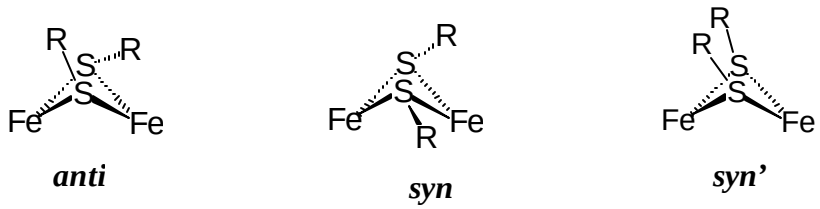

the largest known SRS has a 5-atom S-to-S link, SCH_2CH_2-(O or NH)-CH_2CH_2S.[29] It is of course possible that larger ring sizes might access the *anti* form.

According to Bor and coworkers (1971), the orientation of the R groups attached to the sulfurs in the dimeric iron dithiolate hexacarbonyl complexes is a compromise between the repulsive forces exerted by the CO ligands and the steric hindrance between R groups.[30] The molecular structures of known $(\mu\text{-SR})_2[Fe(CO)_3]_2$ complexes (R = Et,[31] ^{t}Bu,[32] and 2,4,6-^{i}*Pr*-C_6H_2,[33] among others) show that the *anti* conformation is favored over the *syn* conformation, indicating the balance between the repulsion forces mentioned above. In the case of R = Et, Ph the *syn* isomer has also been structurally characterized. Equilibrium constants determined for the *anti-syn* isomerization process for $(\mu\text{-SMe})_2[Fe(CO)_3]_2$ and $(\mu\text{-SEt})_2[Fe(CO)_3]_2$ show that the equilibrium shifts towards the *anti* isomer as the size of the organic group increases.[30]

Experimental studies on the kinetics and thermodynamics of the isomerization of $[(\mu\text{-SMe})Fe(CO)_3]_2$ conducted by Mattson and Mueting (1981)[34] showed that the *syn* isomer is only 1.4 kcal/mole more stable than the *anti* isomer. These researchers also found a solvent effect in the value of the equilibrium constant, K, and in the rate of the isomerization process. At 50 °C, K = [anti]/[syn] = 2.0 in $CHCl_3$, and 3.8 in hexane; the rate of isomerization is about 4 times faster in $CHCl_3$ and CH_3CN than in hexane. Mattson and Mueting provide tables of mole fraction ratios which indicate that *ani-syn* mixtures exist at all normal temperatures (up to 70 °C).

The coordination sphere around each Fe atom in complexes $(\mu\text{-SR})_2$-$[Fe(CO)_2L]_2$ and $(\mu\text{-SRS})[Fe(CO)_2L]_2$ can be described as square pyramidal, where

the basal plane of the pyramid is defined by the two sulfur atoms and the two ligands *trans* to them. The axial position of the pyramid is occupied by a fifth ligand bound to Fe. The electron pair in the Fe-Fe bond completes the 18-electron count for each iron center. Substitution of one or two CO ligands by electron-rich ligands like phosphines to afford mono- and di-substituted complexes has been extensively studied. This substitution reaction proceeds thermally, photolytically, or with the use of chemical agents that promote CO loss. In most cases the di-substituted product shows one L on each iron rather than the asymmetric (μ-SR)$_2$[Fe(CO)$_3$Fe(CO)L$_2$] possibility. Chart III-2 presents the possible conformational isomers for the disubstituted products.

Chart III-2

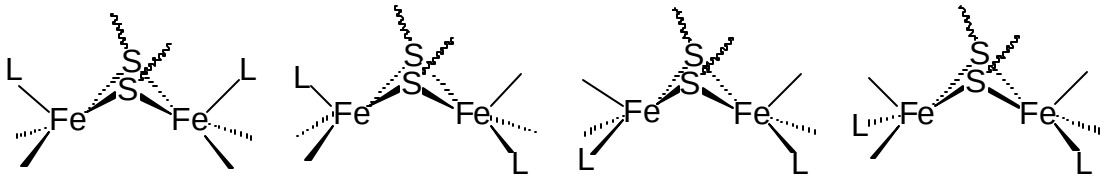

ap/ap **ap/ba** **ba/ba** ***cisoid*** **ba/ba** ***transoid***

The extent of CO substitution and preference of one site over another is governed by the steric hindrance of the incoming ligand L, and the R groups on the sulfurs. For example, trimethylphosphine forms disubstituted products very readily, while PPh$_3$ forms monosubstituted complexes only. While the known (μ-SR)-bridged bisphosphine diiron complexes present both phosphine ligands in apical positions (the

ap/ap configurational isomer in Chart III-2), rearranging the organic groups attached to the sulfurs, if required, to minimize repulsions, the (μ-SRS)-bridged compounds typically show phosphines coordinated in the basal plane (ba/ba). A notable exception is the ethanedithiolate-bridged complex that accommodates one PMe_3 in the axial position, and the other in the basal plane (ap/ba), *vide infra*.

In studies of the effect of the hydrocarbon chain which links the thiolate sulfurs on the properties and reactivity of (μ-SRS)$[Fe(CO)_3]_2$, a series of compounds with various S-to-S linkers has been prepared by several students in this research group.[8] As described in Chapter I, the two-iron cluster in the active site of [Fe]H_2ase has a three light atom chain linking the bridging sulfurs. Nature's choice of this unusual S-donor ligand rather than two cysteines as was used to bridge the binuclear site in the [Ni-Fe]H_2ase active site is curious. Hence we explored reactivity appropriate to biomimicry of the [Fe]H_2ase with a non-chelating thiol, CH_3CH_2SH, in order to establish differences, if any, there might be between a chelating and a non-chelating thiolate bridge.

Synthesis and Characterization of $[(\mu\text{-}SCH_2CH_3)Fe(CO)_2PMe_3]_2$

The all-CO precursor. As the precursor to the phosphine derivative is [(μ-SEt)$Fe(CO)_3]_2$, I first prepared and compared the properties of this complex to what was reported in the literature. Reaction of $Fe_3(CO)_{12}$ with ethanethiol in toluene afforded the orange $[(\mu\text{-}SEt)Fe(CO)_3]_2$. This diiron dithiolate hexacarbonyl complex has been previously prepared and structurally characterized.[31,35] The solid state

structure of [(μ-SEt)- $Fe(CO)_3]_2$ determined by Dahl and Wei shows that the ethyl groups are arranged in the *anti* fashion, as shown in the following stick drawing.

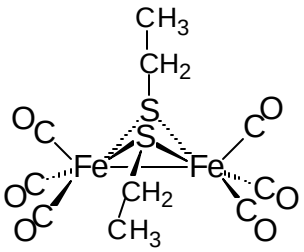

The acetone-d_6 solution ^1H NMR spectrum of the compound which I prepared and isolated, without chromatographic separation, contains a multiplet at δ 2.59-2.49 ppm, a quartet at 2.21 ppm, and three triplets (δ 1.11, 1.33, and 1.40 ppm), Figure III-1. Literature data for the ^1H NMR spectra of pure *syn* and pure *anti* isomers of [(μ-SEt)$Fe(CO)_3]_2$ in $CDCl_3$,[36] show that the *syn* isomer presents two resonances, a quartet at 2.43 ppm, and a triplet at 1.28 ppm, due to the magnetic equivalence of the methyl and methylene protons (Chart III-3). The *anti* isomer, however, contains non-equivalent protons, the spectrum presents two quartets for the methylene protons (2.13 and 2.43 ppm), and two triplets for the methyl protons (1.08 and 1.35 ppm).

Based on the reported data, we can conclude that a mixture of *syn* and *anti* isomers is present in solution. The multiplet that appears at 2.59-2.49 ppm in the ^1H NMR spectrum results form the overlap of two quartets that correspond to methylene protons in the *anti* and *syn* isomers (B' and B'' in Chart III-3). The triplet at δ 1.33 ppm is assigned to the CH_3 protons in the *syn* isomer, while triplets at 1.11, and 1.40 ppm, and the quartet at 2.20 ppm are the remaining signals for the *anti* isomer.

Integration of the signals in the spectrum suggest that the solution has an *anti:syn* ratio of ~ 70:30. The presence of a mixture of *syn* and *anti* isomers in solution was later corroborated by ^{13}C NMR.

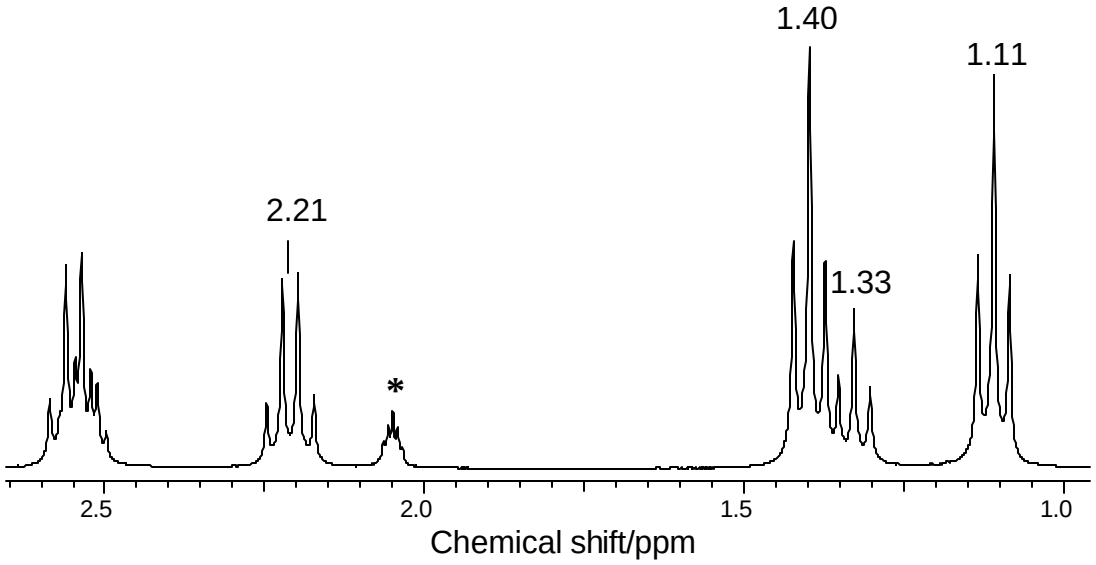

Figure III-1. ^{1}H NMR spectrum of $[(\mu\text{-SEt})Fe(CO)_3]_2$ in acetone-d_6 solution. * Solvent resonance.

Chart III-3

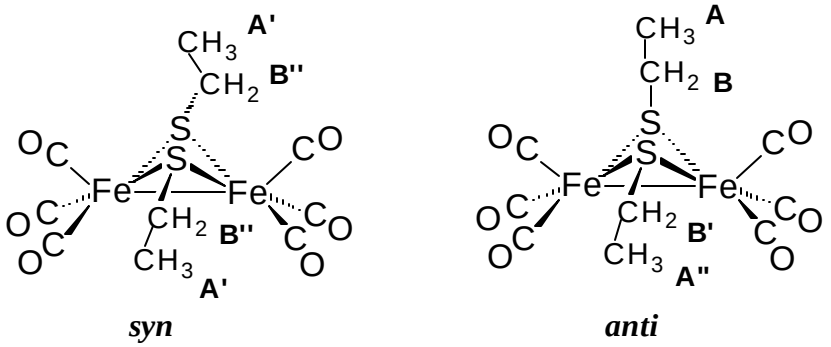

syn ***anti***

The ^{13}C NMR spectra of a ^{13}CO-enriched sample in Figure III-2 shows two sharp signals at 22 °C of unequal intensity, at δ 209.2 and 210.1 ppm. As the $Fe(CO)_3$ units are freely rotating at this temperature, intramolecular CO site exchange makes the CO's magnetically equivalent. Therefore only one signal would be expected for a solution containing one isomer. On the other hand early kinetic studies showed that the intramolecular process that interconverts the *syn* to *anti* isomer is slow at 22 °C. Hence presence of two resonances in the CO region of the spectrum indicates that there are two isomers present in solution. As the temperature is decreased, the signal at 209.2 broadens, reaching coalescence at a slightly higher temperature than the signal at 210.1 ppm. The 209.2 ppm signal separates into three resonances at –70 °C, which are sharp by –80 °C, the low temperature limit. They appear at 211.1, 210.0 and 208.4 ppm, and are assigned as indicated in Figure III-2. The positions of the resonances are consistent with the *anti* isomer, which is the major isomer present in solution, and with the results reported by Cotton and coworkers,[37] for the VT ^{13}C NMR spectroscopic study of a 2-methyltetrahydrofuran solution of *anti* $[(\mu\text{-SEt})Fe(CO)_3]_2$.

The broad signal at 211.8 ppm in the spectrum at –80 °C, Figure III-2, is assigned to the CO's in the *syn* isomer, the minor isomer, of $[(\mu\text{-SEt})Fe(CO)_3]_2$. Instrumental limitations prevented us from going to lower temperatures, so a complete and better-defined spectrum could not be obtained. The delayed appearance of the ^{13}C resonances for the CO ligands in the *syn* isomer indicates that the stopped exchange region has not yet been reached. Thus, the activation barrier for rotation of the $Fe(CO)_3$ units in this isomer is lower than that of the *anti* isomer.

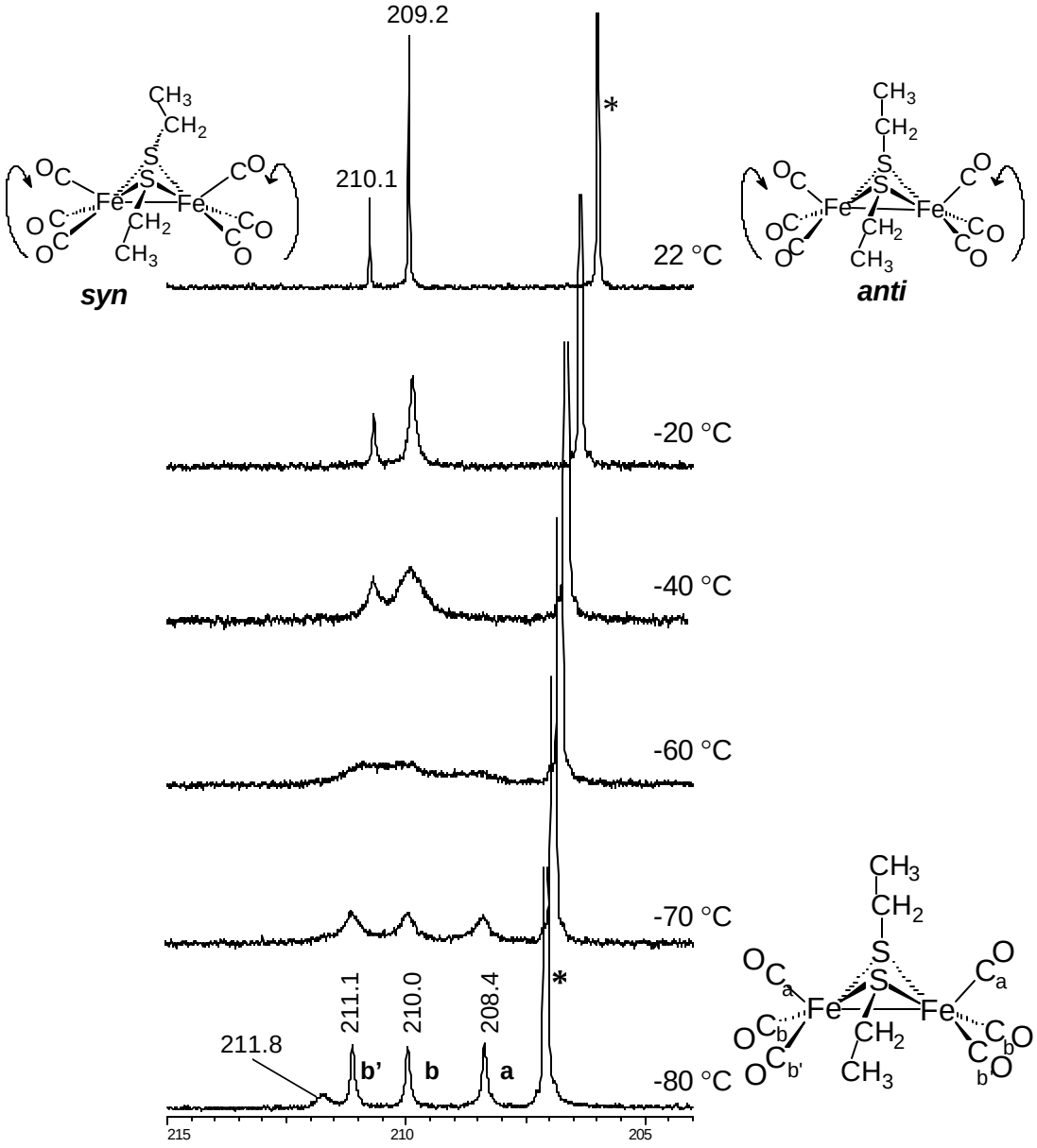

Figure III-2. Variable temperature ^{13}C NMR spectra of $[(\mu\text{-SEt})Fe(CO)_3]_2$ in the **C**O region. Assignments of the individual signals at the low temperature limit for the *anti* isomer are indicated in the stick drawing. * Solvent peak, acetone-d_6.

The PMe_3-substituted derivative. Reaction of $[(\mu\text{-SEt})Fe(CO)_3]_2$ with excess PMe_3 in hexane (40-50 °C, overnight) resulted in the substitution of two CO ligands by PMe_3 with one on each Fe atom to form a symmetrically disubstituted complex. The product, $[(\mu\text{-SEt})\text{-}\ Fe(CO)_2PMe_3]_2$, was obtained as a red oil after removing the solvent in vacuo. It was redissolved in a small amount of hexane and placed in the freezer (-5 °C), where crystals were obtained. The IR spectrum of a CH_3CN solution of $[(\mu\text{-SEt})Fe(CO)_2PMe_3]_2$ in the ν(CO) region presents bands at 1977 cm^{-1} (s), 1931 cm^{-1} (m), and 1908 cm^{-1} (s); in hexane the three bands sharpen and shift to higher frequencies by 11 – 17 cm^{-1}. The ν(CO) IR bands of the phosphine derivative are shifted to lower frequencies by about 90 cm^{-1} from the parent $[(\mu\text{-SEt})Fe(CO)_3]_2$, as expected for the substitution of CO by a better electron donor. Comparison to the IR spectrum of a very closely related compound, the methyl derivative $[(\mu\text{-SMe})Fe(CO)_2PMe_3]_2$,[38] shows that the spectral bands are an almost exact match of each other indicating the close similarity in electron donating ability of the methyl- and ethylthiolate ligands.

The molecular structure of $[(\mu\text{-SEt})Fe(CO)_2PMe_3]_2$ was determined by X-ray diffraction studies (Dr. Matthew Miller, TAMU, PhD 2003) and is presented in Figure III-3. This diiron complex crystallizes in the triclinic system with four molecules per unit cell. The PMe_3 ligands coordinate at the axial position of the square pyramids, *trans* to the Fe-Fe bond, and the ethyl groups on the sulfurs are arranged in the *syn*

a)

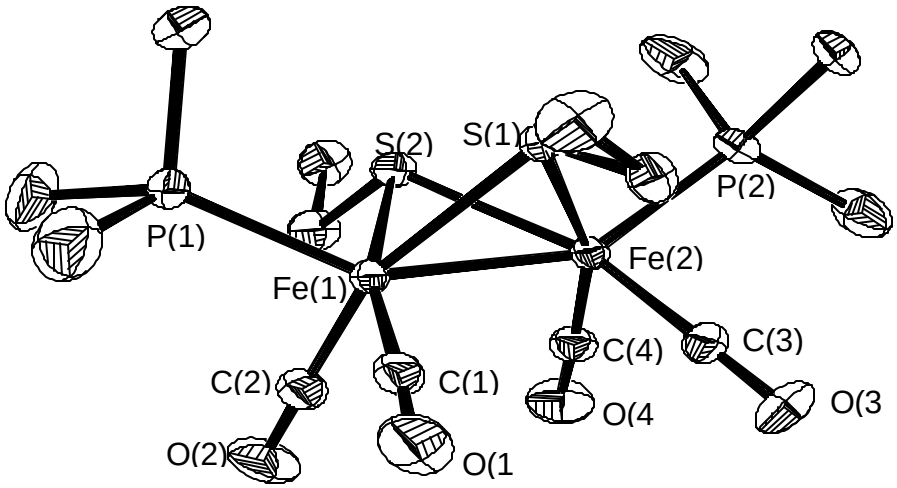

b)

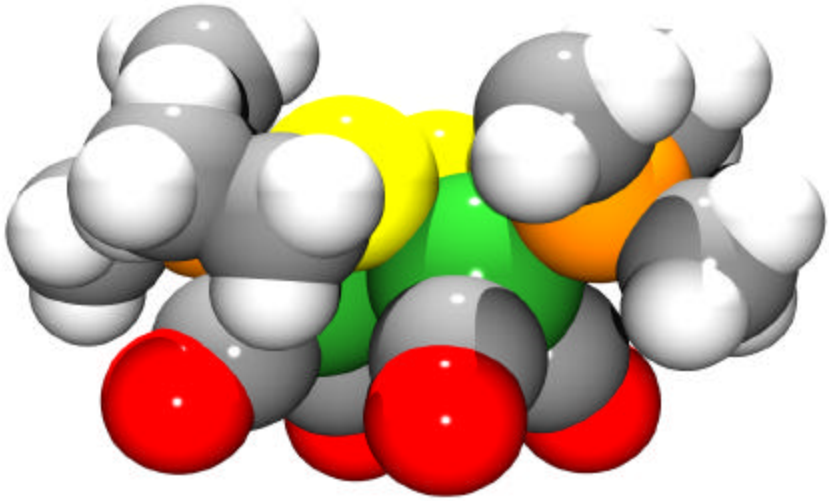

Figure III-3. Solid state structure of $[(\mu\text{-SEt})Fe(CO)_2PMe_3]_2$. a) Thermal ellipsoids set at 50% probability (hydrogen atoms were omitted for clarity), and b) Space filling model.

fashion, a change from the all-CO complex where they were arranged in an *anti* conformation. The *syn* conformation of the ethyl groups attached to the sulfurs minimizes steric interactions with the PMe_3 ligands. This can be seen in the space filling model of $[(\mu\text{-SEt})Fe(CO)_2PMe_3]_2$ presented in Figure III-3 b.

The Fe-Fe bond distance of 2.514(1) Å shows a very small difference from the hexacarbonyl complex, 2.537 (10) Å. Upon substitution of two CO ligands by PMe_3, the Fe-C average distance decreases from 1.813 (5) Å in the $[(\mu\text{-SEt})Fe(CO)_3]_2$ complex to 1.755 (3) Å in $[(\mu\text{-SEt})Fe(CO)_2PMe_3]_2$, as expected for an increase in π-back donation from the electron-richer Fe atoms to the remaining CO ligands. A complete listing of metric parameters is given in the Appendix.

A comparison between selected metric parameters for $[(\mu\text{-SEt})Fe(CO)_2PMe_3]_2$ and related $(\mu\text{-SRS})[Fe(CO)_2PMe_3]_2$ complexes is presented in Table III-1. The most obvious difference between the three complexes presented, $[(\mu\text{-SEt})Fe(CO)_2PMe_3]_2$, $(\mu\text{-edt})[Fe(CO)_2PMe_3]_2$ (prepared and characterized by Chao-Yi Chiang)[8] and $(\mu\text{-pdt})[Fe(CO)_2PMe_3]_2$ (prepared and characterized by Dr. Xuan Zhao, TAMU, PhD 2002)[7e], (edt = $-SC_2H_4S-$; pdt = $-SC_3H_6S$), and a clear example of the influence of steric factors and electronic factors on the CO/PMe_3 substitution reaction, is the position of the PMe_3 ligands. While the complex with the monodentate –SEt bridge presents both PMe_3 ligands coordinated in the apical position of the square pyramid, the thiolate bridge containing a three-carbon linker between sulfurs directs the PMe_3 ligands to the basal plane, where they arrange in a transoid fashion. The coordination

Table III-1. Selected Metric Data for Binuclear Iron Phosphino Carbonyl Complexes Bridged by Thiolates

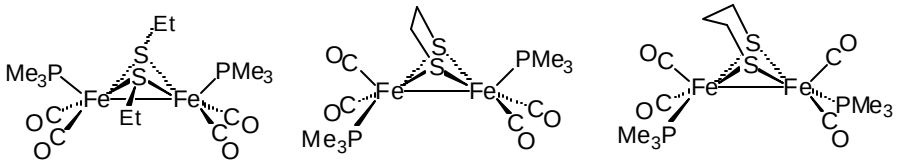

Fe-Fe, Å	2.5097(7)	2.5159(6)	2.555(2)
Fe-$C_{CO,ap}$	N/A	1.769(3)	1.772(9)
Fe-$C_{CO,ba}$	1.7552(3)[a]	1.759(3)[b]	1.742(10)
Fe-Sμ_{-SR}[c]	2.280(1)	2.2521(8)	2.254(2)
S· · · · S	2.798	2.897	3.026
Fe dsp[d]	0.315	0.365	0.376
Dihedral[e] (deg)	94.6	101.7	109.2

[a] Average of four Fe-$C_{CO,ba}$ bonds. [b] Average of three Fe-$C_{CO,ba}$ bonds. [c] Average of four Fe-$S_{\mu\text{-}SR}$ bonds. [d] Fe dsp = Displacement of Fe from best plane of $S_2L_{(ba)2}$ toward L_{ap}. [e] Defined by the intersection of the two SFe_2 planes.

of one PMe_3 ligand in the apical position, and the other in the basal plane in (μ-edt)$[Fe(CO)_2PMe_3]_2$ suggests a compromise between the steric hindrance of the ethanedithiolate bridge, and the repulsive forces imposed by the CO ligands in the basal plane.

The data presented in Table III-1 shows that the Fe-Fe distances vary according to the thiolate bridge. In the bisphosphine compound with $(\mu\text{-SEt})_2$, the Fe--Fe distance is, at 2.5097(7) Å, the shortest of the series, as might be expected for a monodentate thiolate which does not impose an angular constraint as large as a bidentate ligand. Also, the non-chelating –SEt bridge presents the shortest S to S distance. This distance is larger in the propanedithiolate bridge than in the ethanedithiolate bridge, due to the greater number of carbon atoms in the S-to-S linker in the former. The effect of the length of the hydrocarbon chain between sulfurs is also reflected in the dihedral angle (the angle between the two SFe_2 planes); the smallest dihedral angle is observed in the complex that contains the monodentate -SEt thiolate; the (μ-pdt)$[Fe(CO)_2PMe_3]_2$ complex presents the largest dihedral angle.

Protonation of $[(\mu\text{-}SCH_2CH_3)Fe(CO)_2PMe_3]_2$. Characterization of $\{(\mu\text{-}H)[(\mu\text{-}SCH_2CH_3)Fe(CO)_2PMe_3]_2\}(PF_6)$

Oxidative addition of H^+ to $[(\mu\text{-SEt})Fe(CO)_2PMe_3]_2$ occurs readily when excess concentrated HCl acid is added to a methanol solution of the bisphosphine complex, Equation III-3. The resultant monocationic $(\mu\text{-H})Fe^{II}\text{-}Fe^{II}$ complex precipitated from

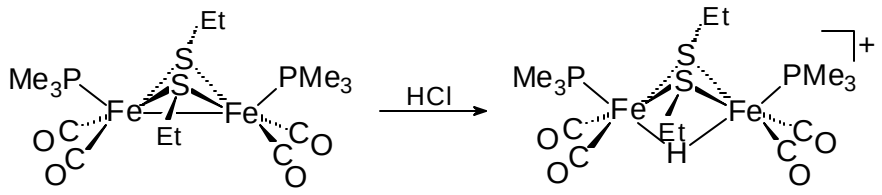

(III-3)

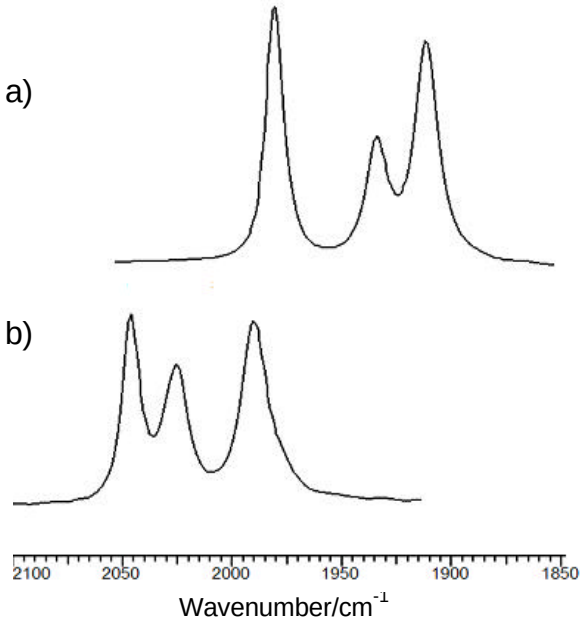

Figure III-4. Infrared spectra of a) $[(\mu\text{-SEt})Fe(CO)_2PMe_3]_2$($\nu_{CO}$ = 1977, 1931, 1908 cm^{-1}) , and b) $\{(\mu\text{-H})[(\mu\text{-SEt})Fe(CO)_2PMe_3]_2\}PF_6$ (ν_{CO} = 2046, 2025, 1990 cm^{-1}) in CH_3CN solution.

solution on addition of an aqueous NH_4PF_6 solution. Infrared spectral data of {(μ-SEt)$_2$(μ-H)[Fe(CO)$_2$PMe$_3$]$_2$}(PF_6), CH_3CN solution, in the CO region shows bands at 2046, 2025 and 1990 cm^{-1}, Figure III-4. The ν(CO) bands are shifted to higher frequencies by 69, 94, and 82 cm^{-1}, respectively, from the neutral [(μ-SEt)-Fe(CO)$_2$PMe$_3$]$_2$ complex, as expected for the oxidation of the Fe^IFe^I complex to $Fe^{II}Fe^{II}$. Crystals suitable for X-ray diffraction studies were grown from a methanol solution layered with hexanes. The solid state structure of {(μ-H)(μ-SEt)$_2$-[Fe(CO)$_2$PMe$_3$]$_2$}(PF_6) (determined by Dr. Matthew Miller, TAMU, PhD 2003) is presented in Figure III-5. This complex crystallizes in the monoclinic system with four molecules in the unit cell. It retains the stereochemistry of the neutral precursor complex, [(μ-SEt)Fe(CO)$_2$PMe$_3$]$_2$, presenting both PMe_3 ligands in apical positions and the ethyl groups attached to the sulfurs in the *syn* conformation.

After Fe-Fe bond protonation, the metal-metal distance increases to 2.571(1) Å from a distance of 2.510(1) Å in the neutral precursor, Table III-1. This is the largest increase, 0.061 Å, in iron-iron distance upon protonation that has been observed in the series of compounds that were examined, Table III-1 and Table III-2. Although the S-to-S distance in the protonated –SEt bridged compound remains almost unchanged (the difference is only 0.01 Å), the dihedral angle increases by 1.9° probably due to a change in position of the iron atoms. The displacement of the Fe atoms from the basal plane of the square pyramids towards the apical PMe_3 was 0.315 Å in the neutral bisphosphine complex; this displacement is only 0.180 Å in the monocationic hydride

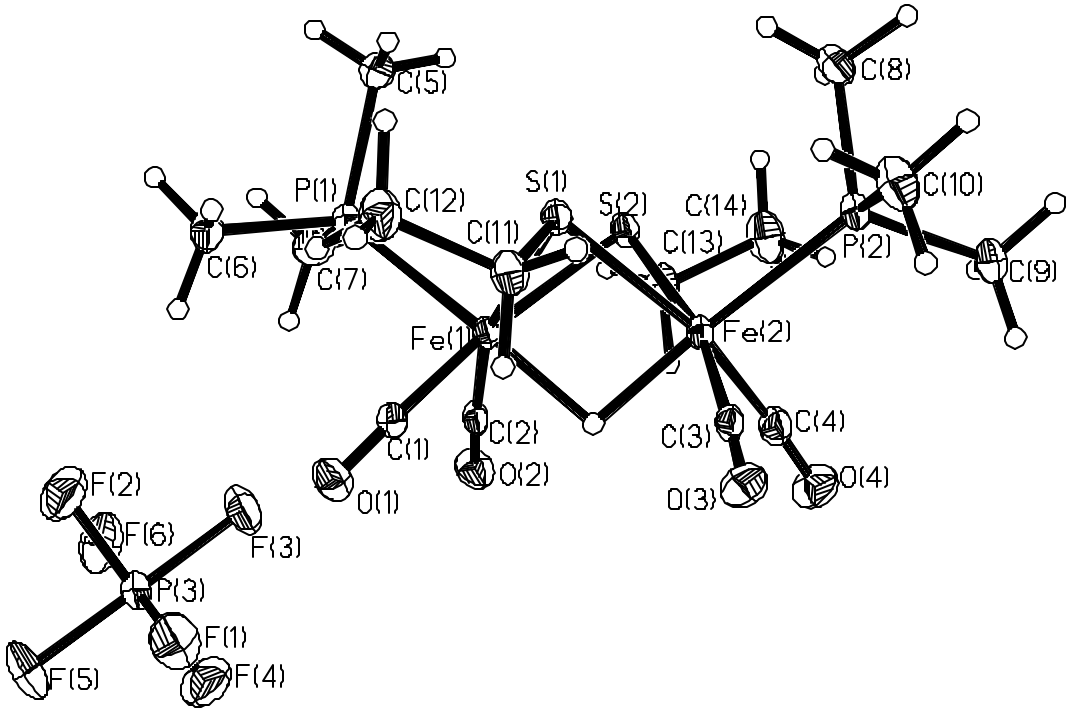

Figure III-5. Solid state structure of $\{(\mu\text{-H})(\mu\text{-SEt})_2[Fe(CO)_2PMe_3]_2\}(PF_6)$ with thermal ellipsoids set at 50% probability.

Table III-2. Selected Metric Data for Monocationic Binuclear Iron Phosphino Carbonyl Complexes Bridged by Thiolates .[a]

	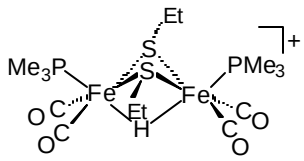	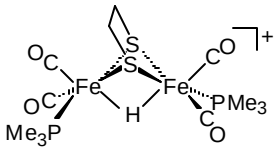	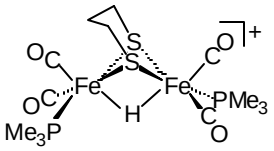
Fe· · · Fe, Å	2.5708(4)	2.5742(13)	2.5784(8)
Fe-H	1.66(2)	1.69(6)	1.710(14)
Fe-$C_{CO,ap}$	N/A	1.774(6)	1.779(4)
Fe-$C_{CO,ba}$	1.778(3)[b]	1.770(6)[c]	1.778(4)[c]
Fe-Sμ_{-SR}[d]	2.2793(7)	2.2562(16)	2.2717(11)
S· · · · S	2.808	2.924	3.064
Fe dsp[e]	0.180	0.197	0.231
Dihedral[f] (deg)	96.5	104.2	109.9

[a] {(μ-H)(μ-edt)[Fe(CO)$_2$PMe$_3$]}(PF$_6$) and {(μ-H)(μ-pdt)[Fe(CO)$_2$PMe$_3$]}(PF$_6$) were prepared by other members of the group.[7e,8] [b] Average of four Fe-$C_{CO,ba}$ bonds. [c] Average of two Fe-$C_{CO,ba}$ bonds. [d] Average of four Fe-$S_{\mu\text{-}SR}$ bonds. [e] Fe dsp = Displacement of Fe from best plane of $S_2L_{(ba)2}$ toward L_{ap}. [f] Defined by the intersection of the two SFe_2 planes.

complex, indicating that the Fe itoms are being pulled back onto the plane by the hydride ligand that is bridging them. The displacement of the iron atoms in the other two complexes considered in this comparison, {(μ-H)(μ-edt)[Fe(CO)$_2$PMe$_3$]$_2$}(PF$_6$) and {(μ-H)(μ-pdt)[Fe(CO)$_2$PMe$_3$]$_2$} (PF$_6$), also decreases.

The {(μ-H)(μ-pdt)[Fe(CO)$_2$PMe$_3$]$_2$}(PF$_6$) complex remains in the same conformation as in the neutral bisphosphine complex; that is, both PMe$_3$ ligands occupy basal positions in a *transoid* fashion. Interestingly, the ethanedithiolate-bridged compound, (μ-edt)[Fe(CO)$_2$PMe$_3$]$_2$ rearranges stereochemistry on protonation to have both PMe$_3$ ligands in the basal plane, i.e. the same stereochemistry as all other hydrides bridged by a bidentate thiolate, a difference from the neutral bisphosphine precursor for which the solid state structure corresponded to the ap/ba isomer.

Hydrogenase-like Activity of {(μ-H)(μ-SCH$_2$CH$_3$)$_2$[Fe(CO)$_2$PMe$_3$]$_2$}(PF$_6$)

As established in the Introduction, model complexes that mimic the active site of [Fe]H$_2$ase can be structural matches for one of the characterized redox states of the enzyme. Synthetic models are designed, also, to present chemical activity or function that is similar to the enzyme. According to the activity assays to test for hydrogenase-like activity, Equations I-1 and I-2, a model complex would mimic the hydrogenase function by catalyzing H/D exchange in H$_2$/D$_2$ mixtures (in the presence of H$_2$O or in the presence of a metal hydride), and by promoting isotopic scrambling in D$_2$/H$_2$O mixtures.

The H/D activity in H_2/D_2 mixtures is expected to be an important reaction for comparing catalysts generated by two base metals in binuclear complexes with those which use noble metals Ir, Pd, and Pt. Hence further studies to explore the effect of the thiolate bridge and the effect of the ligand on these compounds in assays that mimic the function of the enzyme were conducted in a series of $(\mu\text{-SR})_2$- and $(\mu\text{-SRS})[Fe(CO)_2(PMe_3)]_2$ complexes, and the corresponding monocationic bridging hydride species, prepared by several members of this research group.[8] This series of compounds include the bridging hydrides presented as stick drawings in Table III-2, and the correspondent neutral precursors of Table III-1. The studies conducted by Xuan Zhao and Irene Georgakaki, former group members, in which I participated with the complex I synthesized and characterized, $\{(\mu\text{-H})(\mu\text{-SEt})_2[Fe(CO)_2PMe_3]_2\}(PF_6)$, are summarized as follows.

The protocol established by Sellman and others was followed to assess the H_2/D_2 exchange of the Fe^IFe^I and $Fe^{II}(\mu\text{-H})Fe^{II}$ species.[39] A CH_2Cl_2 solution of the compound was prepared in a medium pressure NMR tube which was pressurized with D_2 (7-12 bar). Photolysis was promoted through sunlight exposure by placing the NMR tube on the windowsill. The formation of the $Fe^{II}(\mu\text{-D})Fe^{II}$ complex and HD, Equation III-4, was monitored by ^1H NMR and ^2H NMR. Control experiments placing the NMR tube and its contents in the dark were run at the same time. Competition experiments to establish a relative rate of reaction were performed side by side to ensure identical conditions for all samples.

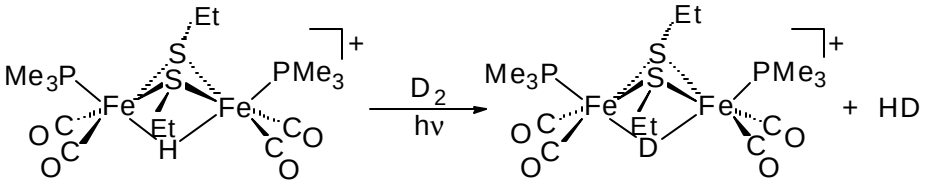

(III-4)

It was found that $\{(\mu\text{-H})(\mu\text{-SEt})_2[Fe(CO)_2PMe_3]_2\}^+$ and all other bridging hydrides bind D_2 and promote H/D exchange under photolytic conditions, while the neutral Fe^IFe^I bisphosphine compounds do not. Exposure to sunlight or to artificial light sources is required to create an open site on one of the Fe atoms where D_2 can bind and initiate the exchange mechanism.

Competition experiments yielded information to categorize the $Fe^{II}(\mu\text{-H})Fe^{II}$ compounds, and in the relative scale of activity the $[(\mu\text{-H})(\mu\text{-SEt})_2Fe_2(CO)_4(PMe_3)_2]^+$ is the most active catalyst in the series. It is also one of the least stable,[8] probably because the ability to maintain the structural integrity is less than that of the chelating thiolates with an S-to-S linker. The monodentate thiolates are subject to isomerization processes in addition to decomposition reactions.

CHAPTER IV

THE HYDROPHILIC PHOSPHATRIAZAADAMANTANE LIGAND IN THE DEVELOPMENT OF H_2-PRODUCTION ELECTROCATALYSTS: IRON HYDROGENASE MODEL COMPLEXES*

The contents of this Chapter are the main components of two manuscripts, one published in *Dalton Transactions***, and the other submitted to the *Journal of the American Chemical Society.*

Hydrogenases have evolved to perform both H_2 production and H_2 uptake reversibly according to the reaction, $2\ H^+ + 2\ e^- \leftrightarrows H_2$, which in the natural systems occur at neutral pH and at *ca.* – 400 mV.[40] These complex biomolecules have drawn the attention of chemists and engineers for the possibility that they might hold the key to a viable macroscale hydrogen economy.[16,41] The H_2-production process is of importance to the ready accessibility of H_2 and is most typically carried out by iron-only hydrogenase, [Fe]H_2ase; the H_2-uptake by nickel-iron hydrogenase, [NiFe]H_2ase, has implications for fuel cell development.[15b,16]

---

* Reproduced with permission from "The Hydrophilic Phosphatriazaadamantane Ligand in the Development of H_2-production Electrocatalysts: Iron Hydrogenase Model Complexes" by Mejia-Rodriguez, R.; Chong, D.; Reibenspies, J. H.; Soriaga, M. P.; Darensbourg, M. Y. *J. Am. Chem. Soc.*, submitted for publication. Unpublished work copyright 2004 by the American Chemical Society.

** Reprinted with permission from "Electrocatalysis of hydrogen production by active site analogues of the iron hydrogenase enzyme: structure/function relationships" by Chong, D.; Georgakaki, I. P.; Mejia-Rodriguez, R.; Sanabria-Chinchilla, J.; Soriaga, M. P.; Darensbourg, M. Y. *Dalton Trans.* **2003**, 4158. Copyright 2003 by The Royal Society of Chemistry.

The [Fe]H_2ase is remarkable in its efficiency for H_2 production. As in the [NiFe]H_2ase, [Fe]H_2ase is outfitted with a series of iron-sulfur clusters that connect the active site to the electron donor/acceptor protein docked into the periphery of the redox-active enzyme. The active site of [Fe]H_2ase in the reduced form has an available coordination position on the distal iron,[5a] the iron that is further removed from the [4Fe4S] cluster, that may be occupied by H_2 or H^-, Figure IV-1, dependent on the direction of reactivity. The spectroscopically-supported oxidation state assignment of this diamagnetic, reduced form of the enzyme is Fe^IFe^I.[42,43] This apparent open site in the reduced form of the enzyme is occupied by a labile H_2O molecule in the oxidized, mixed-valent $Fe^{II}Fe^I$ redox level [42-44] that is responsible for H_2 binding and activation.

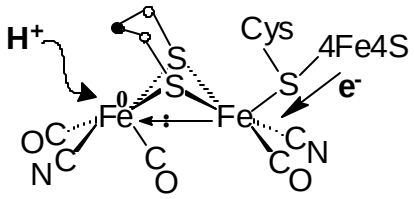

Fig. IV-1 Representation of [Fe]hydrogenase active site in the reduced form and its role in H^+/e^- uptake.

Compositional/structural models which serve as spectroscopic reference points for the active site of [Fe]H_2ase can be readily accessed from $(\mu\text{-}S_2)Fe_2(CO)_6$ (see Equation III-2);[26] Strong acids protonate the $(\mu\text{-SRS})[Fe(CO)_2PMe_3]_2$ complexes, generating the cationic bridging hydride species, $(\mu\text{-H})(\mu\text{-SRS})[Fe(CO)_2PMe_3]_2^+$.[7e,45]

Derivatives in the form of (μ-E)(μ-pdt) $[Fe^{II}(CO)_2PMe_3]_2^+$ (E = H, SMe; pdt = $SCH_2CH_2CH_2S$) have demonstrated ability to promote the same isotopic scrambling reaction[7e,8,46] as used in activity assays for the enzyme, Equation IV-1.

$$H_2 + D_2O \leftrightarrows HD + HOD \qquad \text{(IV-1)}$$

Key to this functional biomimicry is the requirement of light which generates an open site necessary for η^2-H_2 binding to d^6 Fe^{II} complexes.[47] Thus the binuclear $(\eta^2\text{-}H_2)Fe^{II}Fe^{II}$ intermediate in these H_2ase-like activity studies mimics the $(\eta^2\text{-}H_2)Fe^{II}$ interaction of the distal iron of the oxidized form of the enzyme proposed to be in a mixed-valent $Fe^{II}Fe^{I}$ redox level.[42-44]

The quest for H_2 production by synthetic analogues must balance proton source (acid strength) and reduction potential (electron availability or "strength"), with the ultimate goal of finding catalysts that facilitate mild conditions of both proton and electron sources. To achieve this, knowledge of the molecular process(es), including the factors that influence the stability of Fe^0Fe^I radical anions, of the hydrogenic species, Fe^{II}-H or $Fe^{II}(\varsigma^2\text{-}H_2)$ and the barriers to their formation, are critical issues to be addressed.

A mixed ligand system, (μ-pdt) $[Fe(CO)_2PMe_3][Fe(CO)_2CN]^-$ was reported by Rauchfuss *et al.*, to evolve hydrogen at a potential of –1 V in the presence of strong acids.[12,45] The exact order of the uptake of two protons and two electrons by the catalysts has not been established, but most certainly involves initial protonation of the cyanide ligand.

In order to provide evidence for the proposed H_2-production activity, a series of $(\mu\text{-SRS})[Fe^{I}(CO)_2L]_2$, (L = CO, PR_3), complexes were used to explore the potential of these structural models for H_2 production. Based on this particular dinuclear system, modifications can be made in the substituent ligand to improve hydrophilicity, and possibly water solubility, as well as to test the effect of complex charge on the redox potential.

The use of 1,3,5-triaza-7-phosphaadamantane, PTA, as a ligand in transition metal complexes emerged from the interest to have metal catalysts soluble in water. In addition to the benefits of working in a more environmentally friendly solvent, this property is expected to improve product/catalyst separation and the catalyst recovery process. Different moieties, for example sulfonate, carboxylate, and phosphonate, have been used to functionalize tertiary phosphines that then engender water solubility to transition metal-based catalysts.[48] An alternative to sulfonated phosphines is the PTA ligand. PTA is a small, basic ligand that has very similar donor and steric properties to PMe_3 (cone angle of PTA = 102°; PMe_3 = 118°). It is a multifunctional ligand that binds to transition metals through the phosphorus atom leaving nitrogen for reactions with electrophiles, including H-bonding interactions with protic solvents or water. PTA itself is water-soluble and it enhances H_2O-solubility of organometallic complexes. However, complete water solubility is only achieved with a sufficient number of PTA ligands bound to the metal; typically more than two are required for mononuclear complexes.[49]

A detailed electrochemical study of the $Fe^{I}Fe^{I}$ dithiolate models and the electrocatalytic H_2 production at the $Fe^{0}Fe^{I}$ and $Fe^{0}Fe^{0}$ redox level in the presence of a weak acid is discussed in this chapter. The ligand modification effects have been approached with the complexes (μ-pdt)$[Fe(CO)_3][Fe(CO)_2PTA]$, and (μ-pdt)$[Fe(CO)_2PTA]_2$, (PTA = 1,3,5-triaza-7-phosphaadamantane = $P(CH_2)_6N_3$), and protonated and methylated derivatives, $\{(\mu\text{-pdt})[Fe(CO)_2(PTA\text{-}H)]_2\}(PF_6)_2$ and $\{(\mu\text{-pdt})[Fe(CO)_2(PTA\text{-}Me)]_2\}(OTf)_2$, (OTf = CF_3SO_3).

Results and Discussion

Electrochemical studies were performed in collaboration with Dr. Daesung Chong, a postdoctoral fellow in our group in 2001-2003, and with the helpful advice of Dr. Manuel Soriaga. Some of the compounds used in such studies were prepared by other members of the group, as follows: (μ-edt)$[Fe(CO)_3]_2$, and (μ-edt)-$[Fe(CO)_2PMe_3]_2$, (edt = SCH_2CH_2S), by Chao-Yi Chiang; (μ-pdt) $[Fe(CO)_3]_2$, (μ-pdt)$[Fe(CO)_2PMe_3]_2$, (pdt = $SCH_2CH_2CH_2S$), (μ-o-xyldt) $[Fe(CO)_3]_2$, (μ-o-xyldt)$[Fe(CO)_2PMe_3]_2$, (o-xyldt = $SCH_2C_6H_4CH_2S$), by Dr. Irene Georgakaki (PhD, TAMU 2002). The synthesis and characterization of the new compounds prepared within the scope of this research project will be presented first, followed by electrochemical studies on (μ-SRS)$[Fe(CO)_3]_2$ and (μ-SRS)$[Fe(CO)_2PMe_3]_2$ complexes, and studies on electrocatalytical H_2 production by PTA-derivatives of (μ-pdt)$[Fe(CO)_3]_2$.

Synthesis and Characterization of (μ-pdt)$[Fe(CO)_2PTA]_2$ and (μ-pdt)-$[Fe(CO)_2PTA][Fe(CO)_3]$

The PTA ligand was dissolved in MeOH and added to a solution of (μ-pdt)$[Fe(CO)_3]_2$, in CH_3CN in a stoichiometric ratio of 2:1. Following reflux (ca. 70 °C) for 24 h, the ν(CO) infrared spectrum of the resultant red-orange solution indicated almost complete conversion of the hexacarbonyl parent compound (CH_3CN solution spectrum: 2074(m), 2034(vs), 1999(s) cm^{-1}) to the disubstituted (μ-pdt)$[Fe(CO)_2PTA]_2$, (1986(w), 1953(s), 1907(m) cm^{-1}). A reddish orange solid was obtained after evaporating the solvent and washing the residue with hexanes. At a lower temperature (ca. 40 °C for 20 h), the same solvent system and reagent ratio led to the mono-substituted product in >85% yield. The mixture components, (μ-pdt)$[Fe(CO)_3]_2$ (ca. 5-10%) and (μ-pdt)$[Fe(CO)_2PTA]_2$ (5 to 10%), were separated from (μ-pdt)$[Fe(CO)_2PTA][Fe(CO)_3]$ by silica gel column chromatography, eluting them using hexane first, followed by THF. The mono-substituted derivative was obtained as a solid after evaporating the solvent. While the IR spectrum of each chromatographic band presented the expected ν(CO) bands (both in pattern and stretching frequencies), elemental analysis and ^1H NMR of (μ-pdt)$[Fe(CO)_2PTA][Fe(CO)_3]$ indicated that an unidentified impurity(ies) was(were) present, probably due to some interaction of the nitrogen atoms of PTA throughout the column. Nevertheless, the ^{31}P NMR spectrum indicated the presence of only one P-containing species with the expected chemical shift, -18.4 ppm in CD_3CN (85% H_3PO_4 as external reference), as compared to the chemically pure disubstituted complex (μ-pdt)$[Fe(CO)_2PTA]_2$ (δ -17.8 ppm) , obtained

as described above. Efforts made to identify the source and identity of this impurity were unsuccessful.

Both (μ-pdt)[$Fe(CO)_2PTA]_2$ and (μ-pdt)[$Fe(CO)_2PTA$][$Fe(CO)_3$] are air and thermally stable, in contrast to the mildly air sensitive (μ-pdt)[$Fe(CO)_2PMe_3]_2$ complex.[7e] The PTA derivatives are very soluble in THF and CH_2Cl_2; they are soluble in acetone, MeOH and CH_3CN. Their solubility in pure water is limited, however solubility is good in H_2O/organic solvent mixtures.

Crystal of suitable quality to perform X-ray analysis grew after several days at –5 °C from a layered methanol-hexane solution of (μ-pdt)[$Fe(CO)_2PTA]_2$, and from a concentrated THF solution of (μ-pdt)- [$Fe(CO)_2PTA$][$Fe(CO)_3$]. These complexes crystallize in solvate-free forms in the P2(1)/n and P2(1)/c space groups, respectively, each with four molecules per unit cell. Crystallographic data are presented in Table IV-1, and selected metric data are compared in Table IV-2. A complete listing of distances and angles from the CIF file is given in the Appendix.

Shown in Figure IV-2 as thermal ellipsoid plots, the solid state structures find the PTA ligands in the basal positions of the thiolate-edge-bridged, square pyramidal iron species. As in other (μ-pdt)[$Fe(CO)_2L]_2$, L = PMe_3 and PMe_2Ph, the PTA ligands of (μ-pdt)[$Fe(CO)_2PTA]_2$ are transoid to each other.[7e,8] This arrangement minimizes ligand-ligand steric interactions and with the propane-dithiolate bridge. The Fe-Fe distance of 2.5535 (6) Å in (μ-pdt)[$Fe(CO)_2PTA]_2$ is indistinguishable from that in (μ-pdt)[$Fe(CO)_2PMe_3]_2$ and there are no other differences of note in the metric

Table IV-1. X-ray Crystallographic Data for Complexes (μ-pdt)-[Fe(CO)$_2$PTA][Fe(CO)$_3$], and (μ-pdt)[Fe(CO)$_2$PTA]$_2$

	(μ-pdt)[Fe(CO)$_2$PTA]-[Fe(CO)$_3$][a]	**(μ-pdt)[Fe(CO)$_2$PTA]$_2$**[b]
Empirical formula	$C_{14}H_{18}Fe_2N_3O_5PS_2$	$C_{19}H_{30}Fe_2N_6O_4P_2S_2$
Formula weight (g mol^{-1})	515.10	644.25
Crystal system	Monoclinic	Monoclinic
Space group	P2(1)/n	P2(1)/c
Unit cell		
a(Å)	11.8502(16)	12.8193(10)
b(Å)	12.4174(18)	24.0187(19)
c(Å)	13.1985(18)	8.4330(7)
α(deg)	90	90
β(deg)	94.424(8)	105.5690(10)
γ(deg)	90	90
Volume (Å)^3	1936.4(5)	2501.3(3)
Z	4	4
d_{calc}, (g cm^{-3})	1.767	1.711
Absolute coefficient (mm^{-1})	15.107	1.495
RI[c] [I>2σ(I)]	0.0657	0.0555
wR2[d]	0.1346	0.1303
Goodness-of-fit on F^2	0.907	1.099

[a] Obtained using graphite-monochromatic Cu Kα radiation (λ = 1.54178 Å) at 110(2) K. [b] Obtained using graphite-monochromatic MoKα radiation (λ = 0.71073 Å) at 110(2) K. [c] RI = Ó||F$_o$| - |F$_c$||. [d] wR2 = [Ó[w(F$_o^2$ – F$_c^2$)^2]/ Ów(F$_o^2$)^2]]^{½}.

Table IV-2. Selected Metric Data for Binuclear Iron Phosphino Complexes

	(μ-pdt)-[Fe(CO)$_2$PMe$_3$]$_2$[16]	**(μ-pdt)[Fe(CO)$_2$PTA]-[Fe(CO)$_3$]**	**(μ-pdt)-[Fe(CO)$_2$PTA]$_2$**
Fe-Fe (Å)	2.555(2)	2.542(2)	2.5535(6)
Fe-P	2.234(3)[a]	2.215(3)	2.2139(9)[a]
Fe-$C_{CO,ap}$[b]	1.772(9)	1.789(12)	1.776(4)
Fe-$C_{CO,ba}$	1.742(10)	1.757(11)[c]	1.764(4)
Fe-$S_{\mu\text{-}SR}$[d] (Å)	2.254(2)	2.264(3)	2.258(9)
Fe disp[e] (Å)	0.376	0.395	0.389
S···S	3.026	3.050	3.051
dihedral (deg)[f]	109.2	108.4	106.8
Fe-S-Fe (deg)	69.06(8)	68.29(9)	68.85(3)
S-Fe-S α(deg)	84.34(11)	84.66(10)	84.98(3)

[a] Average of two Fe-P_{ba} bonds. [b] Average of two Fe-$C_{CO,ap}$ bonds. [c] Average of three Fe-$C_{CO,ba}$ bonds. [d] Average of four Fe-$S_{\mu\text{-}SR}$ bonds. [e] Fe disp = Displacement of Fe from best plane of $S_2L_{2(ba)}$ toward L_{ap}. [f] Defined by the intersection of the two Fe_2S planes.

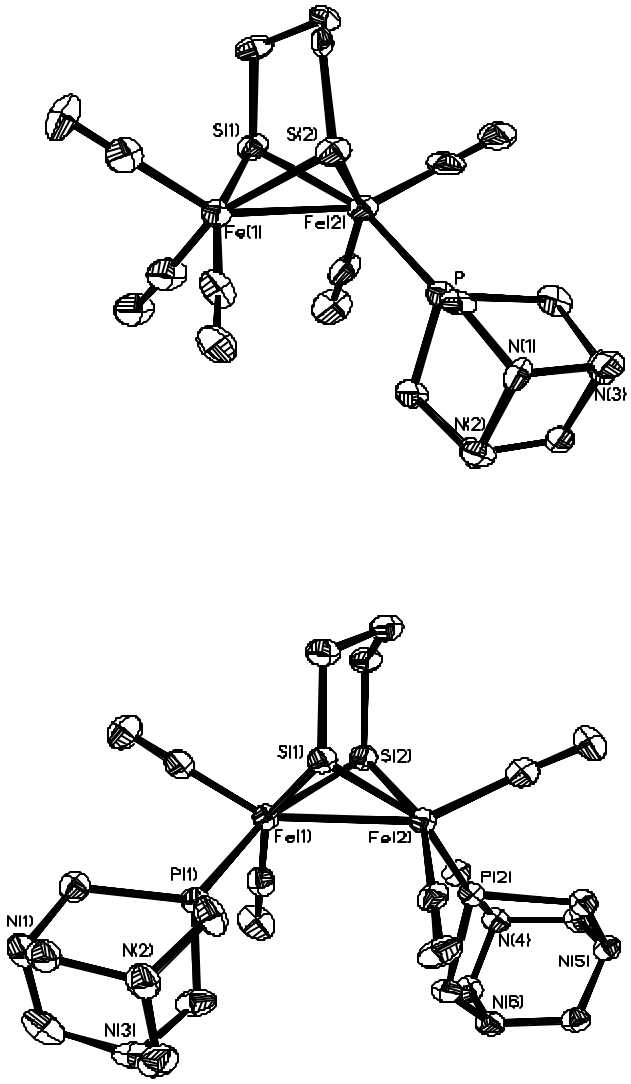

Figure IV-2. Thermal ellipsoid representations (50% probability) of the molecular structures of (a) (μ-pdt)[$Fe(CO)_3$][$Fe(CO)_2$(PTA)], and (b) (μ-pdt)[$Fe(CO)_2$(PTA)]$_2$.

parameters, Table IV-2. The solid-state X-ray structure finds that the boat form of the $Fe_2S_2C_3$ ring is on the $Fe(CO)_2PTA$ side of the asymmetric diiron species. The pseudo-square pyramidal geometry about the iron atoms results in displacement of iron out of the best basal planes and towards the apical carbonyl. The average Fe_{displ} value for both (μ-pdt)$[Fe(CO)_2PTA]_2$ and (μ-pdt)$[Fe(CO)_2PTA][Fe(CO)_3]$ is 0.39 Å, with a 0.06 Å difference between the maximum and minimum Fe_{displ} values for the two irons of (μ-pdt)$[Fe(CO)_2PTA][Fe(CO)_3]$ and 0.03 Å for (μ-pdt)$[Fe(CO)_2PTA]_2$. The iron atoms in the parent compound, (μ-pdt)$[Fe(CO)_3]_2$, are displaced of the best basal plane 0.38 Å.[7a]

The ^1H NMR spectrum of (μ-pdt)$[Fe(CO)_2PTA][Fe(CO)_3]$ indicates rapid intramolecular proton site exchange in the propane dithiolate C_3H_6 unit at room temperature. That is, there is magnetic equivalence of axial and equatorial protons due to the fluxionality of the bridge (see Figure V-1 and text in Chapter V). Similarly, the ^{13}C NMR shows intramolecular CO site exchange at the $Fe(CO)_3$ units. The room temperature spectrum (23 °C) presents one resonance, a doublet at 214.7 ppm (downfield from TMS), J_{P-C} = 16.4 Hz, while there are four distinct resonances at –80 °C: a singlet at 212.1 ppm, a singlet at 212.9 ppm, a doublet at 215.8 ppm (J_{P-C} = 27.1), and a doublet at 216.6 ppm (J_{P-C} = 27.1), indicating the magnetic non-equivalence of the four CO ligands at the stopped exchange region (site exchange processes taking place within the NMR time scale in diiron thiolate complexes will be further discussed in Chapter V).

Donor Ability of PTA and Reactions of Diiron Derivatives with Acids

The 3-band patterns in the ν(CO) IR spectra for the complexes (μ-pdt)[Fe(CO)$_2$PMe$_3$]$_2$ and (μ-pdt)[Fe(CO)$_2$PTA]$_2$ are nearly identical. The somewhat poorer donor ability of the PTA ligand is indicated by an average shift of 9 cm^{-1} to higher frequencies in (μ-pdt)[Fe(CO)$_2$PTA]$_2$ as compared to (μ-pdt)[Fe(CO)$_2$PMe$_3$]$_2$. Both complexes react with excess hydrochloric acid resulting in ionic salts that are obtained as precipitates upon Cl$^-$/PF$_6^-$ ion exchange. Figure IV-3 presents aspects of the IR monitor of these reactions. For (μ-pdt)[Fe(CO)$_2$PMe$_3$]$_2$ the ν(CO) values of the neutral compound are shifted to higher values by ca. 70 cm^{-1} indicating a drastic change in electron density about iron, consistent with the binuclear oxidative addition of a proton. The resultant bridging hydride complex, Fe^{II}(μ-H)Fe^{II}, has been thoroughly characterized by X-ray crystal structure and multi-nuclear NMR analyses.[7e,8] For the (μ-pdt)[Fe(CO)$_2$PTA]$_2$ complex, the ν(CO) band pattern of the protonated derivative, {(μ-pdt)[Fe(CO)$_2$(PTA-H)]$_2$}$^{2+}$, is identical to that of the neutral parent compound and the ν(CO) values are shifted by only 17 cm^{-1} on average. The small shift of the latter is consistent with ligand-based protonation as expected for the exposed tertiary nitrogen atoms on the PTA ligands.[49] Confirming this conclusion is ^{1}H NMR spectral data which shows lack of a high field signal (δ -15 to –17.5 ppm for Fe^{II}(μ-H)Fe^{II} complexes),[8] and ^{31}P NMR spectral data, which shows the expected downfield shift for the phosphorus of the iron-bound ligand, from δ -17.8 ppm in the

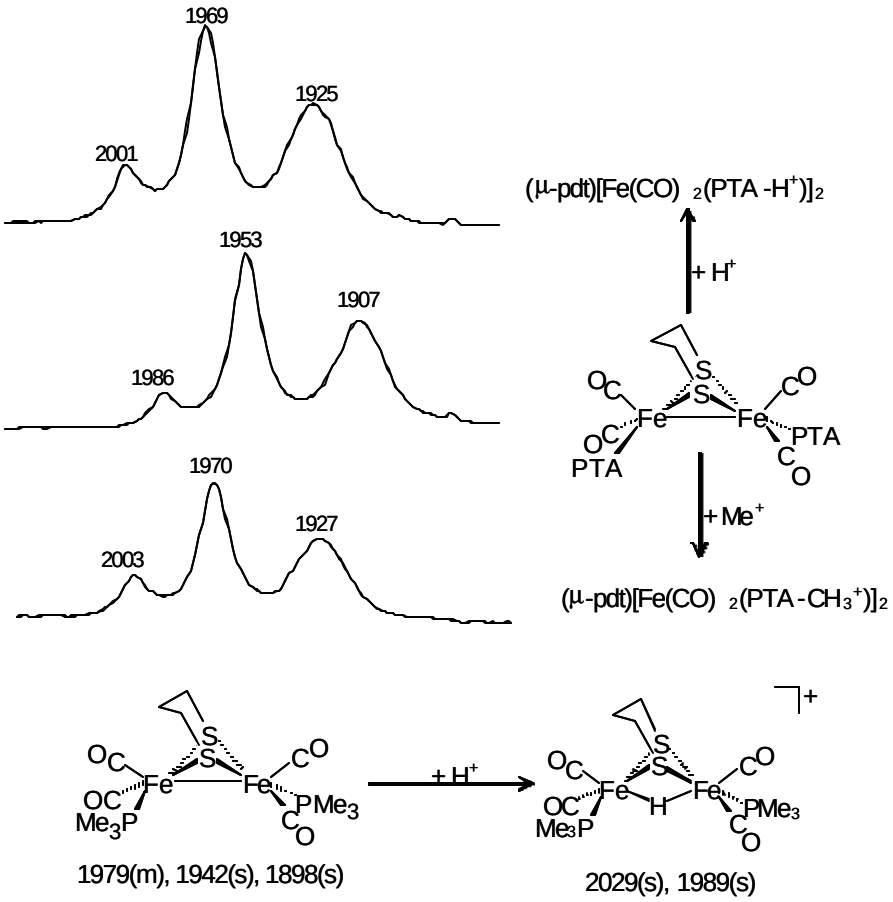

Figure IV-3. Infrared spectra (ν(CO) region, CH_3CN solution) demonstrating ligand-based reactivity of (μ-pdt)[$Fe(CO)_2PTA]_2$ with electrophiles *versus* binuclear oxidative addition of H^+ to Fe^I-Fe^I in (μ-pdt)[$Fe(CO)_2PMe_3]_2$.

neutral (μ-pdt)[Fe(CO)$_2$PTA]$_2$ complex to δ -3.9 ppm in the diprotonated derivative. Also supporting the assignment to a diprotonated species are conductivity measurements in 1.5 mM solutions in CH_3CN, Λ_M = 263 ohm^{-1} cm^2 mole^{-1}, which is within the range of a 3-ion system,[50] and consistent with the formulation {(μ-pdt)-[Fe(CO)$_2$(PTA-H)]$_2$}(PF$_6^-$)$_2$. Similar values were obtained for the product isolated from methylation of (μ-pdt)[Fe(CO)$_2$PTA]$_2$ with excess Me^+OTf^- (Λ_M = 275 ohm^{-1} cm^2 mole^{-1}, ^{31}P NMR δ 1.68 ppm).

Electrochemical Studies of (μ-SRS)[Fe^I(CO)$_2$L]$_2$, (L = CO, PMe$_3$) Complexes

The series of diiron dithiolates used in the first part of this study is given in Table IV-3 along with infrared data in the CO stretching region. While the three-band ν(CO) pattern in the IR is similar for each of the all-CO species, differences arise for the phosphine-substituted series which depend on the positions of the PMe_3 ligands.[8] Reflecting the electron-donating ability of the phosphines (which is similar to cyanides), the average ν(CO) value is ca. 100 cm^{-1} lower in the PMe_3-substituted complexes as compared to the all-CO complexes. The ν(CO) infrared spectral values within the all-CO and the PMe_3-substituted subsets show no significant differences for the μ-SRS derivatives, however the μ-SEt complexes appear to have slightly lower ν(CO) values in each subset, Table IV-3.

Table IV-3. Listing of ν(CO) Infrared and Electrochemical Parameters[a] for (μ-SRS)$[Fe(CO)_2L]_2$ and $(\mu\text{-}SR)_2[Fe(CO)_2L]_2$ Complexes in CH_3CN.

L = CO	ν(CO), cm^{-1}	E_{pc} vs NHE, V E_1 : $Fe^IFe^I \rightarrow Fe^0Fe^I$ (E_2 : $Fe^0Fe^I \rightarrow Fe^0Fe^0$)	E_{pa} vs NHE, V $Fe^IFe^I \rightarrow Fe^{II}Fe^I$
$(\mu\text{-}SEt)_2$	2073 (m), 2034 (vs), 1992 (s)	-1.31 (-1.94)	1.18
(μ-edt)	2087 (m), 2038 (vs), 1997 (s)	-1.30 (-1.84)	1.29
(μ-pdt)	2074 (m), 2036 (vs), 1995 (s)	-1.34 (-1.95)	1.14
(μ-*o*-xyldt)	2076 (m), 2040 (vs), 1999 (s)	-1.16 (-1.81)	1.20
L = PMe_3			
$(\mu\text{-}SEt)_2$	1977 (s), 1931 (m), 1908 (s)	-1.91	0.27
(μ-edt)	1982 (s), 1944 (s), 1908 (s), 1896 (m,br)	-1.87	0.34
(μ-pdt)	1979 (m), 1942 (s), 1898 (s)	-1.85	0.34
(μ-*o*-xyldt)	1983 (m), 1948 (s), 1903 (s)	-1.80	0.35

[a]CH_3CN solution (0.1 M *n*-Bu_4NBF_4) with a glassy carbon working electrode (A = 0.071 cm^2) to NHE using Cp_2Fe/Cp_2Fe^+ standard ($E_{1/2}$ = 0.40 V). Counter electrode: Pt. Scan rate: 0.2 Vs^{-1}. SRS: μ-edt = SCH_2CH_2S, μ-pdt = $SCH_2CH_2CH_2S$, μ-*o*-xyldt = $SCH_2\text{-}C_6H_4\text{-}CH_2S$.

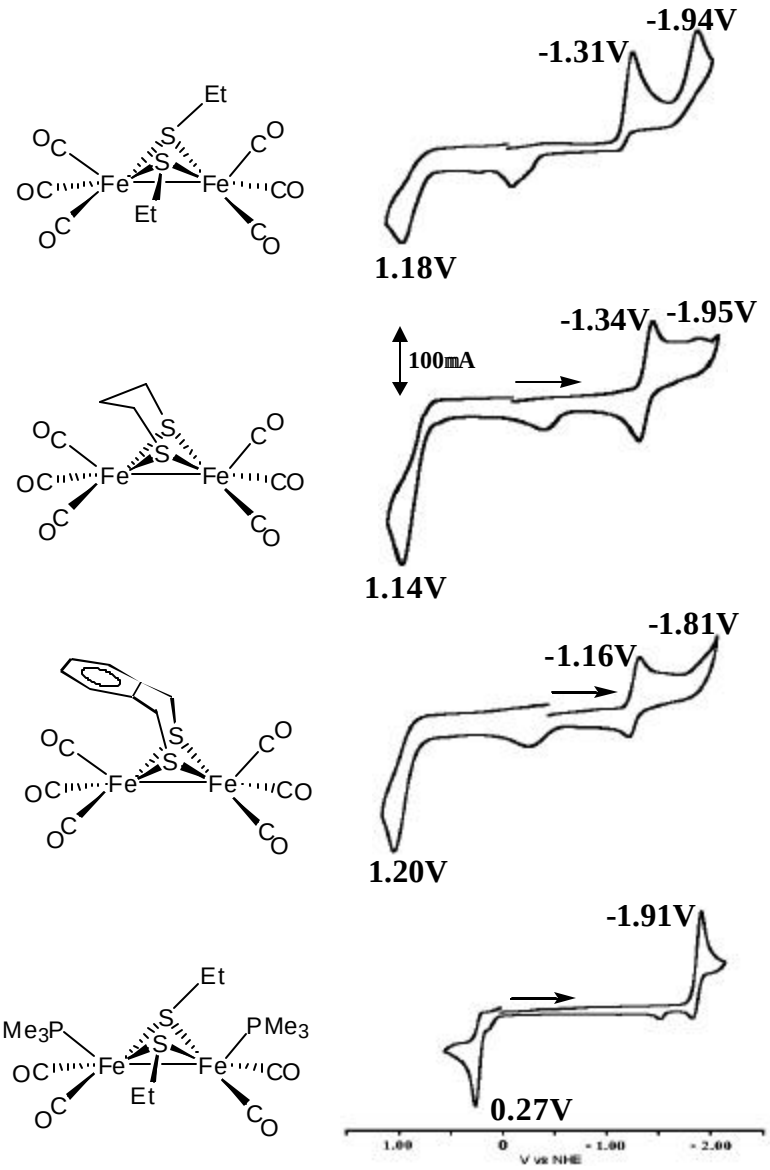

Figure IV-4. Cyclic voltammograms of a series of $Fe^{I}Fe^{I}$ dithiolate complexes in CO-saturated CH_3CN solution (0.1 M *n*-Bu_4NBF_4) with electrochemical parameters as described in Table IV-3.

The cyclic voltammograms shown in Fig. IV-4 were recorded in CO-saturated CH_3CN solution; they were initiated from the rest potentials and proceed as indicated in the cathodic direction. The all-CO species display two reduction events that are typical of all members of the series. A quasi-reversible or electrochemically irreversible reduction (E_1) is observed for the all-CO species in the range of -1.16 to -1.34 V, in agreement with the values obtained by Pickett and co-workers,[51] and an irreversible event (E_2) in the range of -1.81 to -1.95 V.

The assignment of the first event to a one-electron reduction process $Fe^IFe^I + e^- \rightarrow Fe^IFe^0$ is supported by bulk electrolysis and IR data described below. The second reduction event is proposed to correspond to the $Fe^IFe^0 + e^- \rightarrow Fe^0Fe^0$ process. The PMe_3-derivatives show one reduction event at ca. -1.9 V that is assigned to the one-electron reduction of Fe^IFe^I to Fe^IFe^0. Its appearance at more negative potentials than that corresponding to the all-CO complexes is consistent with the better donor character of the PMe_3 ligand relative to CO. At room temperature, controlled-potential coulometry of all complexes at each cathodic peak potential in the absence of added acid shows net consumption of about 0.95 electron per molecule. The peak current of these reduction events is proportional to the square root of the scan rate (50-1000 mV s^{-1}), which indicates that the electrochemical processes are diffusion-controlled.[52]

Also observed for each member of the series is an irreversible anodic or oxidative event which is displaced positively by ca. 2.2 - 2.6 V from the E_1 cathodic feature for all species, Fig. IV-4. As expected, the PMe_3 derivatives destabilize the Fe^IFe^0 form and stabilize the Fe^IFe^{II} as compared to the all-CO parent species.

Spectroelectrochemistry. The E_1 process $Fe^IFe^I \rightarrow Fe^IFe^0$ for complex $(\mu\text{-}SEt)_2[Fe(CO)_3]_2$ is supported by spectroelectrochemical monitors using a ReactIR™ for *in situ* infrared monitoring of solutions during the course of bulk electrolysis (Figs. IV-5-II, and IV-6). For example, electrolysis of a CO-saturated CH_3CN solution of $(\mu\text{-}SEt)_2[Fe(CO)_3]_2$ at an applied potential of -1.34 V over the course of 4 h resulted in a loss of intensity of the three ν(CO) IR bands of the neutral complex (2073, 2034, and 1992 cm^{-1}, Fig. IV-6a with growth of bands at 1999, 1949, 1966, and 1922 cm^{-1}, Fig. IV-6b. On anodic electrolysis at -0.95 V the original IR spectrum was regenerated along with a minor amount of a species with infrared bands at 2115 and 1953 cm^{-1} (Fig. IV-6a'). While the structure of the one-electron reduced species is not known, that it is an anion of similar structure to that of the neutral starting material is a reasonable conclusion based on the IR spectral changes. Furthermore, the EPR spectrum (Fig. IV-6c) of a sample withdrawn from this solution displays an axial EPR signal ($g_\perp$ = 2.117 and g = 1.994) indicative of an odd-electron species (Fe^IFe^0). On addition of acid to the reduced species the EPR signal disappears and the starting complex is reclaimed. The reversible chemical behavior is incongruent with the observed irreversible electrochemical response of the complex $(\mu\text{-}SEt)_2[Fe(CO)_3]_2$ at the $Fe^IFe^I \rightarrow Fe^IFe^0$ reduction event.

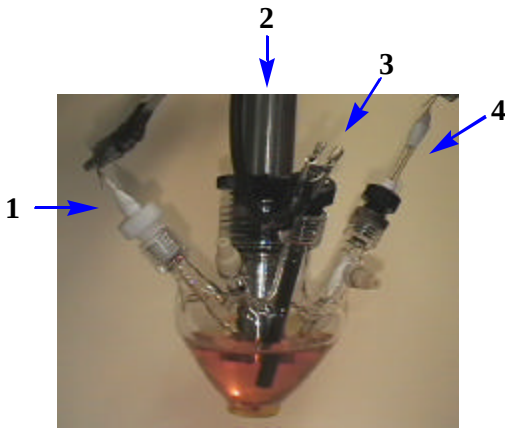

(I)

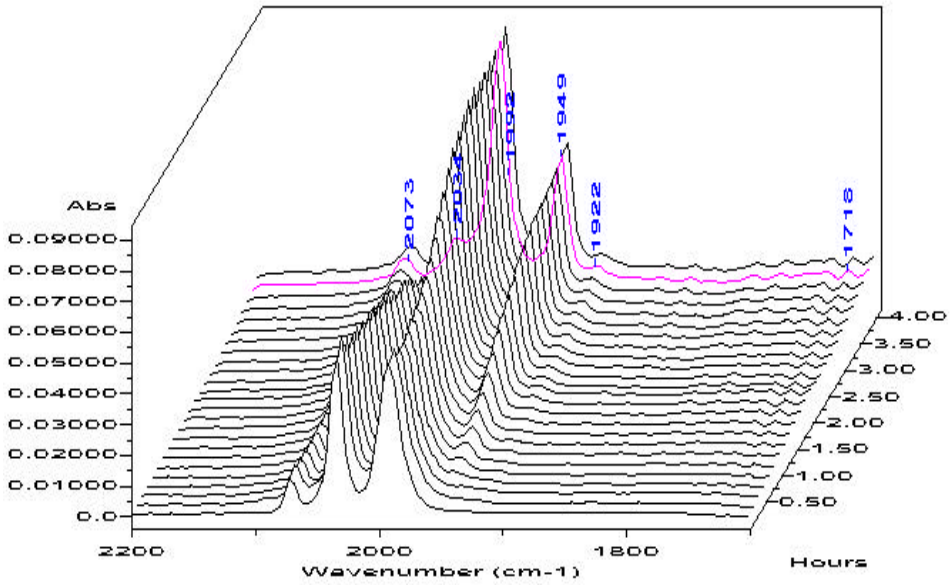

(II)

Figure IV-5. (I) The *in situ* IR/Electrochemical cell: 1) reference electrode (Ag/Ag^{+}), 2) *in situ* IR probe (ReactIR^{TM}), 3) working electrode (carbon rod), and 4) counter electrode (Pt); and (II) sample stacked plot IR spectra for the reduction process at -1.34 V of complex $(\mu\text{-SEt})_2[Fe(CO)_3]_2$ (7.5 mM).

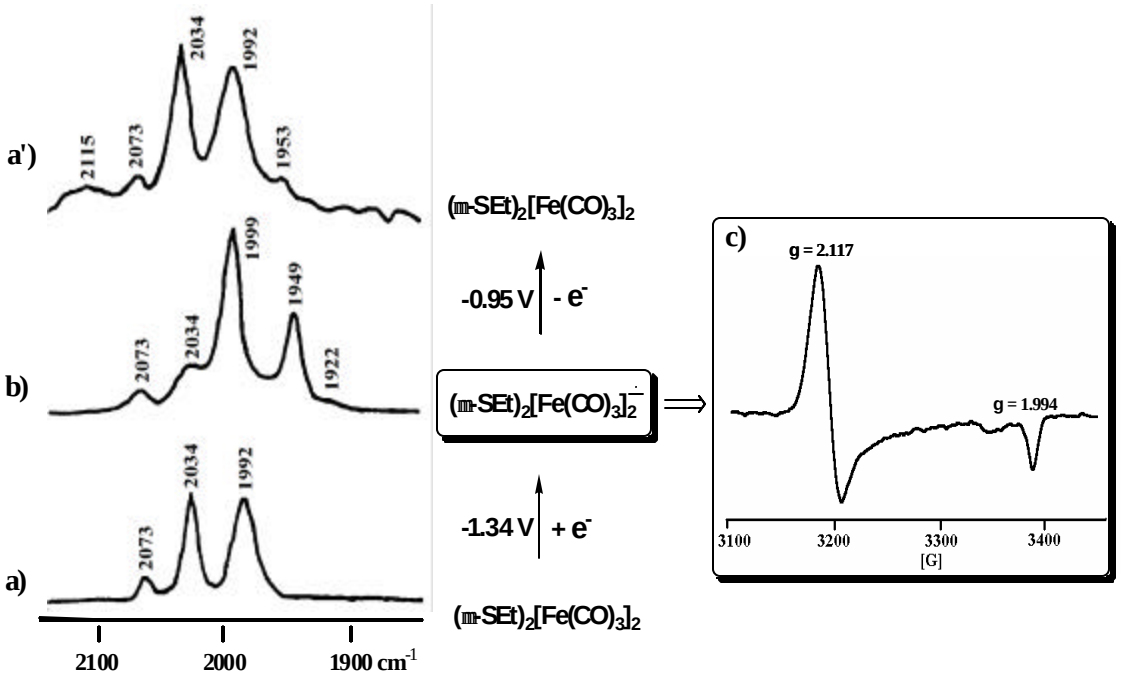

Figure IV-6. *In situ* IR spectra during bulk electrolysis for $(\mu\text{-SEt})_2[Fe(CO)_3]_2$ (7.5 mM). a) neutral starting complex, b) following reduction (E_{app} = -1.34 V), a') re-oxidation (E_{app} = -0.95 V) in 0.1 M *n*-Bt_4NBF_4 solution in CH_3CN and c) EPR spectrum of a sample from b).

Electrocatalysis of H_2 production. Controlled-potential electrolyses were performed in an H-type cell with a rod type glassy carbon electrode (A = 3.34 cm^2). Under the same conditions, acetic acid in CH_3CN (pK_a = 22.6)[53] is reduced at a potential of -2.2 V. For the all-CO complexes, the current height of the first redox wave (E_1 = –1.2 ± 0.1 V, Figure IV-7a-(I)) shows a slight increase with added increments of acid while the second redox wave (E_2 = –1.9 ± 0.05 V, Fig. IV-7a-(II)) shows a significant electrocatalytic response. The current height of the single cathodic event at ca. –1.85 ± 0.05 V of the PMe_3-derivatives increases linearly with the concentration of acetic acid, Figs. IV-7 and IV-8. The steeper slope displayed by the PMe_3-derivative, $(\mu\text{-}SEt)_2[Fe(CO)_2PMe_3]_2$, Figure IV-8, is indicative of its greater sensitivity to acid concentration compared to the all-CO complex $(\mu\text{-}SEt)_2[Fe(CO)_3]_2$. This is consistent with a more stable reaction intermediate of the PMe_3 complex, presumably H-Fe^{II}. The electrolysis of complexes $(\mu\text{-}SEt)_2[Fe(CO)_3]_2$, and $(\mu\text{-}SEt)_2[Fe(CO)_2PMe_3]_2$, at –1.96 V, and -1.93 V, respectively, in the presence of acetic acid (100 mM) for 1 h consumes 12 (*ca.* 6 turnovers per hour), and 34 (ca. 17 turnovers per hour), electrons per molecule, respectively.

The gas which evolved during electrolysis was directed into an NMR tube, purging the *d*-CH_2Cl_2 solvent for 20 min. The ^1H NMR spectrum of this sample showed one resonance at 4.61 ppm for dissolved H_2.[7e,8] A reasonable conclusion is that electrochemical reduction of the diiron complexes initiates the electrocatalysis, followed by protonation of the reduced iron center to produce H_2.

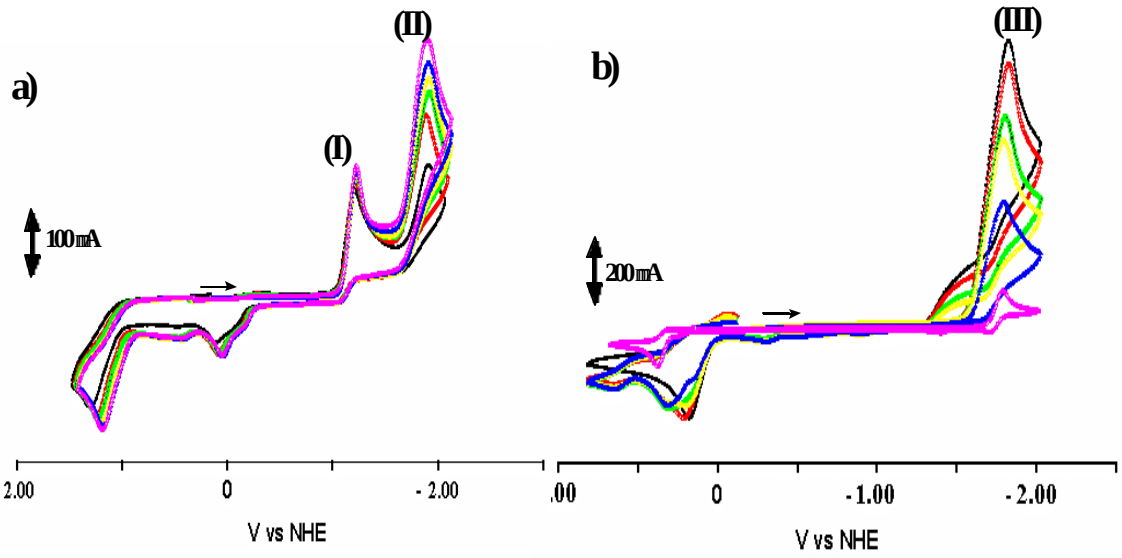

Figure IV-7. Cyclic voltammograms of a) complex $(\mu\text{-SEt})_2[Fe(CO)_3]_2$ (2.5 mM) with HOAc (0-100 mM), and b) $(\mu\text{-SEt})_2[Fe(CO)_2PMe_3]_2$ (2.5 mM) with HOAc (0-100 mM) in 0.1 M *n*-Bu_4NBF_4 in CH_3CN and with electrochemical parameters as described in Table IV-3. (**I**): Fe^IFe^I/Fe^0Fe^I, ca. -1.31 V; (**II**): Fe^0Fe^I/Fe^0Fe^0, ca. -1.94 V; (**III**): Fe^IFe^I/Fe^0Fe^I, ca. -1.91 V.

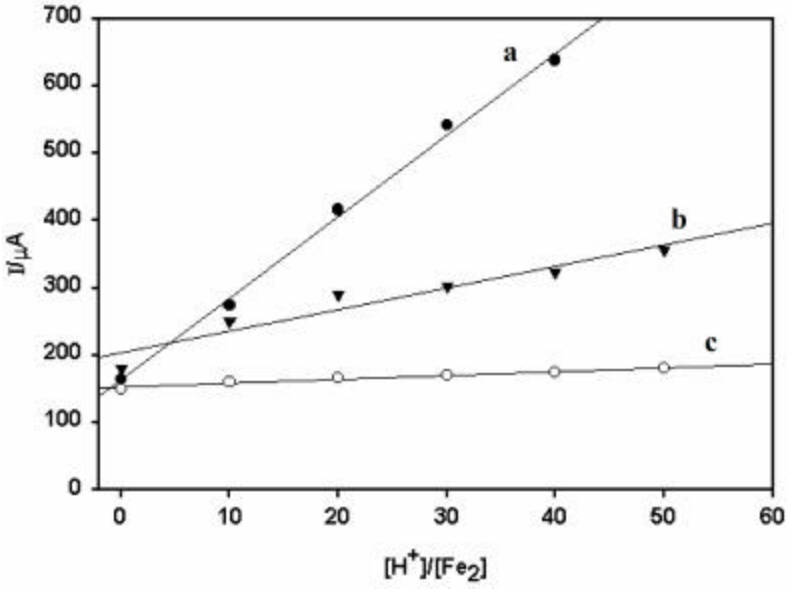

Figure IV-8. Dependence of current heights of electrocatalytic waves on acid concentration. **a**: $(\mu\text{-SEt})_2[Fe(CO)_2PMe_3]_2$ (-1.91 V), **b**: $(\mu\text{-SEt})_2[Fe(CO)_3]_2$ (-1.94 V), and **c**: $(\mu\text{-SEt})_2[Fe(CO)_3]_2$ (-1.31 V).

Electrochemistry of PTA Derivatives of Diiron Complexes, $(\mu\text{-pdt})[Fe(CO)_3][Fe(CO)_2PTA]$, $(\mu\text{-pdt})[Fe(CO)_2PTA]_2$, $\{(\mu\text{-pdt})[Fe(CO)_2(PTA\text{-}H)]_2\}(PF_6)_2$, and $(\mu\text{-pdt})[Fe(CO)_2(PTA\text{-}CH_3)]_2(OTf)_2$

The cyclic voltammograms shown in Figure IV-9 were recorded in CH_3CN solution; they were initiated from the rest potentials and proceed as indicated in the cathodic direction. Complexes $(\mu\text{-pdt})[Fe(CO)_3][Fe(CO)_2PTA]$, $(\mu\text{-pdt})[Fe(CO)_2PTA]_2$, and $\{(\mu\text{-pdt})[Fe(CO)_2(PTA\text{-}Me)]_2\}(OTf)_2$ display an

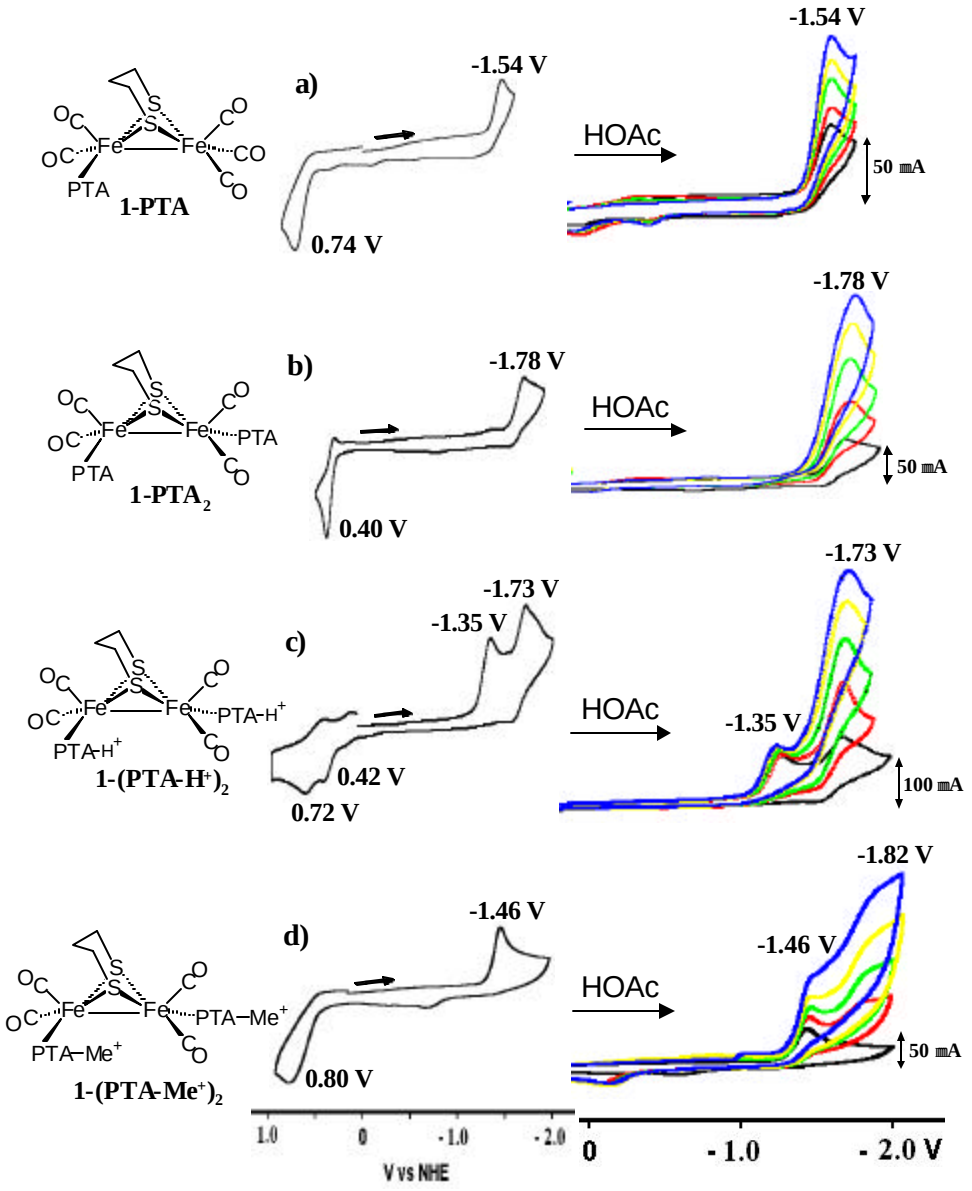

Figure IV-9. Cyclic voltammograms of neutral, and di-cationic complexes, 2.0 mM in a) (μ-pdt)[Fe(CO)$_3$][Fe(CO)$_2$PTA], b) (μ-pdt)[Fe(CO)$_2$PTA]$_2$, c) {(μ-pdt)[Fe(CO)$_2$-(PTA-H)]$_2$}(PF$_6$)$_2$, and d) {(μ-pdt)[Fe(CO)$_2$(PTA-Me)]$_2$}(OTf)$_2$ with HOAc (0, 25, 50, 75 and 100 mM) in CH_3CN solution (0.1 M *n*-Bu_4NBF_4) with electrochemical parameters as described in Table IV-4.

electrochemically irreversible reduction event at –1.54, –1.78, and –1.46 V, respectively. Bulk electrolysis demonstrated these events to be one-electron reduction processes, assigned to the $Fe^{I}Fe^{I} + e^{-} \rightarrow Fe^{I}Fe^{0}$ couple in each, analogous to the all-CO parent complex (μ-pdt)$[Fe(CO)_3]_2$. In comparison to (μ-pdt)$[Fe(CO)_3]_2$, the $Fe^{I}Fe^{I}/Fe^{I}Fe^{0}$ couples of the (μ-pdt)$[Fe(CO)_3][Fe(CO)_2PTA]$ and (μ-pdt)$[Fe(CO)_2PTA]_2$ diiron complexes are negatively shifted, consistent with the increase in electron density about the two-iron core as a CO is replaced by the better donor P-ligand. The positive charge on the methylated-PTA derivative, $\{(\mu\text{-pdt})[Fe(CO)_2(PTA\text{-}Me)]_2\}^{2+}$, results in a smaller shift of the reduction potential; it is only 110 mV more negative than (μ-pdt)$[Fe(CO)_3]_2$. A summary of the reduction potentials in CH_3CN and in CH_3CN/H_2O mixtures is given in Table IV-4.

The doubly protonated PTA complex $\{(\mu\text{-pdt})[Fe(CO)_2(PTA\text{-}H)]_2\}(PF_6)_2$ exhibits two irreversible reduction events at –1.35 and –1.73 V, Figure IV-9 and Table IV-4. The assignment of the first event to a two-electron reduction process, Equation IV-2, with formation of the neutral precursor is supported by coulometry and by *in situ* IR monitoring data as described below.

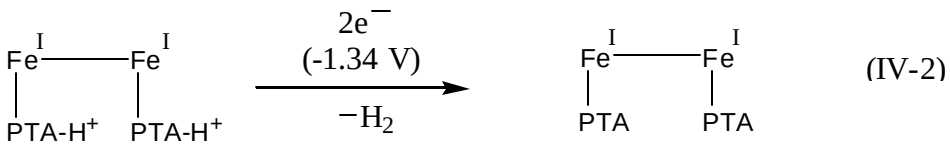

(IV-2)

Table IV-4. Listing of Reduction Potentials[a] for (μ-pdt)[$Fe(CO)_2L]_2$ and (μ-pdt)-[$Fe_2(CO)_5L$] Complexes in CH_3CN and CH_3CN/H_2O at Ambient Temperature.

Complexes	E_{pc} vs NHE, V E : $Fe^IFe^I \rightarrow Fe^0Fe^I$				
	CH_3CN		$CH_3CN:H_2O$, v/v		
	E_1	ton/h[b]	3:1	1:1	1:3
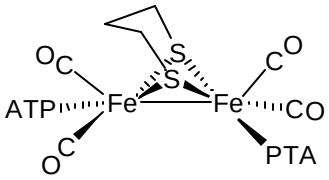	-1.78	16	-1.60	-1.57	-1.53
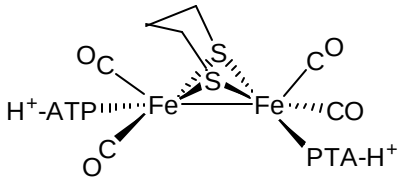	-1.35 -1.73	 21[c]	-1.36 -1.62[e]	-1.34 -1.61	-1.32 -1.59
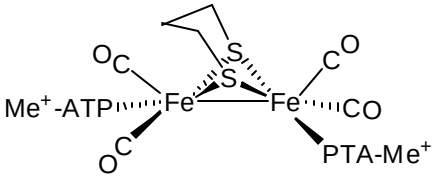	-1.46	10[d]	-1.60	-1.61	-1.59
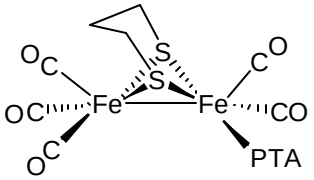	-1.54	7	-1.43	-1.40	-1.38

[a]CH_3CN solution (0.1 M n-Bu_4NBF_4) with a glassy carbon working electrode (A = 0.071 cm^2), referenced to NHE using Cp_2Fe/Cp_2Fe^+ standard ($E_{1/2}$ = 0.40 V).[19] Counter electrode: Pt. Scan rate: 0.2 Vs^{-1}. H_2O solution (0.1 M KCl). μ-pdt = -SCH_2CH_2CHS-. [b]ton = turnovers, ton/h determined as described in text. [c]Determined for the –1.73 V event. [d]Determined for the –1.46 V. [e]ton/h = 44, determined at –1.68 V.

Electrolysis of $\{(\mu\text{-pdt})[Fe(CO)_2(PTA\text{-}H)]_2\}^{2+}$ at an applied potential of –1.47 V found a net consumption of 1.9 electrons per molecule. As the potential of the second cathodic response was identical to the single reductive event of the parent $(\mu\text{-pdt})[Fe(CO)_2PTA]_2$ neutral complex, it was assumed to correspond to $(PTA)Fe^{I}\text{-}Fe^{I}(PTA) + e^{-} \rightarrow (PTA)Fe^{I}\text{-}Fe^{0}(PTA)$; that this reduction was a one-electron process was also confirmed by controlled-potential coulometry.

The *in situ* ReactIR spectroelectrochemical monitor of the infrared spectrum during the course of bulk electrolysis at an applied potential of –1.47 V over the course of 5 h showed a loss of intensity of the three ν(CO) IR bands of the dicationic starting material $\{(\mu\text{-pdt})[Fe(CO)_2(PTA\text{-}H)]_2\}^{2+}$, 1999, 1966, and 1924 cm^{-1}, with growth of bands at 1989, 1960, and 1916 cm^{-1}. While not exact matches, the latter are sufficiently similar to those of the neutral PTA complex, $(\mu\text{-pdt})[Fe(CO)_2PTA]_2$, (1986, 1953, and 1907 cm^{-1}) to conclude the species are the same. The differences in infrared spectra of the electrochemically generated species and the pure compound are assumed to be due to the use of different infrared spectrophotometers to record the IR spectra; a small band at 2040 cm^{-1} is of unknown origin. We note that electrochemical/electrocatalytic studies of the protonated species, isolated as the PF_6^- salt at negative potentials should give identical results as with the neutral $(\mu\text{-pdt})[Fe(CO)_2PTA]_2$ complex. In fact, as will be seen below, electropotential/electrocatalysis values are slightly different for isolated and purified $(\mu\text{-pdt})[Fe(CO)_2PTA]_2$ and that derived electrochemically *in situ* from the $\{(\mu\text{-pdt})\text{-}[Fe(CO)_2(PTA\text{-}H)]_2\}^{2+}$ precursor. Whether these slight differences are significant or

are a measure of the inherent irreproducibility in the electrochemical studies is at present unknown.

Consistent with the spectroelectrochemical changes described above, the cyclic voltammograms of dicationic complex $\{(\mu\text{-pdt})[Fe(CO)_2(PTA\text{-}H)]_2\}^{2+}$ display different electrochemical responses before and after bulk electrolysis at –1.47 V. After bulk electrolysis of the dicationic complex shows only one reduction event remains and its position at –1.75 V is indicative of the neutral complex $(\mu\text{-pdt})[Fe(CO)_2PTA]_2$ (–1.78 V).

Comparison of the cyclic voltammograms of the diprotonated $\{(\mu\text{-pdt})\text{-}[Fe(CO)_2(PTA\text{-}H)]_2\}^{2+}$ with the monoprotonated bistrimethylphosphine analogue, $\{(\mu\text{-}H)(\mu\text{-pdt})[Fe(CO)_2PMe_3]_2\}^{+}$ shows that for the latter, for which protonation is metal based in binuclear oxidative addition, see Figure IV-3, the resultant $Fe^{II}Fe^{II}$ bridging hydride complex, $(\mu\text{-H})(\mu\text{-pdt})[Fe(CO)_2PMe_3]_2^{+}$, shows a quasi-reversible redox process at –1.1 V, assigned to the $Fe^{II}Fe^{II} + e^- \leftrightarrows Fe^{II}Fe^{I}$ redox couple (Figure IV-10b). An irreversible reduction at –1.86 V is similar in position and shape to the single irreversible reduction event at –1.85 V in the neutral PMe_3 complex, $(\mu\text{-pdt})[Fe(CO)_2PMe_3]_2$, (Figure IV-10a). For the latter, the reduction is confidently assigned to $Fe^{I}Fe^{I} + e^- \rightarrow Fe^{I}Fe^{0}$. Hence, we conclude the analogous waves at –1.86 V in solutions of $(\mu\text{-H})(\mu\text{-pdt})[Fe(CO)_2PMe_3]_2^{+}$ and at –1.75 V for $\{(\mu\text{-pdt})[Fe(CO)_2(PTA\text{-}H)]_2\}^{2+}$ are due to the presence of the neutral complexes

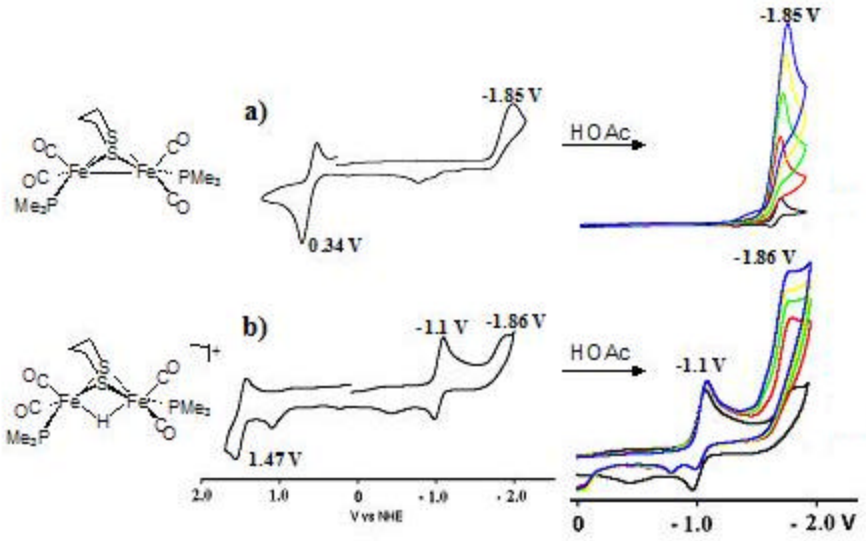

Figure IV-10. Cyclic Voltammograms of neutral and mono-cationic complexes, 2.0 mM, a) (μ-pdt)[Fe(CO)$_3$PMe$_3$]$_2$ and b) {(μ-H)(μ-pdt)[Fe(CO)$_2$PMe$_3$]$_2$}$^+$ with HOAc (0, 25, 50, 75 and 100 mM) in CH_3CN solution (0.1 M *n*-Bu$_4$NBF$_4$) with electrochemical parameters as described in Table IV-4.

(μ-pdt)[Fe(CO)$_2$PMe$_3$]2 and (μ-pdt)[Fe(CO)$_2$PTA]$_2$, the both of which are produced by H-atom loss following reduction of the protonated species.[54]

The electrochemical processes of the neutral (μ-pdt)[Fe(CO)$_2$PTA]$_2$ and its cationic derivatives are diffusion-controlled, analogous to the all-CO diiron complexes, *vide supra*. Also observed for each PTA derivative is an irreversible oxidative event

which is displaced positively by ca. 2.4 V for all species, tracking the reductive event, Figure IV-9. This oxidation is assumed to be due to the $Fe^{I}Fe^{I}/Fe^{I}Fe^{II}$ couple, which experiences a greater stabilization by the better electron donor ability of the PTA ligand as compared to the all-CO neutral complex.

Electrocatalysis of H_2 production in CH_3CN solution. The current height of the single cathodic event at −1.78 V for (μ-pdt)[Fe(CO)$_2$PTA]$_2$ and at –1.54 V for (μ-pdt)[Fe(CO)$_3$][Fe(CO)$_2$PTA], derived from results in Figure IV-9, shows a linear dependence on the concentration of acetic acid. Only a minor increase in current height with added increments of acetic acid is observed for the redox wave at −1.35 V for $\{(\mu\text{-pdt})[Fe(CO)_2\text{-}(PTA\text{-}H)]_2\}^{2+}$ while the second redox wave, at –1.73 V, shows a more significant electrocatalytic response (Figure IV-9c). That is, the greater acid sensitivity is derived from the more negative potential, which, in the case of the $\{(\mu\text{-pdt})[Fe(CO)_2(PTA\text{-}H)]_2\}^{2+}$ species is actually the reduction of the parent (μ-pdt)[Fe(CO)$_2$PTA]$_2$ produced *in situ* from the protonated species, $\{(\mu\text{-pdt})[Fe(CO)_2\text{-}(PTA\text{-}H)]_2\}^{2+}$, *vide supra*.

Complex $\{(\mu\text{-pdt})[Fe(CO)_2(PTA\text{-}Me)]_2\}(OTf)_2$ undergoes a one-electron irreversible reduction at –1.46 V, assigned to the $Fe^{I}Fe^{I} \rightarrow Fe^{I}Fe^{0}$ couple of the dicationic complex. The cyclic voltammograms of the $\{(\mu\text{-pdt})[Fe(CO)_2(PTA\text{-}Me)]_2\}(OTf)_2$ in the presence of HOAc display two reduction waves at –1.46 V and –1.82 V, respectively, in CH_3CN solution. The similarity of the latter event to the potential of the neutral (μ-pdt)[Fe(CO)$_2$PTA]$_2$ complex, suggests its presence. The

degradation of the $\{(\mu\text{-pdt})[Fe(CO)_2(PTA\text{-}Me)]_2\}(OTf)_2$ cation will be further discussed below.

Controlled-potential electrolyses in CH_3CN solution were performed in to obtain the detailed electrocatalytic activities of the PTA derivatives. The electrolysis of complexes $(\mu\text{-pdt})[Fe(CO)_3][Fe(CO)_2PTA]$, $(\mu\text{-pdt})[Fe(CO)_2PTA]_2$, $\{(\mu\text{-pdt})[Fe(CO)_2(PTA\text{-}H)]_2\}(PF_6)_2$, and $\{(\mu\text{-pdt})[Fe(CO)_2(PTA\text{-}Me)]_2\}(OTf)_2$ (5 mM) at −1.60, −1.84, −1.79, and −1.52 V, respectively, in the presence of acetic acid (100 mM) for 1 h consumes 14, 32, 42, and 20 electrons per molecule per hour, respectively, corresponding to 7, 16, 21 and 10 turnovers per hour, respectively.

A reasonable interpretation of these results is that reduction of the $(\mu\text{-pdt})[Fe(CO)_3][Fe(CO)_2PTA]$ and $(\mu\text{-pdt})[Fe(CO)_2PTA]_2$, derivatives initiates the electrocatalysis, followed by double protonation of the one-electron reduced diiron species. A second reduction of an intermediate produces H_2 and the starting complex is reclaimed, as represented in the ECCE mechanism of Scheme 1,*vide infra*.

Electrocatalysis in the presence of water. While the water solubility of the diiron carbonyl complexes is increased by the presence of the hydrophilic PTA ligands, it is still insufficient for detailed electrochemical studies in pure water. However, in CH_3CN/H_2O mixtures the compounds show good solubility, and they are stable in a variety of CH_3CN and H_2O ratios (3:1, 1:1, and 1:3, v/v) for several hours. The electrochemical reduction processes of $(\mu\text{-pdt})[Fe(CO)_2PTA]_2$ and $(\mu\text{-pdt})[Fe(CO)_3][Fe(CO)_2PTA]$ in these mixed solvent systems are positively shifted, by ca. 100 - 250 mV (Table IV-4, Figure IV-11). For instance, the reduction potential of

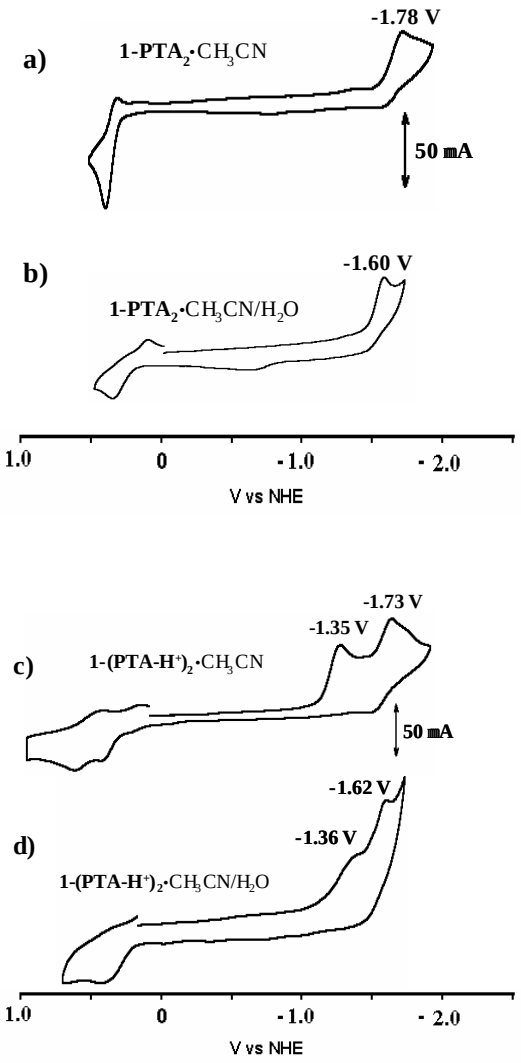

Figure IV-11. Cyclic voltammograms in CH_3CN solution (0.1 M *n*-Bu_4NBF_4) of a) neutral (μ-pdt)[$Fe(CO)_2PTA]_2$ (2.0 mM) and c) dicationic $\{(\mu\text{-pdt})[Fe(CO)_2(PTA\text{-}H)]_2\}^{2+}$ (2.0 mM) complexes, and in CH_3CN (0.1 M *n*-Bu_4NBF_4)/H_2O (0.1 M KCl) = 3:1, v/v, of b) neutral (μ-pdt)[$Fe(CO)_2PTA]_2$ and d) dicationic $\{(\mu\text{-pdt})[Fe(CO)_2(PTA\text{-}H)]_2\}^{2+}$ complexes with electrochemical parameters as described in Table IV-4.

(μ-pdt)[Fe(CO)$_2$PTA]$_2$ moves to −1.60 V in CH_3CN/H_2O mixtures from −1.78 V in CH_3CN; optimal values are with the 3:1 CH_3CN/H_2O mixture. Amongst the possible reasons for this shift are pK_a lowering, H-bonding interactions to the N of the PTAligand and product stabilization. It should be noted that our results, and published data (using a Pt electrode)[55] find the potential window for electrochemistry in CH_3CN/H_2O mixtures is +1.6 to ca. –1.7 V, and the observed events are within this window.

Figure IV-12 presents plots of current vs. acid concentration in pure CH_3CN and with varying CH_3CN:H_2O ratios for the electrocatalysis from the $Fe^IFe^I \rightarrow Fe^IFe^0$ couple of (μ-pdt)[Fe(CO)$_2$PTA]$_2$ (derived from $\{(\mu\text{-pdt})[Fe(CO)_2(PTA\text{-}H)]_2\}^{2+}$). The steeper slopes in the presence of H_2O as compared to the pure CH_3CN solution are indicative of greater sensitivity of the reduced species to acid concentration. Enhanced sensitivity, i.e., greater catalytic activity, is seen with only 10% added water, even though the reduction potential is still at -1.72 V, i.e., roughly the same as in pure CH_3CN. With a 3:1 CH_3CN/H_2O mixture, the reduction potential is shifted positively by ca. 100 mV, and the sensitivity to acid concentration is nearly as great as the 10:1 mixture. With greater water concentrations, the potential is invariant and the sensitivity appears to slightly decrease.

In contrast to (μ-pdt)[Fe(CO)$_2$PTA]$_2$ and $\{(\mu\text{-pdt})[Fe(CO)_2(PTA\text{-}H)]_2\}^{2+}$ the cyclic voltammogram of $\{(\mu\text{-pdt})[Fe(CO)_2(PTA\text{-}Me)]_2\}^{2+}$ in CH_3CN shows a negative shift of the cathodic event from –1.46 V to –1.60 V in the presence of water

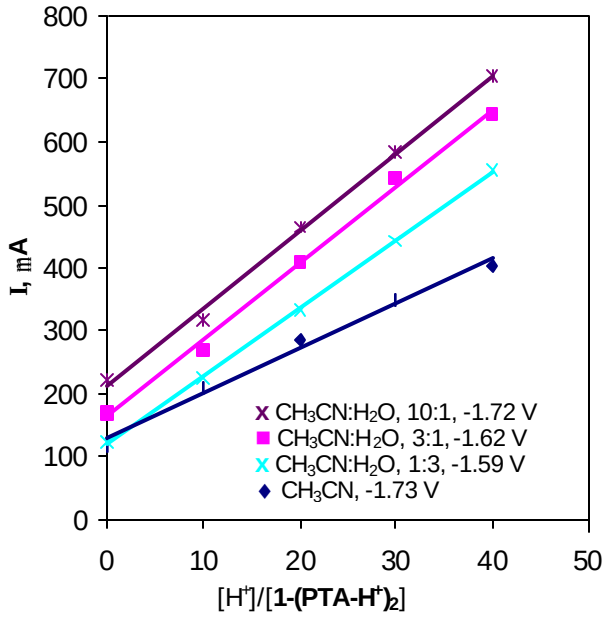

Figure IV-12. Dependence of current heights of electrocatalytic waves for {(μ-pdt)-$[Fe(CO)_2(PTA\text{-}H)]_2$}$(PF_6)_2$ (2 mM) on acid concentration (0, 25, 50, 75 and 100 mM) in CH_3CN and CH_3CN/H_2O (10:1, 3:1, 1:1, and 1:3, v/v) mixed solvent systems.

(CH_3CN/H_2O 3:1) (Table IV-4). As the more negative potential is the same as the reduction of the neutral complex (μ-pdt)$[Fe(CO)_2PTA]_2$ in the CH_3CN/H_2O mixture, this observation is interpreted in terms of a demethylation of the quaternary nitrogen atom of the Fe-PTA-Me^+ moiety. That this demethylation is a chemical event, a result of degradation of the alkylated PTA ligand in the presence of the electrolytes, was also suggested by infrared spectral measurements on non-electrolyzed solutions. Degradation of the methylated PTA complex {(μ-pdt)$[Fe(CO)_2(PTA\text{-}Me)]_2$}$^{2+}$ was

also found in CH_3CN solutions in the absence of water and in the presence of aliquots of glacial acetic acid, as shown in Figure IV-9d. While there is literature precedent for demethylation of quaternary ammonium salts (R_3MeN^+) by RSeH or RSH,[56] whether HOAc might be similarly effective is not known.

Occurrence and significance of "curve-crossing".[57-59] In the mixed CH_3CN/H_2O solvent system in the presence of HOAc reproducible curve crossings were observed for (μ-pdt)$[Fe(CO)_2PTA]_2$ and {(μ-pdt)$[Fe(CO)_2(PTA\text{-}H)]_2$}$(PF_6)_2$ upon reversing the scan following the reduction at -1.62 V. Although the {(μ-pdt)$[Fe(CO)_2(PTA\text{-}H)]_2$}$^{2+}$ complex is at this potential in the form of (μ-pdt)$[Fe(CO)_2PTA]_2$, solutions derived from it as precursor show more clearly defined curve crossing phenomena. As shown in Figure IV-13 for the dicationic complex {(μ-pdt)$[Fe(CO)_2(PTA\text{-}H)]_2$}$^{2+}$ the curve crossing cathodic event is at –1.28 V; its current height increases with increasing acid concentrations. It seems that this response is an integral property of the electroactive (-1.62 V) species following the formation of which a chemical reaction produces a more easily reducible product or intermediate, most reasonably an (ς^2-H_2)$Fe^{II}Fe^{I}$ or H-$Fe^{II}Fe^{I}$ species. These observations suggest that a one-electron step, at –1.62 V, followed by a one-electron reduction of a mono- or di-protonated species at –1.28 V are involved in the electrocatalytic reaction for H_2 production in the model systems.

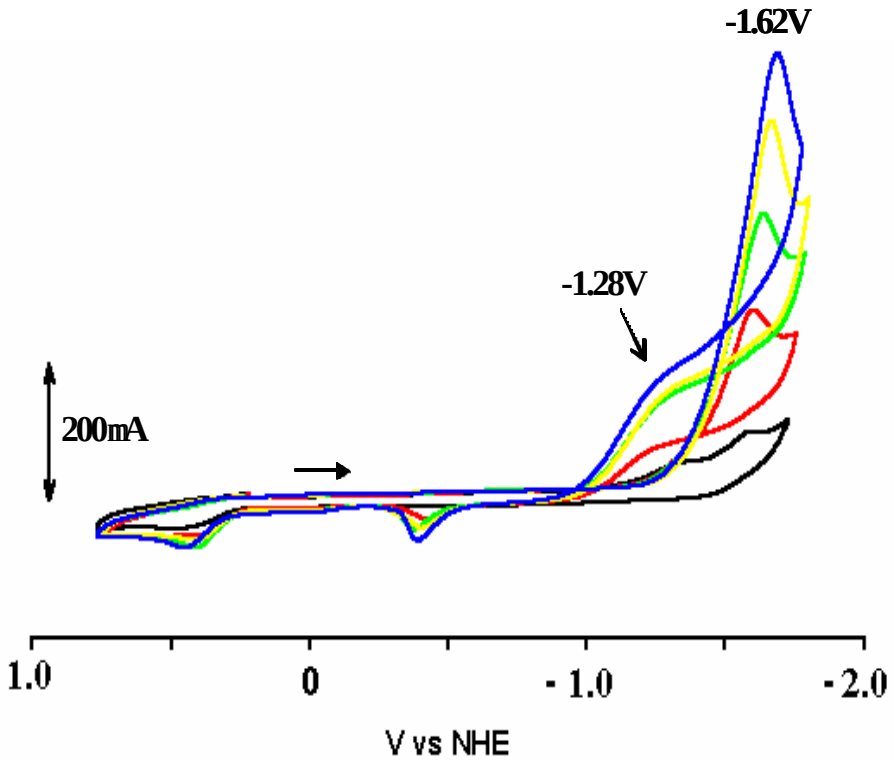

Figure IV-13. Cyclic voltammograms of $\{(\mu\text{-pdt})[Fe(CO)_2(PTA\text{-}H)]_2\}^{2+}$ (2.0 mM) with HOAc (0, 25, 50, 75 and 100 mM) in CH_3CN (0.1 M *n*-Bu_4NBF_4)/H_2O (0.1 M KCl) = 3:1, v/v, with electrochemical parameters as described in Table IV-4.

Mechanisms of H_2 Production by (μ-SRS)[$Fe^I(CO)_2L]_2$, (L = CO, PMe_3, and PTA), Complexes

The results presented in this chapter point to two reductive routes to electrocatalysis of H_2 production from binuclear Fe^IFe^I complexes in the presence of weak acid, HOAc, as a proton source. For the all-CO complexes, the electrocatalysis occurs at the second reduction potential (E_2) that corresponds to an Fe^0Fe^0 species. The Fe^{II}-hydride that results from oxidative addition of a proton to Fe^0 is set up to accept another proton, generating an $(\eta^2\text{-}H_2)Fe^{II}\text{-}Fe^0$ complex according to Scheme IV-1. An EECC (electrochemical-electrochemical-chemical-chemical) mechanism accounts for this process.

Scheme IV-1

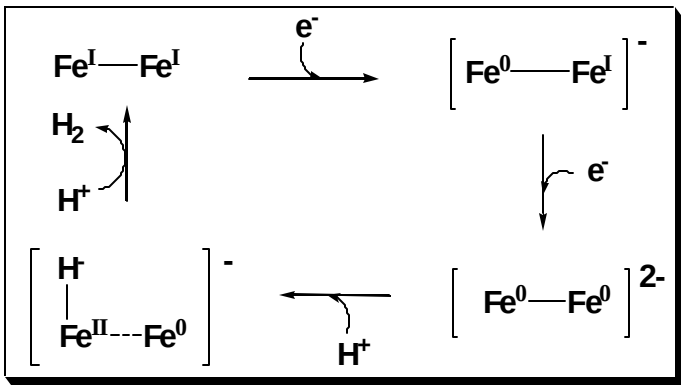

With the PTA and PMe_3 substituents in the Fe^IFe^I complexes the Fe^0Fe^0 state is not accessible within the solvent window, however the electrocatalysis occurs at the Fe^0Fe^I oxidation level that is analogous to that expected for the [Fe]H_2ase enzyme active site.[43,44] The ECCE (electrochemical-chemical-chemical-electrochemical) process as shown in Scheme IV-2a applies to the Fe^I-Fe^I model complexes, (μ-SRS)$[Fe(CO)_2L]_2$ (L = CO (ca. -1.2 to -1.3 V), PMe_3 (-1.8 to -1.9 V), and PTA (-1.78 V)), with HOAc in CH_3CN. An alternative EC (electrochemical-chemical) route expressed in Scheme IV-2b can be proposed based on the bimolecular reaction of two Fe^{II}-hydride (H-Fe^{II}-Fe^I) species derived from oxidative addition of two protons to two separate Fe^0Fe^I species. Such an EC mechanism was previously proposed to account for the electrocatalysis of H_2 production by the mononuclear complex, (η^5-C_5H_5)$Co(PR_3)_2$.[54] However, the formation of a tetranuclear cluster intermediate from two [H-$Fe^{II}Fe^I$] species is poorly favored by steric factors.

For both the mono-cationic, (μ-H)(μ-pdt)$[Fe(CO)_2PMe_3]_2^+$, and the di-cationic species $\{(\mu\text{-pdt})[Fe(CO)_2(PTA\text{-}H)]_2\}^{2+}$, the first reduction events, at –1.1 V and –1.35 V, respectively, generate the Fe^I-Fe^I species from which electrocatalysis occurs, as outlined in Scheme IV-3. Thus there is no apparent advantage in the synthesis of the cationic species when the weak acetic acid is to be used as proton source as only the Fe^0Fe^I species is active in oxidative addition. When strong acids such as triflic acid are used, the more positive reduction potential of (μ-H)(μ-pdt)$[Fe(CO)_2PMe_3]_2^+$, (at –1.1 V) is catalytically active, however the advantage of the more positive potential is

Scheme IV-2

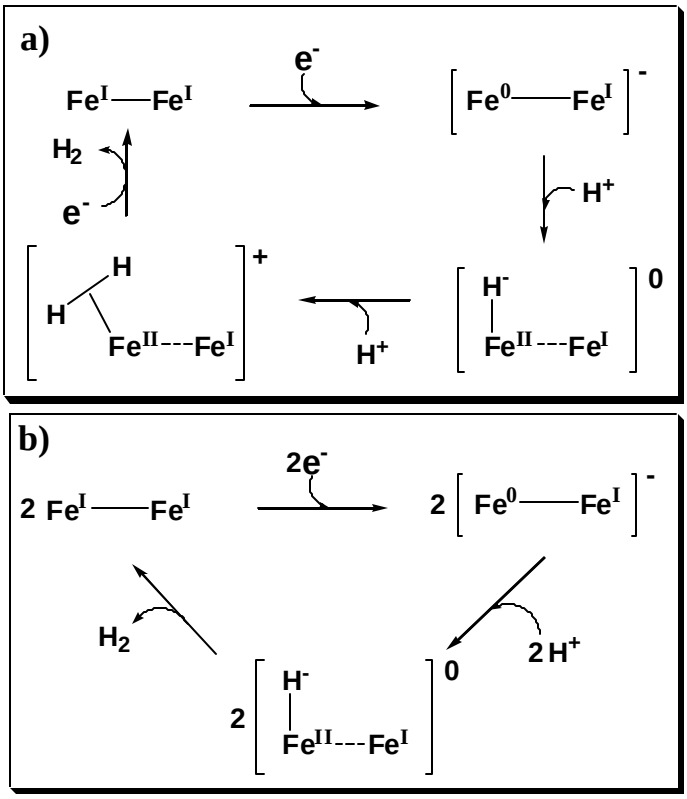
a)
e-
Fe^I—Fe^I
[Fe^0—Fe^I]-
H2
e-
H+
[H
H
Fe^II---Fe^I]+
H+
[H-
Fe^II---Fe^I]0
b)
2e-
2 Fe^I—Fe^I
2 [Fe^0—Fe^I]-
H2
2 H+
2 [H-
Fe^II---Fe^I]0

Scheme IV-3

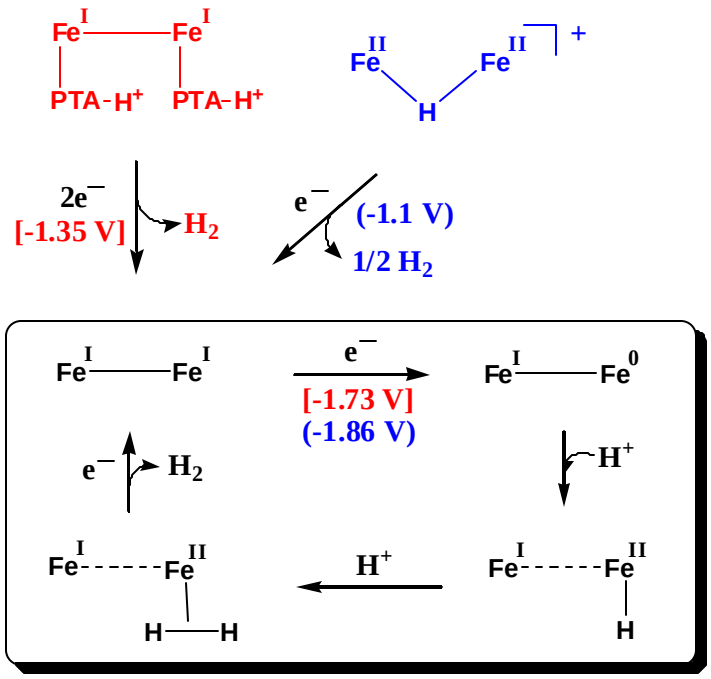

ameliorated by the necessity for a strong acid. While the all-CO complex (μ-pdt)[Fe(CO)$_3$]$_2$ is an electrocatalyst only at the fully reduced Fe^0Fe^0 redox level, the asymmetric mono-substituted complex, (μ-pdt)[Fe(CO)$_3$][Fe(CO)$_2$PTA] shows electrocatalysis at its first reduction event, i.e., the Fe^0Fe^I oxidation level which at –1.54 V is the most positive potential of all electrocatalysts based on (μ-pdt)[Fe(CO)$_3$]$_2$ or its derivatives. The mechanism is presumed to be the same as for the (μ-pdt)-[Fe(CO)$_2$PTA]$_2$ derivative, ECCE, however the preferred site of electron-uptake (the Fe(CO)$_3$ or Fe(CO$_2$)(PTA) positions) and the preferred site for Fe^{II}-H formation are issues that are unknown at this moment.

Although there is no spectroscopic evidence for the $(\eta^2\text{-}H_2)Fe^{II}Fe^{I}$ species, proposed as an intermediate in the ECCE mechanism, its presence would account for the cathodic curve crossing electrochemical event at –1.28 V observed to follow reduction of $(\mu\text{-pdt})[Fe(CO)_2PTA]_2$ to the Fe^0Fe^I level. That is, the cationic charge of an $(\eta^2\text{-}H_2)Fe^{II}Fe^{I}$ species should engender a more positive reduction potential, consistent with the curve crossing event and the ECCE mechanism.

CHAPTER V

EFFECTS OF ASYMMETRY IN DIIRON COMPLEXES: THE N-HETEROCYCLIC CARBENE DERIVATIVE OF (μ-pdt)[Fe(CO)$_3$]$_2$

A fundamental feature of the Fe^IFe^I model complexes is the intramolecular site exchange of CO ligands at individual $Fe(CO)_3$ or $Fe(CO)_2L$ centers via a turnstile rotation process. Cotton, *et al.* (1975), and Flood, *et al.* (1978), studied this process in several diiron complexes bridged by thiolates, phosphines, and arsines.[37,60] Nevertheless, the fluxionality present in dinuclear iron compounds bridged by a chelating dithiolate was first studied in our group by Dr. Erica Lyon (PhD TAMU, 2000) and Dr. Irene Georgakaki (PhD TAMU, 2002) using (μ-SRS)[Fe(CO)$_3$]$_2$ (SRS = SCH_2CH_2S (edt), $SCH_2CH_2CH_2S$ (pdt), and $SCH_2C_6H_4CH_2S$ (o-xyldt)) complexes.[61] The latter studies can be briefly described as follows. The intramolecular site exchange of protons and CO ligands was monitored by variable temperature (VT) nuclear magnetic resonance spectroscopy. The (μ-pdt)[Fe(CO)$_3$]$_2$ complex presented rapid interconversion of axial and equatorial protons in the $Fe(SCH_2)CH_2$ metallodithiacyclohexane ring at room temperature. This dynamic process stops at –60 °C, the temperature at which the bridge "freezes" in one position rendering asymmetry to the individual $Fe(CO)_3$ units. In contrast, the S-to-S linker in (μ-o-xyldt)[Fe(CO)$_3$]$_2$ is fixed in one position even at 50 °C, as evidenced by the ^{1}H NMR spectrum which shows that the hydrogens of the methylene units are magnetically non-equivalent. The second process taking place in (μ-SRS)[Fe(CO)$_3$]$_2$ complexes, CO site exchange in

each $Fe(CO)_3$ unit, equilibrates apical and basal CO positions in the square pyramidal $S_2Fe(CO)_3$ units. The ^{13}C NMR spectrum in the CO region of $(\mu\text{-pdt})[Fe(CO)_3]_2$ presents one resonance, indicating the magnetic equivalence of the six CO ligands. Lowering the temperature slows down the rotation at the iron centers, and at –85 °C, where the stopped exchange region is reached, four distinct resonances are present in the spectrum. As indicated in Figure V-1 these correspond to two distinct apical CO's and two distinct basal CO sets. The two fluxional processes described above are schematically presented in Figure V-1.

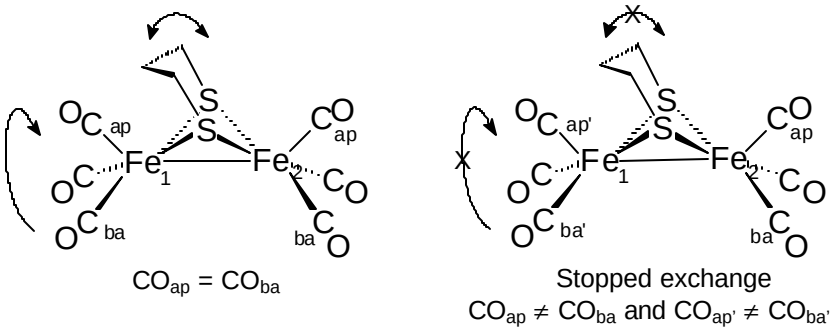

Figure V-1. Fluxional characteristics of $(\mu\text{-pdt})[Fe(CO)_3]_2$

The barrier for rotation ($\Delta G^{\neq}$) in the $Fe(CO)_3$ units can be calculated from line widths in the slow-exchange region of the spectrum,[62] from the exchange rate constant at the coalescence temperature according to Equation V-1,[63] or from rate constants derived from spectral simulations using available NMR computer programs such as gNMR.[64] Even though calculations using the coalescence temperature have inherent

errors, the values obtained for the barriers for rotation for the $Fe(CO)_3$ termini in (μ-edt)- $[Fe(CO)_3]_2$, (μ-pdt)$[Fe(CO)_3]_2$, and (μ-o-xyldt)$[Fe(CO)_3]_2$ using such methods suggested a trend which was consistent with observations and DFT computations.[61]

$$\Delta G^{\neq} = RT \ln (k_B T / k_r h), \quad k_r = \pi \Delta\nu / \sqrt{2} \qquad \text{(V-1)}$$

k_B = Boltzmann's constant h = Planck's constant;

R = gases constant T = absolute coalescence temperature;

$\Delta\nu$ = line separation in the stopped exchange region (in Hz)

Density functional calculations were performed to further study the intramolecular CO site exchange and to gain insight into the differences observed for the activation barriers of each $Fe(CO)_3$ unit on (μ-pdt)$[Fe(CO)_3]_2$, and (μ-*o*-xyldt)-$[Fe(CO)_3]_2$.[61,65] Calculations for the monocyanide derivative (μ-pdt)$[Fe(CO)_3]$-$[Fe(CO)_2CN]^-$, a complex that can be prepared through a CO/CN conversion reaction, were also performed to study the influence of a better donor ligand on the activation energy of the rotation process.[65] It was shown that in (μ-*o*-xyldt) $[Fe(CO)_3]_2$ there is a lower barrier for rotation for the $Fe(CO)_3$ end that is underneath the dithiolate bridge. A rationale for the "assistance" furnished to ease this rotation was based on the necessity to release some of the steric and electronic hindrance imposed on the molecule by the close proximity of the apical CO to the phenyl ring of the *o*-xylyldithiolate moiety. There is an analogous, albeit much smaller steric effect, for (μ-pdt)$[Fe(CO)_3]_2$.

In the monocyanide complex, (μ-pdt)[$Fe(CO)_3$][$Fe(CO)_2CN$]$^-$, the barrier for rotation of the $Fe(CO)_3$ end is lower than that calculated for the all-CO complex. As there are no obvious steric differences, the conclusion was that a better donor might facilitate the rotation by stabilizing the transition state generated in this process.[65]

As shown in Scheme V-1, the DFT optimized structure for the transition state of (μ-SRS)[$Fe(CO)_2L]_2$ features a rotation and rearrangement of the $Fe(CO)_3$ unit so as to present an inverted square pyramid with an apparent semi-bridging CO group, and a vacant open site on iron. This transition state structure looks very similar to the enzyme active site, suggesting that the protein, in which the active center is deeply buried, facilitates a rotation or orientation at which the structure is ready for H^+ uptake or H_2 binding at that open site. Such a conclusion leads to further questions regarding

Scheme V-1

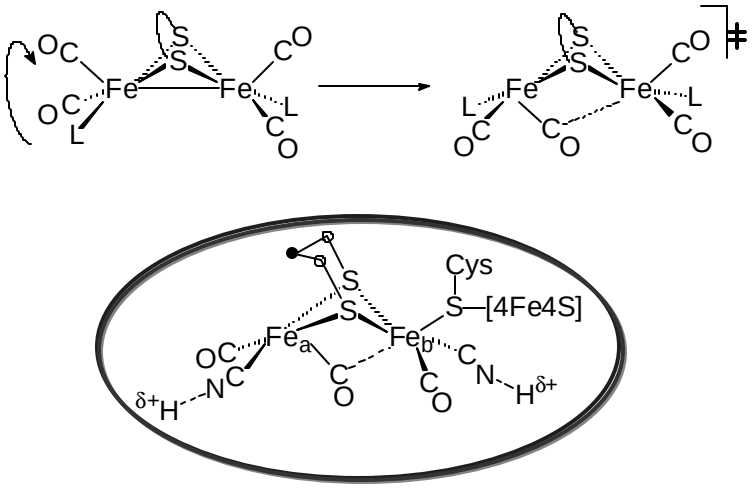

conditions that might stabilize this transition state, or in fact, produce an intermediate of similar structure.

In pursuit of complexes appropriate for exploring features which control intramolecular dynamics that might influence electrocatalysis of H_2 production, a sterically encumbered ligand, the N-heterocyclic carbene 1,3-bis(2,4,6-trimethyl phenyl)imidazol-2-ylidene, IMes, was employed for the generation of a singly substituted derivative of $(\mu\text{-pdt})[Fe(CO)_3]_2$. Our ultimate objective was to determine whether an asymmetric complex which has one end locked in position by a sterically encumbered ligand might have special features conducive to H_2 electrocatalysis via Equation V-2.

$$2H^+ + 2e^- \xrightarrow{Fe^I Fe^I cat.} H_2 \qquad \textbf{(V-2)}$$

N-heterocyclic carbenes (NHCs), are 2-electron donors that behave like typical σ-donor ligands with little π-back bonding.[66] This class of ligands has been called "phosphine mimics" for their similarities in coordination to metals and in synthetic methods.[67] Nevertheless, Nolan, *et al.* showed through solution calorimetric experiments that NHCs are, in fact, better donors than phosphines.[68] Furthermore, many are less O_2-sensitive than phosphines. Theoretical calculations performed by Herrmann and coworkers for a Ru(II) model complex demonstrated that the Ru-L dissociation energy increases in the series $PH_3 < PMe_3 <$ NHC, corroborating the higher strength of the metal-carbene bond.[69]

In the late '70s and '80s a major synthetic effort of Lappert and coworkers successfully produced several NHC complexes of Fe^0, Fe^I, and Fe^{II} (some examples shown in Figure V-2).[70] Carbonyls, phosphines, or the cyclopentadienyl ligand completed the coordination sphere of the iron centers. More recently (1993) Öfele and coworkers[71] prepared $Fe(CO)_4$(IMe), (IMe = 1,3-dimethylimidazol-2-ylidene), and Grubbs and Louie (2000)[72] synthesized $FeX_2(I^iPr)$ (I^iPr = 1,3-diisopropylimidazol-2-ylidene) (Figure V-2). In 2003 Guerchais and coworkers synthesized and characterized a "piano stool" complex, $CpFe^{II}(CO)(I)$IMes.[73]

The importance of NHCs as ligands, particularly those with bulky groups on N, has been recognized in recent research. It has been shown that the substitution of a phosphine with a N-heterocyclic carbene improves the catalytic activity of metal catalysts participating in several different organic reactions, i.e. ring-closing metathesis, olefin metathesis, atom transfer radical polymerization, ring-opening metathesis polymerization, etc.[72, 74] The effects of complexation of these ligands to biologically relevant metal complexes is not known and has yet to be investigated.[66] It is an attractive area as the M—C bond in the M-(NHC) is very strong and should increase stability. Also it is a "biologically compatible" ligand, resembling an N-protected form of histidine.

In this chapter the synthesis, characterization and properties of (μ-pdt) $[Fe(CO)_3][Fe(CO)_2$IMes], an asymmetrically substituted diiron complex, are reported.

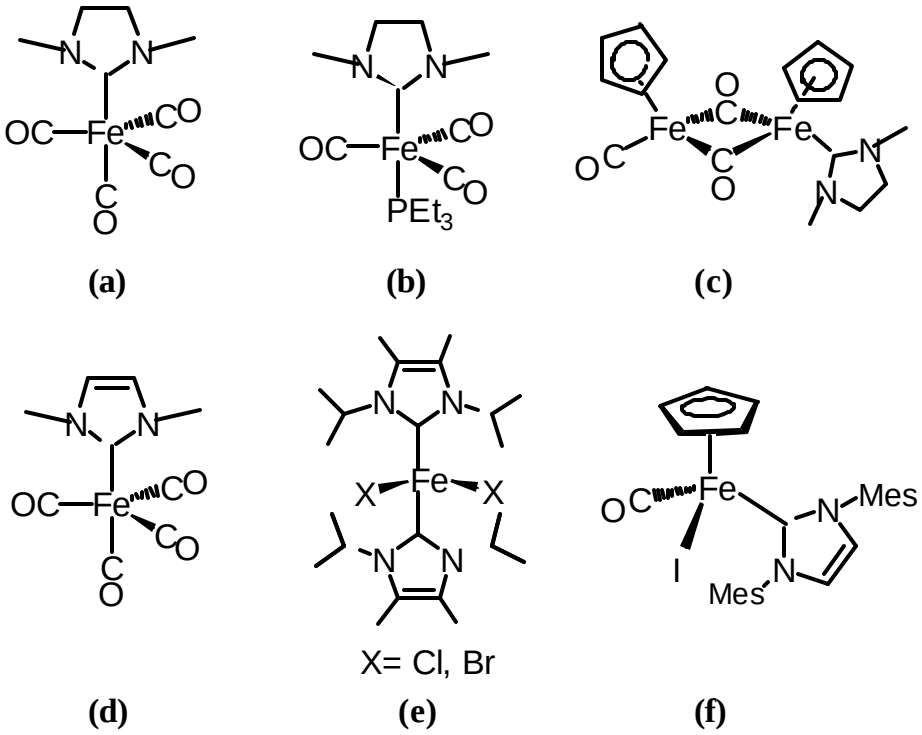

Figure V-2. Representative Iron-N-heterocyclic carbene complexes. Compounds prepared by (a), (b), and (c) Lappert *et al.*,[70] (d) Öfele and coworkers,[71] (e) Grubbs and Louie,[72] and (f) Guerchais and coworkers.[73]

Synthesis and Characterization of (μ-pdt)[Fe(CO)$_3$][Fe(CO)$_2$IMes]

The procedure of Arduengo, *et al.*[25] was followed for deprotonation of 1,3-bis(2,4,6-trimethylphenyl)imidazolium chloride and isolation of the neutral 1,3-*bis*(2,4,6-trimethylphenyl)imidazol-2-ylidene (IMes) ligand. On mixing a THF solution of (μ-pdt)[Fe(CO)$_3$]$_2$ and IMes (1:1.2 molar ratio) and warming to 50 °C, a color change from orange to red-orange ensued over the course of 1.5 h concomitantly with changes in the ν(CO) infrared spectrum as indicated in equation V-3. The shift of CO stretching frequencies to lower values is in agreement with the superior electron donor ability of the IMes ligand over CO. The 4-band IR pattern is typical of monosubstituted derivatives of (μ-SRS)[Fe(CO)$_3$]$_2$,[75] and is similar to that of the (μ-pdt)[Fe(CO)$_3$][Fe(CO)$_2$PTA], (PTA = 1,3,5-triaza-7-phosphaadamantane) complex (see complete characterization of this complex in Chapter IV), Figure V-3.

The IR ν(CO) of (μ-pdt)[Fe(CO)$_3$][Fe(CO)$_2$IMes] is also comparable to the monosubstituted cyanide complex, {(μ-pdt)[Fe(CO)$_3$][Fe(CO)$_2$CN]}(Et$_4$N), although the spectrum for this monocyanide complex presents 5 bands (2029 cm^{-1} (s), 1974 cm^{-1} (vs), 1955 cm^{-1} (s), 1941 cm^{-1} (s), and 1917 cm^{-1} (m)).[76] The differences in band pattern in the IR spectra of (μ-pdt)[Fe(CO)$_3$][Fe(CO)$_2$IMes] and {(μ-pdt)[Fe(CO)$_3$][Fe(CO)$_2$CN]}$^-$ could be attributed to the symmetry of each compound, *vide infra*.

$$(\mu\text{-pdt})[Fe(CO)_3]_2 \xrightarrow[THF,\ 50\ ^oC]{IMes} (\mu\text{-pdt})[Fe(CO)_3][Fe(CO)_2IMes] \quad \text{(V-3)}$$

n(CO): 2074, 2035, 1995 cm^{-1} **2035, 1969, 1947, 1916 cm^{-1}**

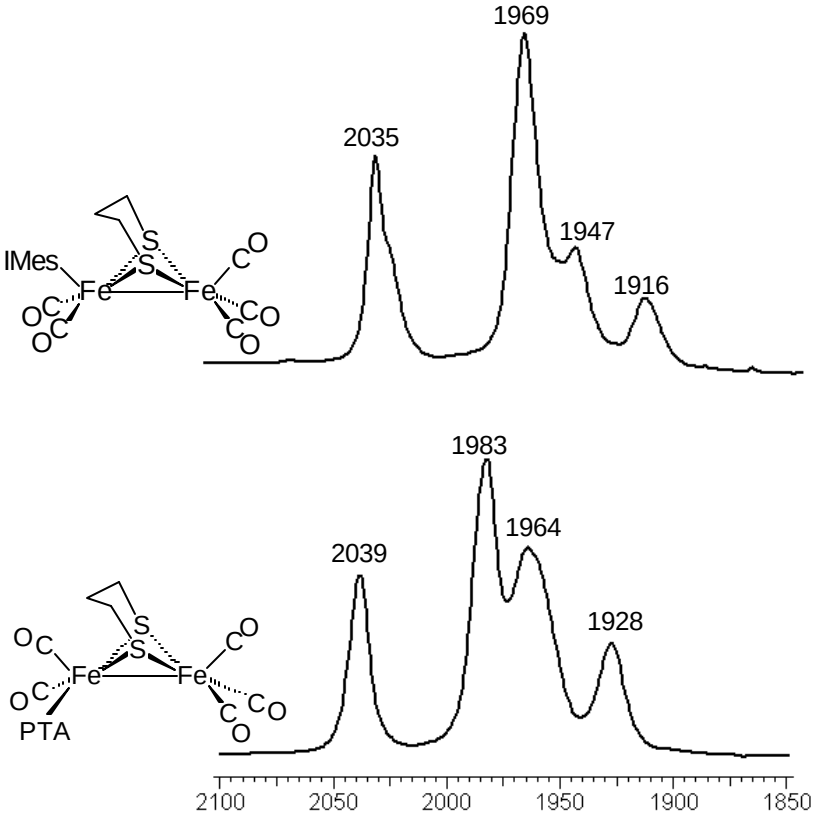

Figure V-3. Infrared spectra in the CO region of the asymmetric complexes (μ-pdt)[Fe(CO)$_3$][Fe(CO)$_2$IMes] and (μ-pdt)[Fe(CO)$_3$][Fe(CO)$_2$PTA] in THF solution.

The product was isolated by evaporating the solvent under vacuum, yielding a thick red oil that solidified after being washed with diethyl ether, and dried under vacuum overnight. Crystals suitable for X-ray analysis were obtained from THF/hexane layering. Complex (μ-pdt)[$Fe(CO)_3$][$Fe(CO)_2$IMes] crystallizes in the monoclinic system with 8 molecules per unit cell and 4 molecules of THF. X-ray diffraction studies determined the molecular structure of (μ-pdt)[$Fe(CO)_3$]-[$Fe(CO)_2$IMes] as given in Figure V-4. As in the parent hexacarbonyl diiron complex, the propanedithiolate unit serves to edge-bridge two square pyramids, creating an Fe_2S_2 butterfly core. The IMes ligand occupies the apical position of the $S_2Fe(CO)_2L$ square pyramid. Selected distances and bond angles are given in Table V-1. A complete listing of metric parameters is given in the Appendix, Tables A-13 to A-15.

The Fe(1)-Fe(2)-C(6)-N(2) dihedral angle is 60.1° such that the plane defined by the C(6), N(1), and N(2) atoms of the carbene nearly eclipses the Fe-S(2) and Fe-C(1) bonds. The Fe-Fe distance of (μ-pdt)[$Fe(CO)_3$][$Fe(CO)_2$IMes], 2.524(3) Å, does not differ significantly from that of the parent complex, (μ-pdt)[$Fe(CO)_3$]$_2$ (2.510(1) Å). The central CH_2 group of the propanedithiolate bridge is oriented towards the IMes ligand. The overlay of the structures of complexes (μ-pdt)[$Fe(CO)_3$]$_2$ and (μ-pdt)[$Fe(CO)_3$][$Fe(CO)_2$IMes] in Figure V-5 suggests that some distortion about Fe(1) is a consequence of the steric bulk of the IMes ligand, repelling the basal CO ligands, and engendering a slight bend in the basal Fe-C-O angles, averaging to 173°. The Fe(1) is displaced from the $S_2(CO)_2$ basal plane of the square pyramid by 0.508 Å,

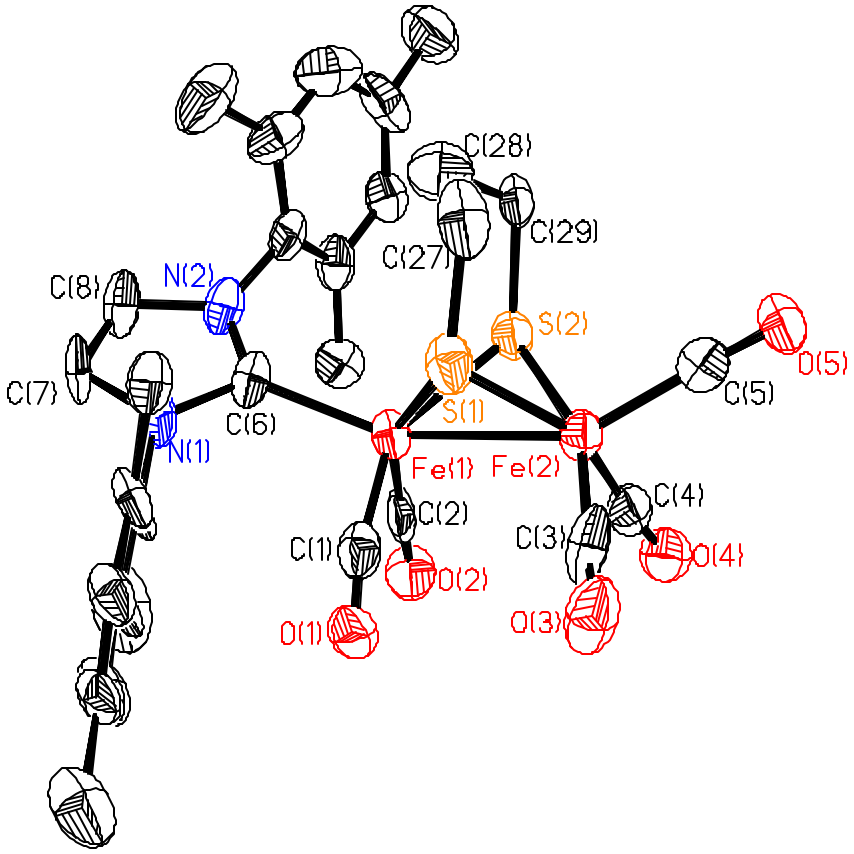

Figure V-4. Thermal ellipsoid representation (50% probability) of (μ-pdt)[$Fe(CO)_3$] [$Fe(CO)_2$IMes] indicating the numbering system. Hydrogens and solvent molecule were omitted for clarity.

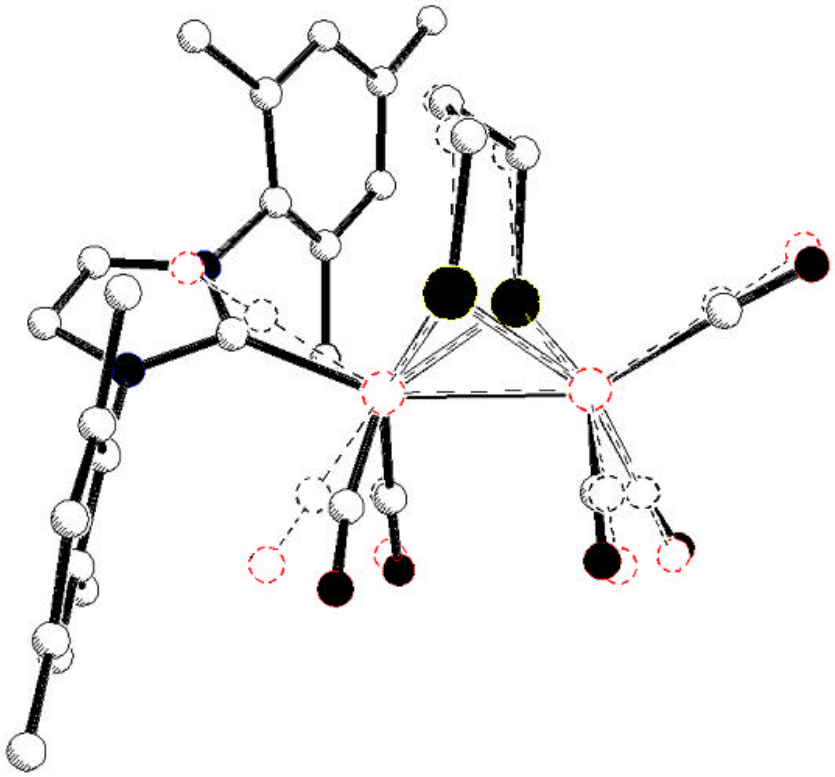

Figure V-5. Overlay of the Fe_2S_2 portions of complexes (μ-pdt)$[Fe(CO)_3]_2$ and (μ-pdt)$[Fe(CO)_3][Fe(CO)_2$IMes]. The solid lines represent the latter complex and the dashed lines and circles represent (μ-pdt)$[Fe(CO)_3]_2$.

Table V-1. Selected Bond Distances [Å] and Angles [deg] for (μ-pdt)[$Fe(CO)_3$]-[$Fe(CO)_2$IMes]

Bond distances		Bond Angles	
Fe(1)-Fe(2)	2.525(3)	Fe(1)-S(1)-Fe(2)	67.33(11)
Fe(1)-S(1)	2.282(4)	Fe(1)-S(2)-Fe(2)	67.46(10)
Fe(1)-S(2)	2.277(3)	S(2)-Fe(1)-S(1)	84.53(11)
Fe(2)-S(1)	2.274(3)	S(2)-Fe(2)-S(1)	84.88(12)
Fe(2)-S(2)	2.270(3)	C(1)-Fe(1)-C(2)	86.0(5)
Fe(1)-C(1)	1.771(13)	C(3)-Fe(2)-C(4)	94.1(5)
Fe(1)-C(2)	1.758(12)	C(6)-Fe(1)-C(2)	86.0(5)
Fe(1)-C(6)	2.012(10)	C(6)-Fe(2)-C(1)	94.1(5)
Fe(2)-C(3)	1.785(14)	C(5)-Fe(2)-C(3)	98.3(5)
Fe(2)-C(4)	1.782(13)	C(5)-Fe(2)-C(4)	99.8(4)
Fe(2)-C(5)	1.820(12)	C(5)-Fe(2)-S(1)	104.4(3)
C(1)-O(1)	1.146(12)	C(5)-Fe(2)-S(2)	103.8(3)
C(2)-O(2)	1.168(11)	C(6)-Fe(1)-S(1)	108.9(3)
C(3)-O(3)	1.138(13)	C(6)-Fe(1)-S(2)	110.7(3)
C(4)-O(4)	1.179(11)	C(5)-Fe(1)-Fe(2)	150.8(3)
C(5)-O(5)	1.115(11)	C(6)-Fe(1)-Fe(2)	158.4(3)
C(6)-N(1)	1.355(11)	N(1)-C(6)-N(2)	101.4(8)
C(6)-N(2)	1.394(13)		
C(7)-C(8)	1.286(14)		

whereas the analogous displacements for Fe(2), and for the iron atoms in complex (μ-pdt)[Fe(CO)$_3$]$_2$ towards the apical CO is 0.38 Å.

The observed solid state geometries for ligand substituted diiron dithiolate carbonyl complexes are determined by the interplay of subtle electronic and steric effects involving the μ-SR or μ-SRS, and the L group. Substitution of two CO ligands in the bis(μ-SR) parent compound, (μ-SR)$_2$[Fe(CO)$_3$]$_2$, by a phosphine (PMe$_3$) occurs at the axial position of the square pyramid, forming a symmetric disubstituted complex.[8,38] The R groups on the sulfurs are typically in a *syn* orientation (see Chart III-1). The preference for an axial coordination in such complexes suggests that substitution in the basal plane is hindered by steric repulsion from the CO ligands. In the other hand, the presence of linked dithiolate bridges (μ-SRS) eliminates the complication of anti-syn isomers observed for the bis-μ(SR) bridged complexes. In this case the basal position is favored for substitution by "small" ligands such as PMe$_3$, PTA, and CN$^-$. Only the more sterically encumbered PPh$_3$ is found in the apical position, and only one PPh$_3$ can be exchanged.

Table V-2 lists the four complexes of the form (μ-pdt)[Fe(CO)$_3$][Fe(CO)$_2$L] that have been structurally characterized, along with IR spectral data. The (μ-pdt)[Fe(CO)$_3$][Fe(CO)$_2$IMes] complex is the only one of these complexes to feature an apical coordinated L in the solid state. Comparison of either the individual ν(CO) stretching frequencies, or the average value, shows that IMes is the best neutral donor of the set. From the ν(CO) one can make the conclusion that the IMes ligand is a

Table V-2. IR data for Complexes (μ-pdt) $[Fe(CO)_3][Fe(CO)_2L]$

L	position of L	ν(CO), cm^{-1}	average ν(CO)	solvent
CO	n/a	2074, 2035, 1995	2035	THF[a]
C(OEt)(Ph)	basal	2050, 1995, 1972, 1948	1991	Hexane[b]
PTA	basal	2039, 1983, 1964, 1928	1979	THF[c]
IMes	apical	2035, 1969, 1947, 1916	1967	THF[c]
CN^- [a]	basal	2029, 1974, 1955, 1941, 1917	1963	THF[d]

[a] Ref 7a; [b] ref 77; [c] this dissertation; [d] as Et_4N^+ salt, ref 76.

much better donor than the C(OEt)(Ph) carbene and PTA, and it appears that IMes has very similar electronic characteristics to the anionic cyanide ligand.

To gain a deeper insight into the factors governing the position that a ligand L may take upon CO substitution in (μ-SRS)$[Fe(CO)_3]_2$ complexes, Jesse Tye, a PhD student in our group, carried out density functional theory (DFT) calculations to determine the relative energy of the positional isomers of an NHC-complex. To make calculations tractable, the mesityl groups on (μ-pdt)$[Fe(CO)_3][Fe(CO)_2$IMes] were replaced with hydrogen atoms. The computations for (μ-pdt)$[Fe(CO)_3][Fe(CO)_2$(I-H)], (I-H = imidazol-2-ylidene) showed that the isomer with the carbene ligand in the basal plane of the square pyramid is 2.7 kcal mol^{-1} more stable than the most stable rotomer

of the apical isomer. These results suggest that the basal position is favored for less sterically demanding ligands, and is consistent with the solid state structure found for other (μ-pdt)[Fe(CO)$_3$][Fe(CO)$_2$L] complexes, (L = PTA (see Chapter IV), CN^-,[76] C(OEt)(Ph)[77]). Steric interactions induced by the mesityl groups, present in the real molecule, probably account for the observation of the apical isomer for (μ-pdt)[Fe(CO)$_3$][Fe(CO)$_2$IMes], *vide infra*.

In contrast to the solid state structure of (μ-pdt)[Fe(CO)$_3$][Fe(CO)$_2$IMes], the (μ-pdt)[Fe(CO)$_3$][Fe(CO)$_2$PTA] complex, presents the PTA ligand in the basal plane, indicating that PTA is less sterically demanding that IMes. In fact, PTA is considered very similar in size to PMe_3 (see Chapter IV for structural details of (μ-pdt)[Fe(CO)$_3$][Fe(CO)$_2$PTA]).

Protonation Studies of (μ-pdt)[Fe(CO)$_3$][Fe(CO)$_2$IMes]

Previous studies conducted by several members of this research group showed that when the good donor ligand PMe_3 substitutes two CO ligands in the parent (μ-SRS)[Fe(CO)$_3$]$_2$ to form disubstituted complexes of the form (μ-SRS)[Fe(CO)$_2$PMe$_3$]$_2$, the electron density at the Fe-Fe bond is sufficient to undergo oxidative addition of nucleophiles such as H^+, and SMe^+ to form $\{(\mu\text{-H})Fe^{II}Fe^{II}\}^+$, and $\{(\mu\text{-SMe})Fe^{II}Fe^{II}\}$, respectively.[7e,8,46] Having in mind the superior electron donor ability of N-heterocyclic carbenes over phosphines, the protonation of the monosubstituted (μ-pdt)[Fe(CO)$_3$]-[Fe(CO)$_2$IMes] was studied using strong acids such as HCl and triflic acid (CF_3SO_3H).

Addition of concentrated HCl to a MeOH solution of (μ-pdt)[Fe(CO)$_3$][Fe(CO)$_2$IMes] did not show the expected shift in the IR ν(CO), indicating that protonation at the Fe-Fe bond was not taking place. A decrease in the absorbance of the starting IR bands suggested some decomposition of the complex, probably due to the reported water sensitivity of N-heterocyclic carbene ligands.[78] Further exploration of the protonation reaction was attempted by using the strong CF_3SO_3H acid. The lack of an upfield resonance in the ^{1}H NMR spectrum for either a terminal or a bridging hydride that would form should protonation occur, indicated that the complex (μ-pdt)[Fe(CO)$_3$][Fe(CO)$_2$IMes] is not sufficiently basic, or does not provide the electron richness required, to undergo oxidative addition of a proton.

Effects of Asymmetry on the Dynamic Properties and Electrochemistry of (μ-pdt)[Fe(CO)$_3$][Fe(CO)$_2$L] Complexes

The natural abundance ^{13}C NMR spectrum of (μ-pdt)[Fe(CO)$_3$][Fe(CO)$_2$IMes] at 23 °C in CD_3CN shows a resonance at 190 ppm for the carbene carbon of the IMes ligand; two sharp resonances at 212 and 216 ppm are assigned to the Fe(**C**O)$_3$ and Fe(**C**O)$_2$ units, respectively. Photolysis for 2 hr under a ^{13}CO atmosphere produced an enriched complex suitable for variable temperature studies. Figure V-6 presents the results of this study. On cooling the sample the upfield resonance for the Fe(CO)$_3$ unit broadens and completely coalesces at –50 °C. By –60 °C, two resonances begin to appear and are sharp by –70 °C. The low field resonance broadens but remains

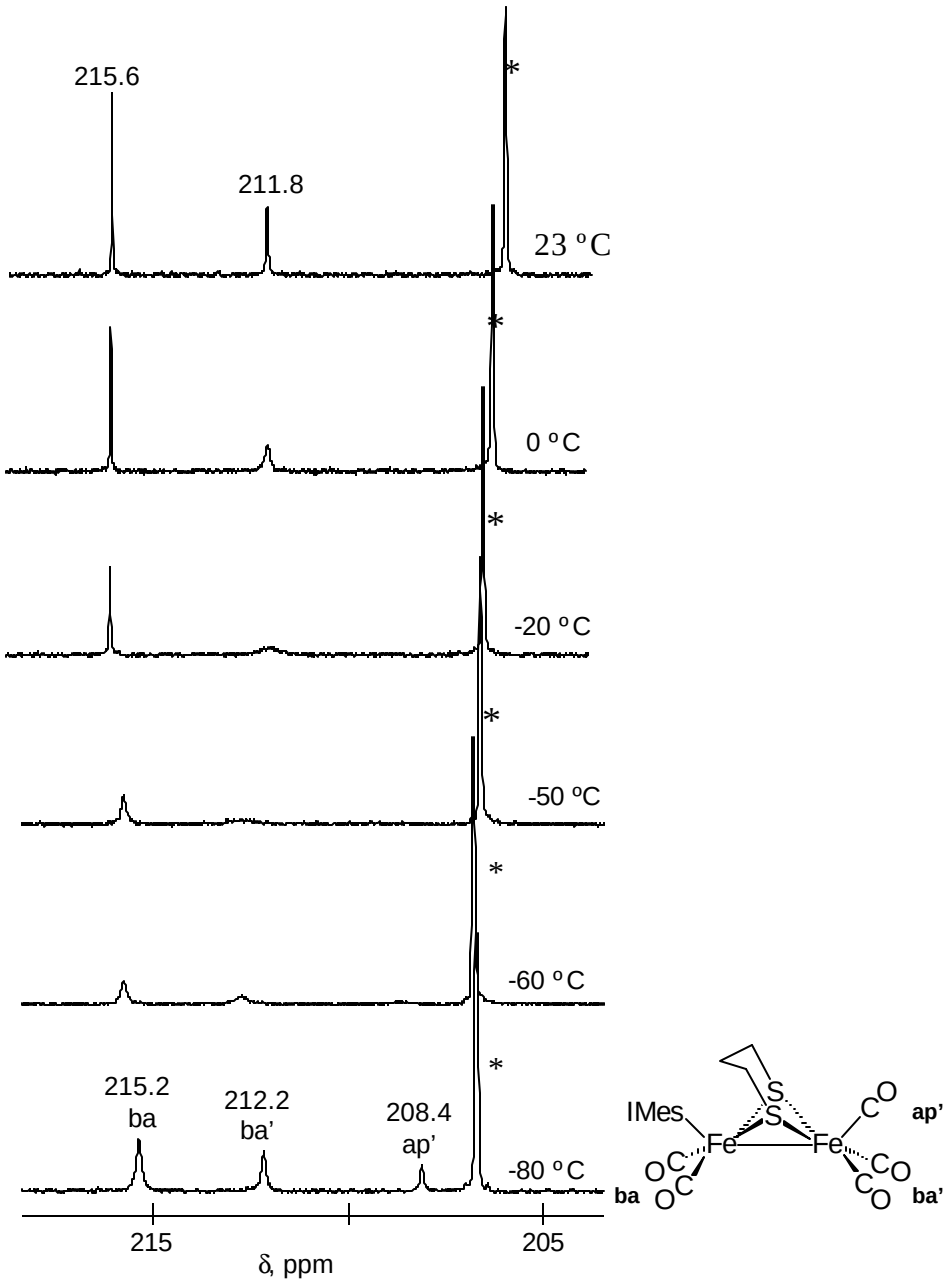

Figure V-6. Variable temperature ^{13}C NMR of (μ-pdt)[Fe(CO)$_3$][Fe(CO)$_2$IMes]. * Solvent peak, acetone-d$_6$.

distinct, maintaining its 215 – 216 ppm position. This resonance is assigned to the basal (ba) CO groups about Fe(1) while the two upfield resonances in the stopped-exchange region at 212.2 and 208.4 ppm are assigned to the basal (ba') and apical (ap') CO groups of Fe(2), as shown in Figure V-7.

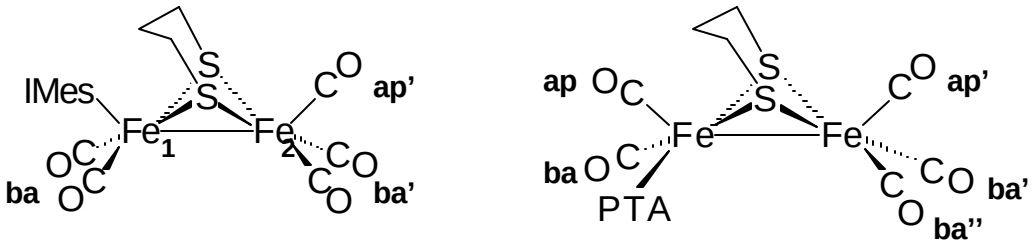

Figure V-7. Stick drawings of (μ-pdt)[Fe(CO)$_3$][Fe(CO)$_2$IMes and (μ-pdt)[Fe(CO)$_3$]-[Fe(CO)$_2$PTA] with the labels assigned to ^{13}C NMR resonances.

For the (μ-pdt)[Fe(CO)$_3$][Fe(CO)$_2$PTA] complex, whose stick drawing is shown in Figure V-7, the room temperature ^{13}C NMR spectrum in the carbonyl region consists of a singlet at 211.6 ppm assigned to the Fe(**C**O)$_3$ end, and a doublet at 213.5 ppm (J_{P-C} = 17.3 Hz) assigned to the Fe(**C**O)$_2$PTA end, Figure V-8. The fact that there is one resonance for the two CO ligands on the latter indicates that they are magnetically equivalent due to an intramolecular site exchange process that is rapid on the NMR time scale. We assume this fluxional behavior is that of a turnstile rotation of the Fe(CO)$_2$PTA end. On lowering the temperature the upfield signal broadens at a

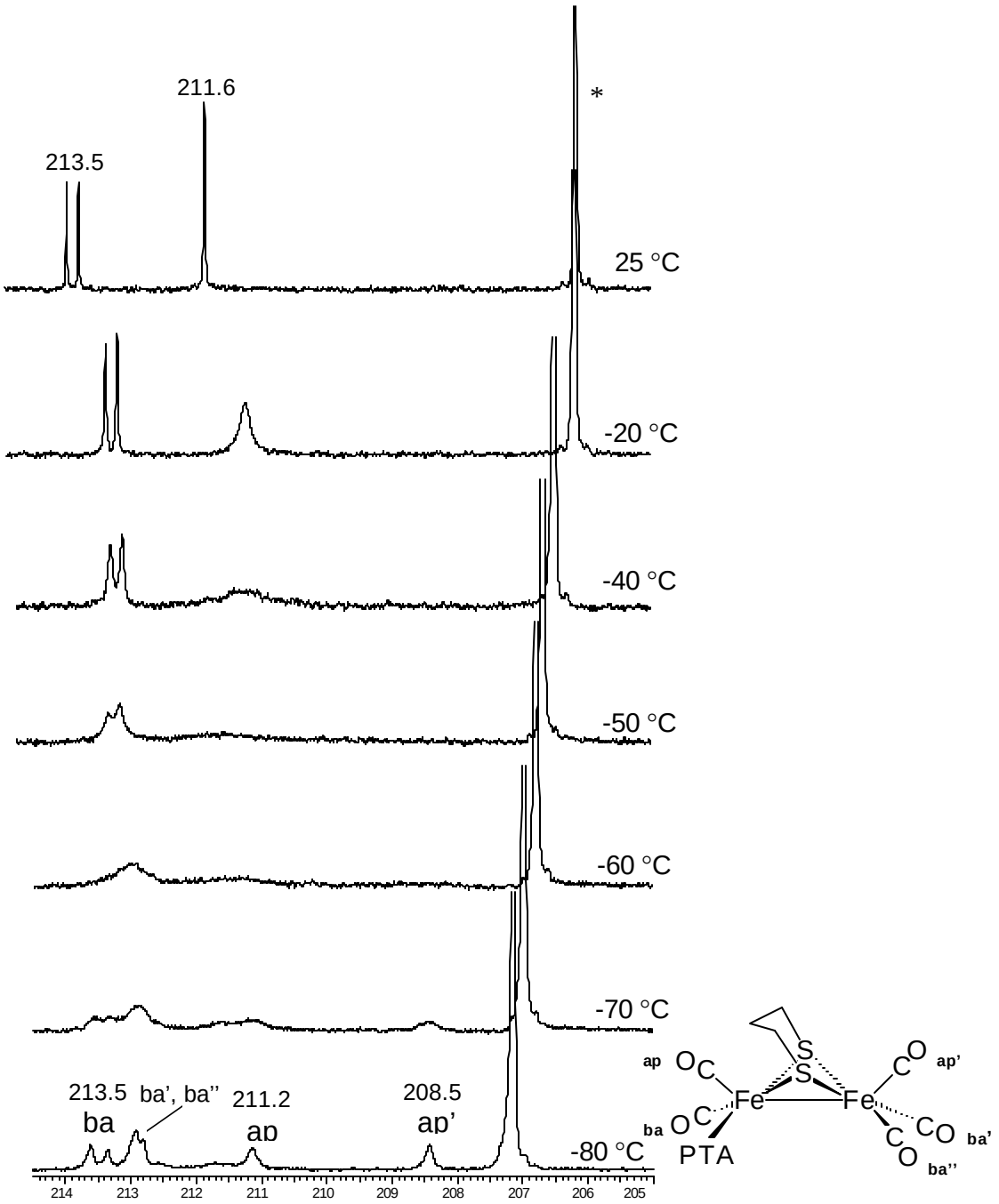

Figure V-8. Variable temperature ^{13}C NMR of (μ-pdt)[Fe(CO)$_3$][Fe(CO)$_2$PTA]. * Solvent peak, acetone-d$_6$.

faster rate than the downfield signal. By –50 °C the upfield signal has coalesced onto the base line, while the doublet is still distinguishable. At –70 °C new resonances are appearing, and at –80 °C, the low temperature limit, there are five distinct resonances present in the spectrum: a doublet at 213.5 ppm (J_{P-C} = 26.3 Hz), assigned to the basal (ba) CO in the $Fe(CO)_2PTA$ end; a singlet at 211.2 ppm assigned to the apical (ap) CO on the same iron center; a singlet at 208.5 ppm for the apical (ap') CO on the $Fe(CO)_3$ end; two overlapping singlets, one at 212.9 ppm, and the other at 212.8 ppm, assigned to the two basal (ba' and ba'') COs in the $Fe(CO)_3$ end. These two basal CO ligands on the $Fe(CO)_3$ end are non-equivalent due to the effect the PTA ligand has over them. The above individual NMR chemical shift assignments were based on results previously obtained by other members of this research group for the parent (μ-pdt)$[Fe(CO)_3]$ complex.[61]

Summarizing the variable temperature NMR studies it can be concluded that at room temperature intramolecular CO site exchange takes place at both ends in the monosubstituted (μ-pdt)$[Fe(CO)_3][Fe(CO)_2PTA]$. In contrast, the $Fe(CO)_3$ end in (μ-pdt)$[Fe(CO)_3][Fe(CO)_2IMes]$ exhibits fluxionality, while the $Fe(CO)_2IMes$ end is fixed, as no change in the chemical shift of the two CO ligands is observed in the NMR time scale even at 50 °C.

Computed and experimental values for the barrier for rotation ($\Delta G^{\neq}$) for the (μ-pdt)$[Fe(CO)_3][Fe(CO)_2IMes]$ and (μ-pdt)$[Fe(CO)_3][Fe(CO)_2PTA]$ complexes are listed in Table V-3. Experimental values were obtained using the coalescence temperature

Table V-3. Computed and Experimental Free Energy of Activation ($\Delta G^{\neq}$), kcal mol^{-1}, for the Rotation of $Fe(CO)_3$ Units in (μ-pdt)[$Fe(CO)_3$][$Fe(CO)_2L$] Complexes*

	Fe_a	Fe_b
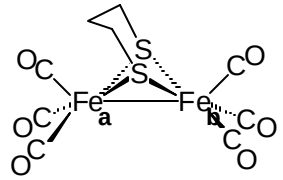	13.7 (10.4)	15.3 (10.4)
	Fe(CO)L	**$Fe(CO)_3$**
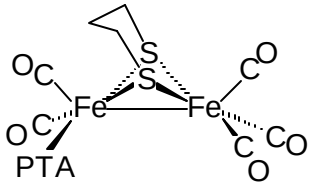	n/a (9.7)	n/a (9.4)
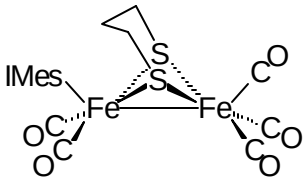	n/a	12.2 (10.1)
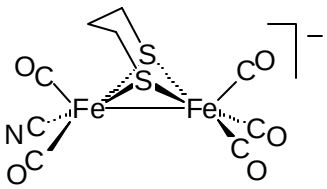	n/a	8.9 (n/a)

* Experimental values, determined using the coalescence temperature and equation V-1, are in parenthesis.

and equation V-1. Computed values were obtained through DFT calculations. It should be noted that the computed value listed for (μ-pdt)[Fe(CO)$_3$][Fe(CO)$_2$IMes], 12.20 kcal mol^{-1}, is the value obtained through computations that used a model which had hydrogens bound to the N atoms instead of mesityl groups. As can be seen in Table V-3 experimental values are lower than the computed ones by 2.1 to 4.9 kcal mol^{-1}, suggesting discrepancies of theory and experiments. Nevertheless, they are considered to be a reasonable approximation.

Comparison of experimental values show that substitution of one CO by a better donor ligand lowers the activation barrier for rotation for the Fe(CO)$_3$ unit in (μ-pdt)[Fe(CO)$_3$][Fe(CO)$_2$PTA], and (μ-pdt)[Fe(CO)$_3$][Fe(CO)$_2$IMes]. Such barriers go from 10.4 kcal mol^{-1} for the unencumbered end of the parent (μ-pdt)[Fe(CO)$_3$]$_2$ complex,[65] to 9.4 kcal mol^{-1} for (μ-pdt)[Fe(CO)$_3$][Fe(CO)$_2$PTA], and 10.1 kcal mol^{-1} for (μ-pdt)[Fe(CO)$_3$][Fe(CO)$_2$IMes]. This result is in agreement with a previous VT ^{13}C NMR study of {(μ-pdt)[Fe(CO)$_3$][Fe(CO)$_2$CN]}$^-$ that showed that one end of this molecule is still fluxional at –80 °C, while the other is not, indicating the lower barrier for rotation for the Fe(CO)$_3$ end in the monocyanide derivative.[79] However, it was expected that the barrier for rotation for (μ-pdt)[Fe(CO)$_3$][Fe(CO)$_2$IMes] would be smaller than the one for (μ-pdt)[Fe(CO)$_3$][Fe(CO)$_2$PTA], due to the fact that the IMes ligand is a better donor than phosphines; the inherent difficulty of the coalescence temperature method used to estimate the activation barrier for rotation could probably account for the disagreement.

Although only three computed values for the activation barrier for rotation of the $Fe(CO)_3$ unit in complexes of the type (μ-pdt)[$Fe(CO)_3$][$Fe(CO)_2L$] are available at the moment of this writing, Table V-3, a tentative comparison among them is appropriate. They show that this barrier decreases with increasing electron donating character of the ligand L. That is, $\Delta G^{\neq}[Fe(CO)_3]$ (L = CO) > (L = IMes) > ($L = CN^-$). Computations to extend the series and to enhance our understanding of the dynamic processes taking place on diiron dithiolate carbonyl complexes, are being conducted by Jesse Tye.

Electrochemistry of (μ-pdt)[$Fe(CO)_3$][$Fe(CO)_2$IMes]

Cyclic voltammetry of the complex (μ-pdt)[$Fe(CO)_3$][$Fe(CO)_2$IMes] was carried out in CH_3CN solution with *n*-Bu_4NBF_4 as supporting electrolyte, Figure V-9. The CV was started from the rest potential and proceeded in the anodic direction. It shows an irreversible reduction at –1.73 V vs. NHE. This reduction event is confidently assigned to a one-electron reduction process, $Fe^IFe^I + e^- \rightarrow Fe^0Fe^I$, based in extensive electrochemical studies for a series of Fe^IFe^I dithiolate complexes (see Chapter IV). The shift in potential to a more negative value relative to the parent compound (μ-pdt)[$Fe(CO)_3$]$_2$ (first reduction event at –1.34 V vs. NHE) is in agreement to the increased electron density in the Fe centers due to the superior electron donor ability of the IMes ligand over CO. The second reduction event that would take the complex to the Fe^0Fe^0 level is not observed within the solvent window.

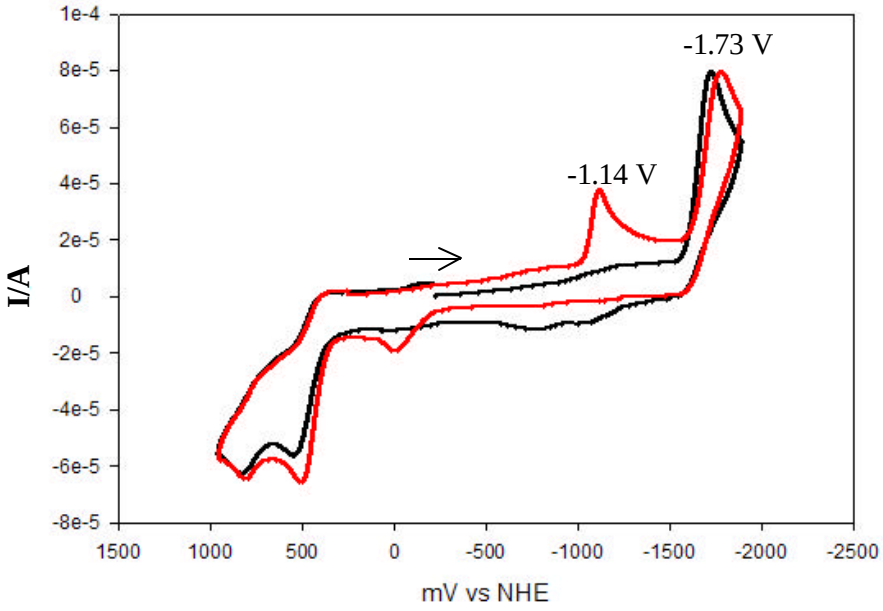

Figure V-9. Cyclic voltammograms of (μ-pdt)[Fe(CO)$_3$][Fe(CO)$_2$IMes] in CH_3CN, 0.1 M *n*-Bu_4NBF_4, in the absence of acid, and 1 eq CF_3SO_3H added.

Comparison of the cyclic voltammograms for the monosubstituted complexes (μ-pdt)[Fe(CO)$_3$][Fe(CO)$_2$IMes], and (μ-pdt)[Fe(CO)$_3$][Fe(CO)$_2$PTA] corroborates the increased electron donor ability of the IMes ligand over PTA. While the reductionj event occurs at –1.73 V for the former complex, it takes place at –1.54 V for the latter, a shift of 390 mV, and 200 mV, respectively, from the reduction of the all-CO parent complex. The $Fe^IFe^I + e^- \rightarrow Fe^0Fe^I$ reduction process for the disubstituted (μ-pdt)-[Fe(CO)$_2$PTA]$_2$, under the same experimental conditions, occurs at –1.78 V; the small

50 mV difference between the mono-IMes and the di-PTA complexes suggests that the electron richness of both diiron complexes is similar.

The cyclic voltammogram of (μ-pdt)[$Fe(CO)_3$][$Fe(CO)_2$IMes] in the presence of 1 eq of CF_3SO_3H (triflic acid) presented two major differences from the CV in the absence of acid, Figure V-9. The first reduction event occurred at –1.14 V vs. NHE. As this reduction does not take place in the absence of acid, our initial interpretation was that protonation of an Fe^I center could be occurring, and as reduction of a cationic species is expected to be more accessible, the more positive potential is reasonable. However, the ^1H NMR spectrum showed that this was not the case because the upfield resonance typical of a hydride was not present in the spectrum, *vide supra*. Thus, the cyclic voltammogram of the free IMes ligand, under identical conditions, was recorded as a control experiment. While in the absence of acid no reduction events are observed, when 1 eq of triflic acid was added the CV of the IMes ligand presented an irreversible wave at –1.00 V vs. NHE. Even though there is a 140 mV difference between this reduction event and the one at –1.14 V in (μ-pdt)[$Fe(CO)_3$][$Fe(CO)_2$IMes], we can conclude that the reduction is ligand based. The difference may be due to changes in the electronic environment of the IMes ligand upon coordination to the Fe center.

Cyclic voltammetry in the presence of acetic acid was conducted to determine the electrocatalytic production of H_2 by (μ-pdt)[$Fe(CO)_3$][$Fe(CO)_2$IMes] when a weak acid is added. Figure V-10 shows the results of this study. The reduction event that

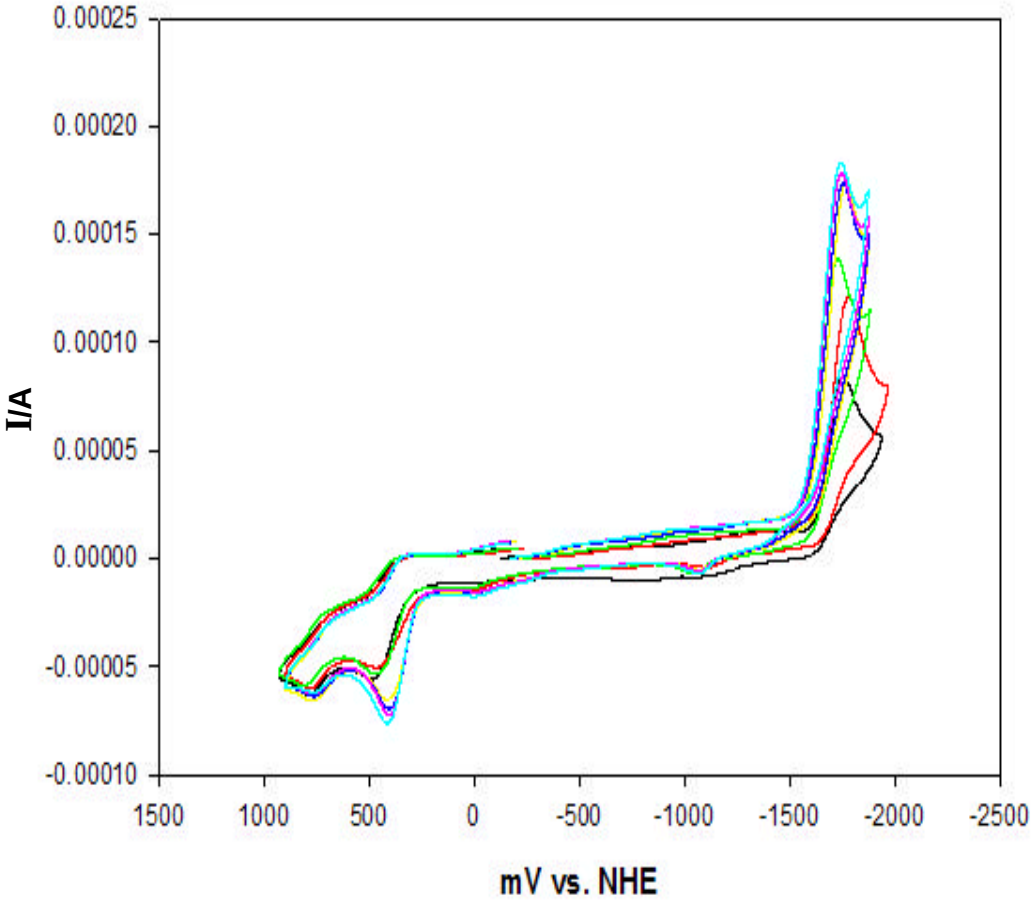

Figure V-10. Cyclic voltammetry of (μ-pdt)[Fe(CO)$_3$][Fe(CO)$_2$IMes], 2.5 mM solution in CH_3CN (0.1 M *n*-Bu_4NBF_4 as supporting electrolyte), 0 eq HOAc 5 eq HOAc, 10 eq HOAc, 20 eq HOAc, 30 eq HOAc, 40 eq HOAc, 50 eq HOAc.

occured at −1.14 V in the presence of triflic acid is not present in this case, suggesting that the ligand based reduction might be due to a protonated species formed only upon addition of a strong acid. The $Fe^{I}Fe^{I} + e^{-} \rightarrow Fe^{0}Fe^{I}$ event in the presence of acetic acid takes place at −1.73 V vs. NHE. Adding 5, 10, and 20 eq of HOAc to a 2.5 mM solution in CH_3CN (0.1 M *n*-Bu_4NBF_4) increases the current of the reduction wave, indicating that an electrocatalytic process is occurring. Further addition of HOAc (30, 40, and 50 eq) does not have any effect. More in depth studies of the electrochemical processes taking place upon addition of HOAc to (μ-pdt)[$Fe(CO)_3$][$Fe(CO)_2$IMes] are required in order to be able to identify possible reaction intermediates and to quantify the catalytic activity of this complex in the production of H_2.

CHAPTER VI

CONCLUSIONS

The understanding of the factors that affect the reactivity of metal complexes is a prerequisite for a chemist to be able to design a model compound that mimics the function of an enzyme's active center. The ultimate goal would be the synthesis of a metal complex that participates in catalytic reactions in a reversible manner, and by "disturbing" the system, in other words, varying the experimental conditions, favor the reactivity in one direction or the other.

My graduate research at the Chemistry Department of Texas A&M University was directed towards the understanding of the effects that different ligands coordinated to the iron atoms in model complexes for the [Fe]H_2ase active site might have. To attempt to understand how asymmetry might affect different fundamental properties of diiron complexes, the monosubstituted (μ-pdt)[$Fe(CO)_3$][$Fe(CO)_2$PTA](PTA = 1,3,5-triaza-7-phosphaadamantane; pdt = SC_3H_6S) and (μ-pdt)[$Fe(CO)_3$][$Fe(CO)_2$IMes] (IMes = 1,3-bis- (2,4,6-trimethylphenyl)imidazol-2-ylidene) were prepared. The disubsituted (μ-pdt)[$Fe(CO)_2PTA]_2$, and its protonated and methylated derivatives, were also synthesized and investigated as electrocatalysts for H_2 production.

The study of [(μ-SEt)$Fe(CO)_2L]_2$ complexes has expanded fundamental knowledge that might provide a plausible explanation for the three light atom chain bridging the sulfurs in the active center of [Fe]H_2ase rather than monodentate thiolates.

As the dinuclear active site of [NiFe]H_2ase contains two cysteine sulfurs which bridge nickel and iron, it is curious that the iron-only hydrogenase is different. Features of the $[(\mu\text{-SEt})Fe(CO)_3]_2$ and $(\mu\text{-pdt})[Fe(CO)_3]_2$ are largely the same with respect to: 1) electron richness, as indicated by the infrared spectrum in the CO region; 2) intramolecular CO site exchange; and, 3) electrochemical properties and H_2 production. They differ in the orientation of the carbons attached to sulfurs; the SRS moieties are in the *syn'* conformation and the carbons are pulled back and away from the coordination sphere. In contrast, in the monodentate thiolates the attached carbons are oriented downwards into the coordination sphere. This provides a steric hindrance to substituents in the basal position of individual square pyramids. Whether there is a definite advantage of apical vs. basal substituents in the active site of the enzyme is not known. Hence from our studies one might conclude that two monodentate μ-SR would work equally well as a μ-SRS. Some possible reasons for nature's choice of ligands present in [Fe]H_2ase are as follows: 1) the active center in the hydrogenase enzyme was formed with what was available at that point in the evolutionary path, which was largely organometallic-like chemistry; and, 2) on another level of evolution, it could be possible that at the beginning of the existence of [Fe]H_2ases, the active center actually contained sulfurs from cysteine. However, evolution has modified them to have the bridging thiolate present at this time, perhaps because it improves the stability of the enzyme, or because it enhances the catalytic activity.

The electrocatalytic production of H_2 studies found that the diiron complexes studied follow different mechanisms for the production of H_2 dependent on the strength

of the acid source and the extent of CO/phosphine substitution. The all-CO complexes produce H_2 at their second reduction event, $Fe^IFe^0 \rightarrow Fe^0Fe^0$, which occurs at ca. –1.9 V. An EECC mechanism accounts for the H_2 production mediated by these compounds. In the other hand, the phosphine derivatives, PMe_3 and PTA, produce H_2 from its first reduction event, $Fe^IFe^I \rightarrow Fe^0Fe^I$, following an ECCE mechanism. These results indicate that sufficient electron density at the Fe-Fe bond has to be achieved for the compound to undergo the oxidative addition of a proton from a weak acid. Good electron donors, phosphines for example build up the electron density in the diiron complex, so this species accepts the proton from HOAc at the Fe^IFe^0 oxidation level, while the all-CO complex requires another electron, to achieving the Fe^0Fe^0 level, to accomplish the same result.

The curve-crossing phenomenon present in the cyclic voltammogram of $\{(\mu\text{-pdt})[Fe(CO)_2(PTA\cdot H)]_2\}(PF_6)_2$ in the mixed solvent system $CH_3CN:H_2O$ 3:1 indicates the reduction of a species that forms after the cathodic scan and reduction of the Fe^IFe^I complex. Although characterization of such species has not been accomplished at the time of this writing, the proposed intermediate in the catalytic cycle, Scheme VI-1, the $(\eta^2\text{-}H_2)Fe^{II}Fe^I$ species, is a reasonable candidate.

Scheme VI-1

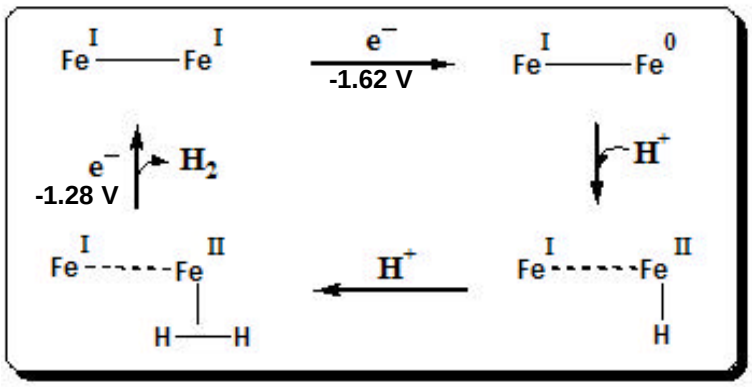

Precedence for the formation of the $(\eta^2\text{-}H_2)Fe^{II}Fe^{I}$ by successive protonations at an Fe^0 center comes from the work of Morris and coworkers.[80] Scheme VI-2 presents the analogy to his work. In this analogy the {(pdt)Fe(CO)$_2$L} moiety in our diiron complexes is viewed as a 4-electron donor ligand that stabilizes the $(\eta^2\text{-}H_2)Fe^{II}$ species in the same way as the diphosphine in Morris' compounds.

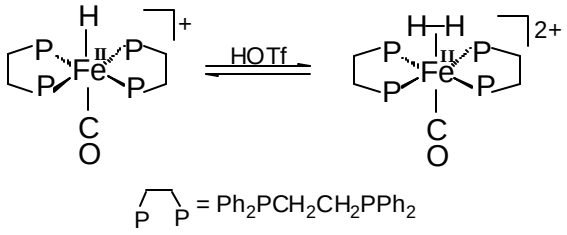

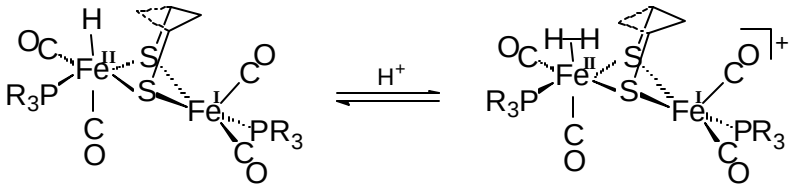

The efficiency of the diiron complexes in the production of H_2 was assessed in terms of the TON, turnover number, and the potential at which H_2 is produced. In the series of catalysts studied, the asymmetric complex $(\mu\text{-pdt})[Fe(CO)_3][Fe(CO)_2PTA]$ produces H_2 at the most positive potential, -1.54 V. However, the TON/h for this complex is only 7, the smallest for the series.

Lowering the overvoltage in the production of H_2 is of great importance to move closer to natural conditions, pH 7, and ca –400 mV. A step in this direction was possible by the addition of H_2O to CH_3CN in the electrochemical studies of $(\mu\text{-pdt})[Fe(CO)_2L]_2$, L = PTA, PTA· H^+, and PTA· Me^+. Reduction of these complexes in CH_3CN:H_2O mixtures is shifted to more positive potentials by 100-250 mV as compared to the pure acetonitrile solutions.

The assignment of oxidation states to the iron centers in the active site of [Fe]H_2ase has not been an easy task. Results from FTIR, EPR, and Mossbaüer studies,[5b,42,43,81] along with theoretical calculations,[82] and with results obtained through the study of model complexes,[7a-d] have been combined to give a consensus in assignment of redox levels to the different states of the enzyme. The H-cluster from the as-isolated, fully oxidized, inactive enzyme has been assigned an $Fe^{II}Fe^{II}$ redox level. Partial reduction takes the $H_{as\text{-}isolated}$ to the oxidized, active form, H_{ox}, which is in a mixed valent, EPR active state assigned as $Fe^{II}Fe^{I}$ redox level. Further reduction of [Fe]H_2ase forms the fully reduced $Fe^{I}Fe^{I}$ state, H_{red}. Dihydrogen uptake or proton binding for the production of H_2 occurs at this mixed valent state.

The mechanisms that we propose for H_2 production involve an Fe^0Fe^I redox level that has not been observed or identified in [Fe]H_2ase. Nevertheless, the protonated H-$Fe^{II}Fe^I$ species, which is a proposed intermediate in the mechanism, is possibly the mixed valent species observed in the enzyme. In the proposed ECCE mechanism for H_2 production using the "low-valent" route of Scheme IV-2a, reproduced in abbreviated form below, three of the likely species are congruent with observed redox levels of the enzyme active site. Experimental evidence has been garnered for two of the redox levels of the model system. We conclude that this is a very reasonable biomimic.

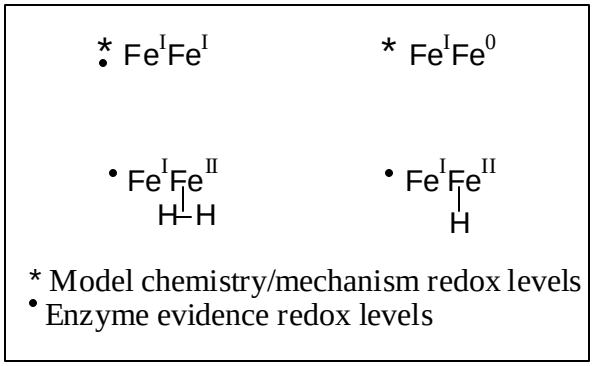

Our goal for the asymmetric complexes was to address the effect of the substituent donor ligand on the barrier to intramolecular site exchange in the $Fe(CO)_3$ terminus. Consistent with earlier work that shows cyanide substitution lowered the barrier in $\{(\mu\text{-pdt})[Fe(CO)_3][Fe(CO)_2CN]\}^-$, the $(\mu\text{-pdt})[Fe(CO)_3][Fe(CO)_2PTA]$ and $(\mu\text{-pdt})[Fe(CO)_3][Fe(CO)_2IMes]$ complexes had a similar yet smaller effect. Theoretical calculations have been performed by Irene Georgakaki, former student in

this group, in collaboration with Drs. Lisa Perez and Michael B. Hall of the Laboratory for Molecular Simulation, TAMU, and currently continued by Jesse Tye. These computations show that the transition state for the $Fe(CO)_3$ rotation that interconverts the apical and basal CO groups is highly similar to the ground state of the enzyme active site. Thus we conclude that the protein matrix, and resultant directed H-bonding, assists in holding a conformation that would relax to what we see in the models were the active site released from the protein. Comparison of experimental and computed values for the activation energy for rotation of the $Fe(CO)_3$ units in (μ-pdt)$[Fe(CO)_2L][Fe(CO)_3]$ (L = CO, PTA, IMes) complexes shows that good electron donors lower this barrier. That is, as in the stick drawing shown below, a donor ligand in the apical position should stabilize the $Fe \rightarrow CO_{bridging}$ interaction.

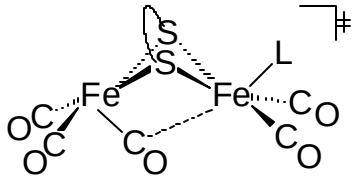

REFERENCES

(1) Lippard, S. J.; Berg, J. M., In *Principles of Bioinorganic Chemistry*; University Science Books: Mill Valley, California, 1994.

(2) (a) Adams, M. W. W.; Mortenson, L. E.; Chen, J.-S. *Biochim. Biophys. Acta* **1981**, *594*, 105. (b) Albracht, S. P. J. *Biochim. Biophys. Acta* **1994**, *1188*, 167. (c) Adams, M. W. W. *Biochim. Biophys. Acta* **1990**, *1020*, 115.

(3) Geirstanger, B. H.; Prasch, T.; Griesinger, C.; Hartmann, G.; Buurman, G.; Thauer, R. K. *Angew. Chem. Int. Ed. Engl.* **1998**, *37*, 3300.

(4) (a) Peters, J. W.; Lanzilotta, W. N.; Lemon, B. J.; Seefeldt, L. C. *Science* **1998**, *282*, 1853. (b) Lemon, B. J.; Peters, J. W. *Biochemistry* **1999**, *38*, 12969.

(5) (a) Nicolet, Y.; Piras, C.; Legrand, P.; Hatchikian, C. E.; Fontecilla-Camps, J. C. *Structure* **1999**, *7*, 13. (b) Nicolet, Y.; De Lacey, A. L.; Vernéde, X.; Fernandez, V. M.; Hatchikian, E. C.; Fontecilla-Camps, J. C. *J. Am. Chem. Soc.* **2001**, *123*, 1596.

(6) Fan, H.-J.; Hall, M. B. *J. Am. Chem. Soc.* **2001**, *123*, 3828.

(7) a) Lyon, E. J.; Georgakaki, I. P.; Reibenspies, J. H.; Darensbourg, M. Y. *Angew. Chem. Int. Ed. Engl.* **1999**, *38*, 3178. b) Lyon, E. J.; Georgakaki, I. P.; Reibenspies, J. H.; Darensbourg, M. Y. *J. Am. Chem. Soc.* **2000**, 123, 3268. c) Schmidt, M.; Contakes, S. M.; Rauchfuss, T. B. *J. Am. Chem. Soc.* **1999**, *121*, 9736. d) Le Cloirec, A.; Best, S. P.; Borg, S.; Davies, S. C.; Evans, D. J.; Hughes, D. L.; Pickett, C. J.; *Chem. Commun.* **1999**, 2285. e) Zhao, X;

Georgakaki, I. P.; Miller, M. L.; Yarbrough, J. C.; Darensbourg, M. Y. *J. Am. Chem. Soc.* **2001**, *123*, 9710.

(8) Zhao, X.; Georgakaki, I. P.; Miller, M. L.; Mejia-Rodriguez, R.; Chiang, C.-Y.; Darensbourg, M. Y. *Inorg. Chem.* **2002**, 41, 3917.

(9) Razavet, M.; Davies, S. C.; Hughes, D. L.; Pickett, C. J. *Chem. Commun.* **2001**, 847.

(10) Razavet, M.; Borg, S. J.; George, S. J.; Best, S. P; Fairhurst, S. A.; Pickett, C. J. *Chem. Commun.* **2002**, 700.

(11) Lawrence, J. D.; Li, H.; Rauchfuss, T. B.; Bénard, M.; Rohmer, M-M. *Angew. Chem., Int. Ed. Engl.* **2001**, *40*, 1768.

(12) Gloaguen, F.; Lawrence, J. D.; Rauchfuss, T. B. *J. Am. Chem. Soc.* **2001**, *123*, 9476.

(13) (a) Ott, S.; Kritikos, M.; Åkermark, B.; Sun, L. *Angew. Chem., Int. Ed. Engl.* **2003**, *42*, 3285. (b) Ott, S.; Kritikos, M.; Åkermark, B.; Sun, L.; Lomoth, R. *Angew. Chem., Int. Ed. Engl.* **2004**, *43*, 1006.

(14) Cammack, R. *Nature* **1999**, *397*, 214.

(15) (a) Tatsumi, H.; Takagi, K.; Fujita, M.; Kano, K.; Ikeda, T. *Anal. Chem.* **1999**, *71*, 1753. (b) Morozov, S. V.; Vignais, P. M.; Cournac, L.; Zorin, N. A.; Karyakina, E. E.; Karyakin, A. A.; Cosnier, S. *Int. J. Hydrogen Energy*. **2002**, *27*, 1501.

(16) Jones, A. K.; Sillery, E.; Albracht, S. P.; Armstrong, F. A. *Chem. Commun.* **2002**, 866.

(17) Seyferth, D.; Womack, G. B.; Gallagher, M. K.; Cowie, M.; Hames, B. W.; Fackler, J. P. Jr.; Mazany, A. M. *Organometallics* **1987**, *6*, 283.

(18) Daigle, D. J. *Inorg. Synth.* **1998**, *32*, 40.

(19) *SMART 1000 CCD*; Bruker Analytical X-ray Systems: Madison, WI, 1999.

(20) *SAINT-Plus*, version 6.02; Bruker: Madison, WI, 1999.

(21) Sheldrick, G. *SHELXS-97*: *Program for Crystal Structure Solution*; Institüt für Anorganische Chemie der Universität: Gottingen, Germany, 1986.

(22) Sheldrick, G. *SHELXL-97: Program for Crystal Structure Refinement*; Institüt für Anorganische Chemie der Universität: Gottingen, Germany, 1977.

(23) *SHELXTL*, version 5.1 or later; Bruker: Madison, WI, 1998.

(24) Gagné, R. R.; Koval, C. A.; Lisensky, G. C. *Inorg. Chem.* **1980**, *19*, 2854.

(25) Arduengo III, A. J.; Dias, H. V. R.; Harlow, R. L.; Kline, M. *J. Am. Chem. Soc.* **1992**, *114*, 5530.

(26) Seyferth, D.; Henderson, R. S.; Song, L.-C. *Organometallics* **1982**, *1*, 125.

(27) King, R. B. *J. Am. Chem. Soc.* **1962**, *84*, 2460.

(28) King, R. B. *J. Am. Chem. Soc.* **1963**, *85*, 1584.

(29) Lyon, E. J. PhD Dissertation, December 2000, Texas A&M University.

(30) Maresca, L.; Greggio, F.; Sbrignadello, G.; Bor, G. *Inorg. Chim. Acta* **1971**, *5*, 667.

(31) Dahl, L.; Wei, C.-H. **1963**, *2*, 328.

(32) Katser, S. B.; Antsyskina, A. S.; Katugin, A. S.; Abdullaev, A. S. *Koord. Khim*. **1987**, *13*, 1132.

(33) Delgado, E.; Hernández, E.; Mansilla, N.; Zamora, F.; Martínez-Cruz, L.-A. *Inorg. Chim. Acta* **1999**, *284*, 14.

(34) Mueting, A.; Mattson, B. M. *J. Inorg. Nucl. Chem.* **1981**, *43*, 749.

(35) Kettle, S. F. A.; Orgel, L. E. *J. Chem. Soc.* **1960**, *82*, 3890.

(36) Lagadec, A.; Dabard, R.; Misterkiewicz, B.; Le Rouzic, A.; Patin, H. *J. Organomet. Chem.* **1987**, *326*, 381.

(37) Adams, R. D.; Cotton, F. A.; Cullen, W. R.; Hunter, D. L.; Mihichuk, L. *Inorg. Chem.* **1975**, *14*, 1395.

(38) Le Borgne, G.; Grandjean, D.; Mathieu, R.; Poilblanc, R. *J. Organomet. Chem.* **1977**, *131*, 429.

(39) (a) Sellmann, D.; Geipel, F.; Moll, M. *Angew. Chem., Int. Ed. Engl.* **2000**, *39*, 561. (b) Sellmann, D.; Fürsattell, A. *Angew. Chem. Int., Ed. Engl.* **1999**, *38*, 6060.

(40) (a) Holm, R. H.; Kennepohl, P.; Solomon, E. I. *Chem. Rev.* **1996**, *96*, 2239. (b) Butt, J. N.; Filipiak, M.; Hagen, W. R. *Eur. J. Biochem.* **1997**, *245*, 116.

(41) Adams, M. W. W.; Stiefel, E. I. *Science* **1998**, *282*, 1842.

(42) Popescu, C. V.; Münck, E. *J. Am. Chem. Soc.* **1999**, *121*, 7877.

(43) De Lacey, A. L.; Stadler, C.; Cavazza, C.; Hatchikian, E. C.; Fernandez, V. M. *J. Am. Chem. Soc.* **2000**, *122*, 11232.

(44) Bennet, B.; Lemon, B. J.; Peters, J. W. *Biochemistry* **2000**, *39*, 7455.

(45) Gloaguen, F.; Lawrence, J. D.; Rauchfuss, T. B.; Bénard, M.; Rohmer, M-M. *Inorg. Chem.* **2002**, *41*, 6573-6582.

(46) Georgakaki, I. P.; Miller, M. L.; Darensbourg, M. Y. *Inorg. Chem.* **2003**, *42*, 2489.

(47) Kubas, G. J. *Metal Dihydrogen and σ-Bond Complexes; Structure, Theory, and Reactivity*, Kluwer Academic/Plenum Publishers: New York 2001.

(48) Darensbourg, D. J.; Decuir, T. J.; Stafford, N. W.; Robertson, J. B.; Draper, J. D.; Reibenspies, J. H. *Inorg. Chem.* **1997**, *36*, 4218.

(49) (a) Fisher, K. J.; Alyea, E. C.; Shahnazarian, N. *Phosphorus, Sulfur and Silicon* **1990**, *48*, 37-40 (b) Darensbourg, D. J.; Robertson, J. B.; Larkins, D. L.; Reibenspies, J. H. *Inorg. Chem.* **1999**, *38*, 2473-2481.

(50) Geary, W. J. *Coord. Chem. Rev.* **1971**, *7*, 81.

(51) Razavet, M.; Davies, S. C.; Hughes, D. L.; Barclay, J. E.; Evans, D. J.; Fairhurst, S. A.; Liu, X.; Pickett, C. J. *J. Chem. Soc., Dalton Trans.* **2003**, 586.

(52) Bard, A. J. *Electrochemical Methods: Fundamentals and Applications*, Wiley: New York, 2001.

(53) Izutsu, K. *Acid-Base Dissociation Constants in Dipolar Aprotic Solvents*; Blackwell Scientific Publications: Oxford, 1990; Vol. 35.

(54) Koelle, U.; Ohst, S. *Inorg. Chem.* **1986**, *25*, 2689.

(55) Tomita, Y.; Teruya, S.; Koga, O.; Hori, Y. *J. Electrochem. Soc.* **2000**, *147*, 4164.

(56) Reich, H. J.; Cohen, M. L. *J. Org. Chem.* **1979**, *44*, 3148.

(57) Houmam, A.; Hamed, E. M.; Still, I. W. J. *J. Am. Chem. Soc.* **2003**, *125*, 7258.

(58) Kuchynka, D. J.; Kochi, J. K. *Inorg. Chem.* **1988**, *27*, 2574.

(59) Saveant, J. M. *Acc. Chem. Res.* **1980**, 323.

(60) Flood, T. C.; DiSanti, F. J.; Campbell, K. D. *Inorg. Chem.* **1978**, *17*, 1643.

(61) Lyon, E. J.; Georgakaki, I. P.; Reibenspies, J. H.; Darensbourg, M. Y. *J. Am. Chem. Soc.* **2001**, *123*, 3268.

(62) Drago, R. S. *Physical Methods for Chemists*, 2nd ed.; Saunders College Publishing: Ft. Worth, TX, 1992; p 291-295.

(63) Kessler, H. *Angew. Chem., Int. Ed. Engl.* **1970**, *9*, 219.

(64) gNMR 5.0, Adept Scientific plc, UK.

(65) Georgakaki, I. P.; Thomson, L. M.; Lyon, E. J.; Hall, M. B.; Darensbourg, M. Y. *Coord. Chem. Rev.* **2003**, *238-239*, 255-266.

(66) Herrmann, W. A. *Angew. Chem., Int. Ed. Eng.* **2002**, *41*, 1290.

(67) Huang, J.; Nolan, S. P. *J. Am. Chem. Soc.* **1999**, *121*, 9889.

(68) Huang, J.; Schanz, H. J.; Stevens, E. D.; Nolan, S. P. *Organometallics* **1999**, *18*, 2370.

(69) Weskamp, T.; Kohl, F. J.; Hieringer, W.; Gleich, D.; Herrmann, W. A. *Angew. Chem., Int. Ed. Eng.* **1999**, *38*, 2416.

(70) a) Lappert, M. F.; Pye, P. L. *J. Chem. Soc., Dalton Trans.* **1977**, 2172. b) Lappert, M. F.; MacQuitty, J. J.; Pye, P. L. *J. Chem. Soc., Chem. Commun.* **1977**, 411. c) Lappert, M. F.; MacQuitty, J. J.; Pye, P. L. *J. Chem. Soc., Dalton Trans.* **1981**, 1583. d) Hitchcock, P. B.; Lappert, M. F.; Thomas, S. A.; Thorne, A. J.; Carty, A. J.; Taylor, N. J. *J. Organomet. Chem.* **1986**, *315*, 27.

(71) Öfele, K.; Herrmann, W. A.; Mihalios, D.; Elison, M.; Herdtweck, E.; Scherer, W.; Mink, J. *J. Organomet. Chem.* **1993**, *459*, 177.

(72) Louie, J.; Grubbs, R. H. *J. Chem. Soc., Chem. Commun.* **2000**, 1479.

(73) Buchgraber, P.; Toupet, L.; Guerchais, V. *Organometallics* **2003**, *22*, 5144-5147.

(74) a) Bourissou, D.; Guerret, O.; Gabbaï , F. P.; Bertrand, G.*Chem. Rev.* **2000**, *100*, 39. b) Huang, J.; Stevens, E. D.; Nolan, S. P.; Petersen, J. L. *J. Am. Chem. Soc.* **1999**, *121*, 2674. c) Scholl, M.; Trnka, T. M.; Morgan, J. P.; Grubbs, R. H. *Tetr. Lett.* **1999**, *40*, 2247.

(75) De Beer, J. A.; Haines, R. J.; Greatrex, R.; Greenwood, N. N. *J. Chem Soc. (A)* **1971**, 3271-3282.

(76) Gloaguen, F.; Lawrence, J. D.; Schmidt, M.; Wilson, S. R.; Rauchfuss, T. B. *J. Am. Chem. Soc.* **2001**, *123*, 12518-12527.

(77) Lotz, S.; Van Rooyen, P. H.; Van Dyk, M. M. *Organometallics* **1987**, *6*, 409-505.

(78) Denk, M. K.; Rodezno, J. M.; Gupta, S.; Lough, A. J. *J. Organomet. Chem.* **2001**, *617-618*, 242.

(79) Georgakaki, I. P. PhD Dissertation, December 2002, Texas A&M University.

(80) Forde, C. E.; Landau, S. E.; Morris, R. H. *J. Chem. Soc., Dalton Trans.* **1997**, 1663.

(81) (a) Nicolet, Y.; Cavazza, C.; Fontecilla-Camps, J. C. *J. Inorg. Biochem.* **2002**, *91*, 1. (b) Pereira, A. S.; Tavares, P.; Moura, I.; Moura, J. J. G.; Huynh, B. H. *J.*

Am. Chem. Soc. **2001**, *123*, 2771. (c) Bennett, B.; Lemon, B. J.; Peters, J. W. *Biochemistry* **2000**, *39*, 7455. (d) Adams, M. M. W. *J. Biol. Chem.* **1987**, *262*, 15054.

(82) Cao, Z.; Hall, M. B. *J. Am. Chem. Soc.* **2001**, *123*, 3734.

APPENDIX

Table A-1. Crystal Data and Structure Refinement for $(\mu\text{-SEt})_2[Fe(CO)_2(PMe_3)]_2$

Empirical formula	$C_{14}H_{28}Fe_2O_4P_2S_2$	
Formula weight	498.12	
Temperature	110(2) K	
Wavelength	0.71073 Å	
Crystal system	Triclinic	
Space group	P-1	
Unit cell dimensions	a = 10.474(2) Å	α= 75.656(4)°.
	b = 14.233(3) Å	β= 89.180(4)°.
	c = 15.932(3) Å	γ = 86.004(3)°.
Volume	2295.6(8) $Å^3$	
Z	4	
Density (calculated)	1.441 Mg/m^3	
Absorption coefficient	1.598 mm^{-1}	
Theta range for data collection	1.32 to 28.32°.	
Index ranges	-13<=h<=13, -18<=k<=18, -14<=l<=21	
Reflections collected	14722	
Independent reflections	10372 [R(int) = 0.0691]	
Refinement method	Full-matrix least-squares on F^2	
Data / restraints / parameters	10372 / 0 / 449	
Goodness-of-fit on F^2	0.634	
Final R indices [I>2sigma(I)]	R1 = 0.0453, wR2 = 0.1159	
R indices (all data)	R1 = 0.0636, wR2 = 0.1317	
Largest diff. peak and hole	0.869 and -1.088 $e.Å^{-3}$	

Table A-2. Atomic coordinates (x 10^4) and equivalent isotropic displacement parameters ($Å^2$x 10^3) for $(\mu\text{-SEt})_2[Fe(CO)_2(PMe_3)]_2$. U(eq) is defined as one third of the trace of the orthogonalized U^{ij} tensor

	x	y	z	U(eq)
Fe(1B)	7249(1)	4760(1)	2180(1)	18(1)
Fe(1A)	2652(1)	10456(1)	2120(1)	18(1)
Fe(2A)	4463(1)	9487(1)	3022(1)	17(1)
Fe(2B)	9140(1)	5462(1)	2701(1)	20(1)
S(1A)	3371(1)	8938(1)	2036(1)	18(1)
S(2B)	8939(1)	3834(1)	2918(1)	21(1)
S(1B)	8987(1)	5227(1)	1347(1)	24(1)
S(2A)	2380(1)	9515(1)	3484(1)	22(1)
P(2A)	5304(1)	8064(1)	3793(1)	23(1)
P(2B)	11246(1)	5579(1)	2756(1)	29(1)
P(1B)	6512(1)	3603(1)	1646(1)	25(1)
P(1A)	619(1)	10494(1)	1738(1)	26(1)
O(3A)	6631(2)	10017(2)	1889(2)	37(1)
O(2B)	5584(2)	4600(2)	3679(2)	36(1)
C(2B)	6246(3)	4646(2)	3090(2)	23(1)
O(4A)	5210(3)	10741(2)	4097(2)	41(1)
O(1B)	5543(2)	6354(2)	1213(2)	38(1)
C(13B)	8550(3)	3223(2)	4033(2)	28(1)
O(2A)	2713(3)	12248(2)	2689(2)	47(1)
C(4A)	4928(3)	10228(2)	3678(2)	25(1)
C(3A)	5769(3)	9795(2)	2339(2)	23(1)
C(1B)	6236(3)	5728(2)	1592(2)	25(1)
O(3B)	8386(3)	7526(2)	2138(2)	45(1)

Table A-2 (continued)

C(1A)	3266(3)	11044(2)	1110(2)	26(1)
O(1A)	3639(3)	11449(2)	443(2)	46(1)
C(13A)	2009(4)	10260(2)	4258(2)	31(1)
C(11A)	4262(3)	8919(2)	1050(2)	24(1)
O(4B)	8505(3)	5495(2)	4477(2)	40(1)
C(2A)	2667(3)	11542(2)	2464(2)	28(1)
C(4B)	8773(3)	5475(2)	3780(2)	25(1)
C(8A)	5525(3)	7119(2)	3211(2)	31(1)
C(10B)	11781(4)	6272(3)	3476(3)	45(1)
C(9A)	4413(4)	7472(3)	4743(2)	45(1)
C(7B)	4935(4)	3844(3)	1151(3)	50(1)
C(3B)	8705(3)	6710(2)	2361(2)	29(1)
C(12A)	3347(4)	8881(3)	329(2)	37(1)
C(14A)	1747(4)	9628(3)	5142(2)	35(1)
C(10A)	6897(4)	8069(3)	4228(3)	46(1)
C(12B)	8272(4)	6157(3)	-325(2)	44(1)
C(14B)	9753(4)	2868(3)	4569(2)	36(1)
C(5A)	4(4)	9327(3)	1769(4)	55(1)
C(11B)	8691(4)	6356(3)	511(2)	35(1)
C(6B)	6288(4)	2458(2)	2438(3)	39(1)
C(6A)	-518(4)	11011(4)	2399(3)	53(1)
C(5B)	7507(5)	3219(3)	833(3)	57(1)
C(7A)	175(4)	11184(3)	649(3)	56(1)
C(9B)	12236(4)	4450(3)	3105(4)	78(2)
C(8B)	11979(5)	6168(4)	1747(3)	66(2)

Table A-3. Bond Lengths [Å] and Bond Angles [°] for $(\mu\text{-SEt})_2[Fe(CO)_2(PMe_3)]_2$.

Fe(1B)-C(1B)	1.757(3)	S(2A)-C(13A)	1.836(3)
Fe(1B)-C(2B)	1.759(3)	P(2A)-C(10A)	1.817(4)
Fe(1B)-P(1B)	2.2191(10)	P(2A)-C(9A)	1.820(4)
Fe(1B)-S(1B)	2.2752(9)	P(2A)-C(8A)	1.814(3)
Fe(1B)-S(2B)	2.2840(9)	P(2B)-C(10B)	1.805(4)
Fe(1B)-Fe(2B)	2.5188(7)	P(2B)-C(9B)	1.819(4)
Fe(1A)-C(1A)	1.755(3)	P(2B)-C(8B)	1.807(4)
Fe(1A)-C(2A)	1.764(3)	P(1B)-C(5B)	1.815(4)
Fe(1A)-P(1A)	2.2163(10)	P(1B)-C(6B)	1.825(4)
Fe(1A)-S(2A)	2.2795(10)	P(1B)-C(7B)	1.815(4)
Fe(1A)-S(1A)	2.2733(9)	P(1A)-C(7A)	1.818(4)
Fe(1A)-Fe(2A)	2.5097(7)	P(1A)-C(5A)	1.811(4)
Fe(2A)-C(4A)	1.755(3)	P(1A)-C(6A)	1.816(4)
Fe(2A)-C(3A)	1.747(3)	O(3A)-C(3A)	1.157(4)
Fe(2A)-P(2A)	2.2216(9)	O(2B)-C(2B)	1.150(4)
Fe(2A)-S(1A)	2.2731(9)	O(4A)-C(4A)	1.160(4)
Fe(2A)-S(2A)	2.2941(10)	O(1B)-C(1B)	1.158(4)
Fe(2B)-C(4B)	1.760(3)	C(13B)-C(14B)	1.517(5)
Fe(2B)-C(3B)	1.754(3)	O(2A)-C(2A)	1.152(4)
Fe(2B)-P(2B)	2.2279(11)	O(3B)-C(3B)	1.154(4)
Fe(2B)-S(1B)	2.2740(10)	C(1A)-O(1A)	1.153(4)
Fe(2B)-S(2B)	2.2812(10)	C(13A)-C(14A)	1.506(5)
S(1A)-C(11A)	1.820(3)	C(11A)-C(12A)	1.521(5)
S(2B)-C(13B)	1.828(3)	O(4B)-C(4B)	1.149(4)
S(1B)-C(11B)	1.827(3)	C(12B)-C(11B)	1.507(5)
C(1B)-Fe(1B)-C(2B)	90.58(14)	C(1B)-Fe(1B)-P(1B)	97.20(11)

Table A-3 (continued)

C(2B)-Fe(1B)-P(1B)	98.61(11)	C(4A)-Fe(2A)-C(3A)	90.97(15)
C(1B)-Fe(1B)-S(1B)	93.68(11)	C(4A)-Fe(2A)-P(2A)	98.97(11)
C(2B)-Fe(1B)-S(1B)	156.27(11)	C(3A)-Fe(2A)-P(2A)	97.37(10)
P(1B)-Fe(1B)-S(1B)	103.98(4)	C(4A)-Fe(2A)-S(1A)	161.19(11)
C(1B)-Fe(1B)-S(2B)	164.22(11)	C(3A)-Fe(2A)-S(1A)	94.06(11)
C(2B)-Fe(1B)-S(2B)	95.28(10)	P(2A)-Fe(2A)-S(1A)	98.34(3)
P(1B)-Fe(1B)-S(2B)	96.39(4)	C(4A)-Fe(2A)-S(2A)	93.30(11)
S(1B)-Fe(1B)-S(2B)	75.24(3)	C(3A)-Fe(2A)-S(2A)	157.94(10)
C(1B)-Fe(1B)-Fe(2B)	108.09(11)	P(2A)-Fe(2A)-S(2A)	103.30(3)
C(2B)-Fe(1B)-Fe(2B)	100.18(11)	S(1A)-Fe(2A)-S(2A)	75.56(3)
P(1B)-Fe(1B)-Fe(2B)	148.12(3)	C(4A)-Fe(2A)-Fe(1A)	104.73(11)
S(1B)-Fe(1B)-Fe(2B)	56.36(3)	C(3A)-Fe(2A)-Fe(1A)	101.56(10)
S(2B)-Fe(1B)-Fe(2B)	56.46(3)	P(2A)-Fe(2A)-Fe(1A)	149.20(3)
C(1A)-Fe(1A)-C(2A)	90.11(15)	S(1A)-Fe(2A)-Fe(1A)	56.50(2)
C(1A)-Fe(1A)-P(1A)	98.46(12)	S(2A)-Fe(2A)-Fe(1A)	56.44(3)
C(2A)-Fe(1A)-P(1A)	101.16(12)	C(4B)-Fe(2B)-C(3B)	90.53(15)
C(1A)-Fe(1A)-S(2A)	165.18(11)	C(4B)-Fe(2B)-P(2B)	98.41(11)
C(2A)-Fe(1A)-S(2A)	93.81(11)	C(3B)-Fe(2B)-P(2B)	97.23(11)
P(1A)-Fe(1A)-S(2A)	94.80(4)	C(4B)-Fe(2B)-S(1B)	161.18(11)
C(1A)-Fe(1A)-S(1A)	94.99(11)	C(3B)-Fe(2B)-S(1B)	93.58(12)
C(2A)-Fe(1A)-S(1A)	155.88(12)	P(2B)-Fe(2B)-S(1B)	99.28(4)
P(1A)-Fe(1A)-S(1A)	101.37(3)	C(4B)-Fe(2B)-S(2B)	94.26(10)
S(2A)-Fe(1A)-S(1A)	75.84(3)	C(3B)-Fe(2B)-S(2B)	157.56(12)
C(1A)-Fe(1A)-Fe(2A)	108.25(11)	P(2B)-Fe(2B)-S(2B)	103.71(3)
C(2A)-Fe(1A)-Fe(2A)	99.55(11)	S(1B)-Fe(2B)-S(2B)	75.32(3)
P(1A)-Fe(1A)-Fe(2A)	145.95(3)	C(4B)-Fe(2B)-Fe(1B)	104.78(11)
S(2A)-Fe(1A)-Fe(2A)	57.00(3)	C(3B)-Fe(2B)-Fe(1B)	101.03(12)
S(1A)-Fe(1A)-Fe(2A)	56.49(2)	P(2B)-Fe(2B)-Fe(1B)	150.17(3)

Table A-3 (continued)

S(1B)-Fe(2B)-Fe(1B)	56.40(2)	C(6B)-P(1B)-C(7B)	100.21(19)
S(2B)-Fe(2B)-Fe(1B)	56.57(2)	C(5B)-P(1B)-Fe(1B)	115.79(15)
C(11A)-S(1A)-Fe(1A)	113.53(11)	C(6B)-P(1B)-Fe(1B)	115.22(13)
C(11A)-S(1A)-Fe(2A)	114.10(11)	C(7B)-P(1B)-Fe(1B)	117.05(14)
Fe(1A)-S(1A)-Fe(2A)	67.01(3)	C(7A)-P(1A)-C(5A)	101.7(2)
C(13B)-S(2B)-Fe(2B)	113.90(12)	C(7A)-P(1A)-C(6A)	102.1(2)
C(13B)-S(2B)-Fe(1B)	113.26(11)	C(5A)-P(1A)-C(6A)	102.9(2)
Fe(2B)-S(2B)-Fe(1B)	66.97(3)	C(7A)-P(1A)-Fe(1A)	117.13(16)
C(11B)-S(1B)-Fe(1B)	113.90(13)	C(5A)-P(1A)-Fe(1A)	115.86(14)
C(11B)-S(1B)-Fe(2B)	113.20(13)	C(6A)-P(1A)-Fe(1A)	115.03(15)
Fe(1B)-S(1B)-Fe(2B)	67.24(3)	O(2B)-C(2B)-Fe(1B)	178.1(3)
C(13A)-S(2A)-Fe(1A)	111.41(12)	C(14B)-C(13B)-S(2B)	111.2(3)
C(13A)-S(2A)-Fe(2A)	115.28(12)	O(4A)-C(4A)-Fe(2A)	177.9(3)
Fe(1A)-S(2A)-Fe(2A)	66.56(3)	O(3A)-C(3A)-Fe(2A)	178.7(3)
C(10A)-P(2A)-C(9A)	102.7(2)	O(1B)-C(1B)-Fe(1B)	178.3(3)
C(10A)-P(2A)-C(8A)	101.81(18)	O(1A)-C(1A)-Fe(1A)	178.0(3)
C(9A)-P(2A)-C(8A)	102.33(18)	C(14A)-C(13A)-S(2A)	110.6(2)
C(10A)-P(2A)-Fe(2A)	115.91(13)	C(12A)-C(11A)-S(1A)	109.9(2)
C(9A)-P(2A)-Fe(2A)	116.65(14)	O(2A)-C(2A)-Fe(1A)	178.1(3)
C(8A)-P(2A)-Fe(2A)	115.30(12)	O(4B)-C(4B)-Fe(2B)	178.4(3)
C(10B)-P(2B)-C(9B)	101.5(2)	O(3B)-C(3B)-Fe(2B)	178.3(3)
C(10B)-P(2B)-C(8B)	101.6(2)	C(12B)-C(11B)-S(1B)	111.0(3)
C(9B)-P(2B)-C(8B)	102.9(3)		
C(10B)-P(2B)-Fe(2B)	116.03(14)		
C(9B)-P(2B)-Fe(2B)	117.01(15)		
C(8B)-P(2B)-Fe(2B)	115.50(16)		
C(5B)-P(1B)-C(6B)	102.6(2)		
C(5B)-P(1B)-C(7B)	103.8(2)		

Table A-4. Crystal Data and Structure Refinement for $\{(\mu\text{-H})(\mu\text{-SEt})_2\text{-}[Fe(CO)_2(PMe_3)]_2\}PF_6$

Empirical formula	C14 H29 F6 Fe2 O4 P3 S2	
Formula weight	644.10	
Temperature	110(2) K	
Wavelength	0.71073 Å	
Crystal system	Monoclinic	
Space group	P2(1)/c	
Unit cell dimensions	a = 10.3731(9) Å	α = 90°.
	b = 12.5853(11) Å	β = 98.0290(10)°.
	c = 20.2228(17) Å	γ = 90°.
Volume	2614.2(4) $Å^3$	
Z	4	
Density (calculated)	1.637 Mg/m^3	
Absorption coefficient	1.514 mm^{-1}	
Theta range for data collection	1.91 to 23.31°.	
Index ranges	-11<=h<=10, -12<=k<=13, -22<=l<=22	
Reflections collected	11188	
Independent reflections	3759 [R(int) = 0.0659]	
Refinement method	Full-matrix least-squares on F^2	
Data / restraints / parameters	3759 / 0 / 292	
Goodness-of-fit on F^2	1.070	
Final R indices [I>2sigma(I)]	R1 = 0.0278, wR2 = 0.0710	
R indices (all data)	R1 = 0.0292, wR2 = 0.0719	
Largest diff. peak and hole	0.591 and -0.404 $e.Å^{-3}$	

Table A-5. Atomic Coordinates (x 10^4) and Equivalent Isotropic Displacement Parameters ($Å^2$x 10^3) for $\{(\mu\text{-H})(\mu\text{-SEt})_2[Fe(CO)_2(PMe_3)]_2\}PF_6$. U(eq) Is Defined as One Third of the Trace of the Orthogonalized U^{ij} Tensor

	x	y	z	U(eq)
Fe(1)	4725(1)	7169(1)	919(1)	13(1)
Fe(2)	3030(1)	6889(1)	-122(1)	14(1)
C(1)	6271(2)	6629(2)	819(1)	17(1)
O(1)	7241(2)	6281(1)	732(1)	24(1)
C(2)	4408(2)	6264(2)	1549(1)	18(1)
O(2)	4135(2)	5686(1)	1939(1)	25(1)
C(3)	3696(2)	6209(2)	-768(1)	18(1)
O(3)	4177(2)	5783(1)	-1166(1)	24(1)
C(4)	1987(2)	5819(2)	25(1)	20(1)
O(4)	1377(2)	5115(1)	148(1)	30(1)
P(1)	5565(1)	8387(1)	1661(1)	15(1)
C(5)	4954(2)	9719(2)	1485(1)	21(1)
C(6)	7313(2)	8558(2)	1756(1)	25(1)
C(7)	5271(3)	8118(2)	2507(1)	24(1)
P(2)	1563(1)	7749(1)	-846(1)	18(1)
C(8)	1073(3)	9039(2)	-573(1)	29(1)
C(9)	44(2)	7053(2)	-1081(1)	25(1)
C(10)	2122(3)	8031(2)	-1636(1)	28(1)
S(1)	4581(1)	8188(1)	-27(1)	15(1)
C(11)	5882(2)	7884(2)	-525(1)	20(1)
C(12)	7074(2)	8564(2)	-301(1)	25(1)
S(2)	2667(1)	7819(1)	801(1)	16(1)
C(13)	1605(2)	7122(2)	1305(1)	22(1)

Table A-5 (continued)

C(14)	194(2)	7387(2)	1063(1)	31(1)
P(3)	8432(1)	5276(1)	2582(1)	20(1)
F(1)	8622(2)	4940(1)	1847(1)	38(1)
F(2)	9159(2)	6376(1)	2495(1)	39(1)
F(3)	7075(1)	5819(1)	2301(1)	37(1)
F(4)	7696(2)	4189(1)	2674(1)	42(1)
F(5)	9790(2)	4750(1)	2867(1)	44(1)
F(6)	8232(2)	5619(1)	3321(1)	40(1)

Table A-6. Bond Lengths [Å] and Angles [°] for $\{(\mu\text{-H})(\mu\text{-SEt})_2\text{-}[Fe(CO)_2(PMe_3)]_2\}PF_6$

Fe(1)-H(1)	1.68(2)	P(1)-C(6)	1.809(2)
Fe(1)-C(2)	1.773(2)	P(1)-C(7)	1.811(2)
Fe(1)-C(1)	1.780(3)	P(1)-C(5)	1.810(2)
Fe(1)-P(1)	2.2348(6)	P(2)-C(9)	1.807(2)
Fe(1)-S(2)	2.2670(7)	P(2)-C(10)	1.809(3)
Fe(1)-S(1)	2.2895(6)	P(2)-C(8)	1.810(3)
Fe(1)-Fe(2)	2.5708(4)	S(1)-C(11)	1.833(2)
Fe(2)-H(1)	1.64(2)	C(11)-C(12)	1.520(3)
Fe(2)-C(4)	1.777(3)	S(2)-C(13)	1.827(2)
Fe(2)-C(3)	1.780(3)	C(13)-C(14)	1.515(4)
Fe(2)-P(2)	2.2384(7)	P(3)-F(1)	1.5842(16)
Fe(2)-S(2)	2.2773(7)	P(3)-F(5)	1.5900(16)
Fe(2)-S(1)	2.2834(7)	P(3)-F(4)	1.5908(16)
C(1)-O(1)	1.133(3)	P(3)-F(3)	1.5968(15)
C(2)-O(2)	1.139(3)	P(3)-F(6)	1.5967(16)
C(3)-O(3)	1.140(3)	P(3)-F(2)	1.5977(16)
C(4)-O(4)	1.137(3)		

H(1)-Fe(1)-C(2)	84.3(8)	C(1)-Fe(1)-S(2)	167.48(7)
H(1)-Fe(1)-C(1)	86.4(9)	P(1)-Fe(1)-S(2)	95.52(2)
C(2)-Fe(1)-C(1)	95.55(10)	H(1)-Fe(1)-S(1)	84.0(8)
H(1)-Fe(1)-P(1)	177.3(8)	C(2)-Fe(1)-S(1)	164.27(7)
C(2)-Fe(1)-P(1)	92.97(7)	C(1)-Fe(1)-S(1)	94.22(7)
C(1)-Fe(1)-P(1)	93.75(7)	P(1)-Fe(1)-S(1)	98.66(2)
H(1)-Fe(1)-S(2)	84.7(9)	S(2)-Fe(1)-S(1)	76.08(2)
C(2)-Fe(1)-S(2)	92.36(7)	H(1)-Fe(1)-Fe(2)	38.5(8)

Table A-6 (continued)

C(2)-Fe(1)-Fe(2)	109.00(7)	O(3)-C(3)-Fe(2)	176.9(2)
C(1)-Fe(1)-Fe(2)	112.27(7)	O(4)-C(4)-Fe(2)	175.9(2)
P(1)-Fe(1)-Fe(2)	143.28(2)	C(6)-P(1)-C(7)	102.75(12)
S(2)-Fe(1)-Fe(2)	55.738(17)	C(6)-P(1)-C(5)	103.21(12)
S(1)-Fe(1)-Fe(2)	55.681(17)	C(7)-P(1)-C(5)	104.95(11)
H(1)-Fe(2)-C(4)	82.5(9)	C(6)-P(1)-Fe(1)	116.32(9)
H(1)-Fe(2)-C(3)	85.5(9)	C(7)-P(1)-Fe(1)	113.89(9)
C(4)-Fe(2)-C(3)	93.77(10)	C(5)-P(1)-Fe(1)	114.25(8)
H(1)-Fe(2)-P(2)	177.6(9)	C(9)-P(2)-C(10)	103.78(12)
C(4)-Fe(2)-P(2)	95.85(7)	C(9)-P(2)-C(8)	104.08(12)
C(3)-Fe(2)-P(2)	92.86(7)	C(10)-P(2)-C(8)	103.41(13)
H(1)-Fe(2)-S(2)	85.4(9)	C(9)-P(2)-Fe(2)	115.19(8)
C(4)-Fe(2)-S(2)	94.53(8)	C(10)-P(2)-Fe(2)	113.62(9)
C(3)-Fe(2)-S(2)	166.81(7)	C(8)-P(2)-Fe(2)	115.32(8)
P(2)-Fe(2)-S(2)	96.47(2)	C(11)-S(1)-Fe(2)	111.63(8)
H(1)-Fe(2)-S(1)	85.2(9)	C(11)-S(1)-Fe(1)	112.01(8)
C(4)-Fe(2)-S(1)	165.11(7)	Fe(2)-S(1)-Fe(1)	68.414(19)
C(3)-Fe(2)-S(1)	93.71(7)	C(12)-C(11)-S(1)	110.47(17)
P(2)-Fe(2)-S(1)	96.62(2)	C(13)-S(2)-Fe(1)	113.60(8)
S(2)-Fe(2)-S(1)	76.00(2)	C(13)-S(2)-Fe(2)	113.09(8)
H(1)-Fe(2)-Fe(1)	39.8(9)	Fe(1)-S(2)-Fe(2)	68.90(2)
C(4)-Fe(2)-Fe(1)	109.27(7)	C(14)-C(13)-S(2)	110.17(17)
C(3)-Fe(2)-Fe(1)	112.05(7)	F(1)-P(3)-F(5)	90.48(9)
P(2)-Fe(2)-Fe(1)	142.56(2)	F(1)-P(3)-F(4)	90.27(9)
S(2)-Fe(2)-Fe(1)	55.358(18)	F(5)-P(3)-F(4)	90.84(9)
S(1)-Fe(2)-Fe(1)	55.905(16)	F(1)-P(3)-F(3)	89.94(8)
O(1)-C(1)-Fe(1)	177.62(19)	F(5)-P(3)-F(3)	179.27(10)
O(2)-C(2)-Fe(1)	176.3(2)	F(4)-P(3)-F(3)	89.76(9)

Table A-6 (continued)

F(1)-P(3)-F(6)	179.61(10)	F(1)-P(3)-F(2)	90.31(9)
F(5)-P(3)-F(6)	89.91(9)	F(5)-P(3)-F(2)	89.62(9)
F(4)-P(3)-F(6)	89.77(9)	F(4)-P(3)-F(2)	179.27(10)
F(3)-P(3)-F(6)	89.67(9)	F(3)-P(3)-F(2)	89.78(9)
		F(6)-P(3)-F(2)	89.66(9)

Table A-7. Crystal Data and Structure Refinement for (μ-pdt)[$Fe(CO)_3$][$Fe(CO)_2$PTA]

Empirical formula	C14 H18 Fe2 N3 O5 P S2	
Formula weight	515.10	
Temperature	110(2) K	
Wavelength	1.54178 Å	
Crystal system	Monoclinic	
Space group	P2(1)/n	
Unit cell dimensions	a = 11.8502(16) Å	α = 90°.
	b = 12.4174(18) Å	β = 94.424(8)°.
	c = 13.1985(18) Å	γ = 90°.
Volume	1936.4(5) $Å^3$	
Z	4	
Density (calculated)	1.767 Mg/m^3	
Absorption coefficient	15.107 mm^{-1}	
Crystal size	0.10 x 0.05 x 0.05 mm^3	
Theta range for data collection	4.90 to 59.08°.	
Index ranges	-13<=h<=12, -13<=k<=13, -14<=l<=14	
Reflections collected	10087	
Independent reflections	2574 [R(int) = 0.1219]	
Absorption correction	Semi-empirical from equivalents	
Max. and min. transmission	0.5188 and 0.3134	
Refinement method	Full-matrix least-squares on F^2	
Data / restraints / parameters	2574 / 0 / 244	
Goodness-of-fit on F^2	0.907	
Final R indices [I>2sigma(I)]	R1 = 0.0657, wR2 = 0.1346	
R indices (all data)	R1 = 0.1258, wR2 = 0.1542	
Largest diff. peak and hole	0.745 and -0.531 $e.Å^{-3}$	

Table A-8. Atomic Coordinates (x 10^4) and Equivalent Isotropic Displacement Parameters (Å^{2}x 10^3) for (μ-pdt)[Fe(CO)$_3$][Fe(CO)$_2$PTA]. U(eq) Is Defined as One Third of the Trace of the Orthogonalized U^{ij} Tensor

	x	y	z	U(eq)
Fe(1)	90(1)	3160(1)	2105(1)	23(1)
Fe(2)	1013(1)	1622(1)	3134(1)	22(1)
P(1)	111(2)	160(2)	2548(2)	21(1)
S(1)	1627(2)	3346(2)	3216(2)	26(1)
S(2)	-689(2)	2333(2)	3423(2)	25(1)
N(1)	-1842(6)	-977(7)	2011(6)	24(2)
N(2)	-218(6)	-1270(7)	950(5)	23(2)
N(3)	-175(6)	-2052(7)	2682(6)	26(2)
O(1)	-891(6)	5337(6)	2204(6)	42(2)
O(2)	-1601(6)	2189(6)	659(5)	34(2)
O(3)	1628(6)	3464(6)	492(5)	40(2)
O(4)	2849(6)	1185(6)	1846(6)	42(2)
O(5)	1989(6)	603(6)	4988(5)	39(2)
C(1)	-521(9)	4495(10)	2165(8)	34(3)
C(2)	-916(8)	2570(9)	1246(7)	25(3)
C(3)	1018(9)	3317(9)	1125(8)	35(3)
C(4)	2118(9)	1344(9)	2357(8)	33(3)
C(5)	1596(9)	1002(9)	4259(8)	33(3)
C(6)	1264(8)	4054(8)	4362(7)	28(3)
C(7)	525(8)	3430(9)	5034(7)	30(3)
C(8)	-647(8)	3209(8)	4557(7)	25(2)
C(9)	-1452(8)	52(8)	2453(7)	27(3)
C(10)	346(8)	-255(8)	1253(7)	27(3)

Table A-8 (continued)

C(11)	414(7)	-1142(9)	3196(7)	25(3)
C(12)	-1476(8)	-1152(9)	975(6)	26(3)
C(13)	122(9)	-2161(8)	1630(7)	27(3)
C(14)	-1436(7)	-1876(8)	2651(7)	23(2)

Table A-9. Bond Lengths [Å] and Angles [°] for (μ-pdt)[$Fe(CO)_3$][$Fe(CO)_2$PTA]

Fe(1)-C(2)	1.743(10)	N(1)-C(14)	1.458(11)
Fe(1)-C(3)	1.771(11)	N(1)-C(9)	1.464(12)
Fe(1)-C(1)	1.813(13)	N(1)-C(12)	1.482(11)
Fe(1)-S(1)	2.260(3)	N(2)-C(13)	1.461(11)
Fe(1)-S(2)	2.276(3)	N(2)-C(10)	1.468(12)
Fe(1)-Fe(2)	2.542(2)	N(2)-C(12)	1.500(11)
Fe(2)-C(4)	1.758(11)	N(3)-C(13)	1.464(11)
Fe(2)-C(5)	1.766(11)	N(3)-C(11)	1.468(12)
Fe(2)-P(1)	2.215(3)	N(3)-C(14)	1.507(11)
Fe(2)-S(2)	2.261(3)	O(1)-C(1)	1.137(12)
Fe(2)-S(1)	2.261(3)	O(2)-C(2)	1.176(11)
P(1)-C(10)	1.828(9)	O(3)-C(3)	1.162(11)
P(1)-C(9)	1.852(9)	O(4)-C(4)	1.155(11)
P(1)-C(11)	1.851(10)	O(5)-C(5)	1.149(11)
S(1)-C(6)	1.829(9)	C(6)-C(7)	1.509(12)
S(2)-C(8)	1.848(9)	C(7)-C(8)	1.506(12)

C(2)-Fe(1)-C(3)	90.2(4)	C(3)-Fe(1)-Fe(2)	101.9(4)
C(2)-Fe(1)-C(1)	99.1(5)	C(1)-Fe(1)-Fe(2)	145.1(3)
C(3)-Fe(1)-C(1)	101.8(5)	S(1)-Fe(1)-Fe(2)	55.81(8)
C(2)-Fe(1)-S(1)	160.4(4)	S(2)-Fe(1)-Fe(2)	55.64(8)
C(3)-Fe(1)-S(1)	87.0(3)	C(4)-Fe(2)-C(5)	98.3(5)
C(1)-Fe(1)-S(1)	100.5(4)	C(4)-Fe(2)-P(1)	89.8(4)
C(2)-Fe(1)-S(2)	90.5(3)	C(5)-Fe(2)-P(1)	94.8(4)
C(3)-Fe(1)-S(2)	156.7(4)	C(4)-Fe(2)-S(2)	152.8(4)
C(1)-Fe(1)-S(2)	101.1(3)	C(5)-Fe(2)-S(2)	108.9(3)
S(1)-Fe(1)-S(2)	84.49(10)	P(1)-Fe(2)-S(2)	88.06(11)
C(2)-Fe(1)-Fe(2)	106.0(4)	C(4)-Fe(2)-S(1)	87.9(4)

Table A-9 (continued)

C(5)-Fe(2)-S(1)	105.6(4)	C(14)-N(1)-C(12)	108.4(7)
P(1)-Fe(2)-S(1)	159.63(12)	C(9)-N(1)-C(12)	112.9(7)
S(2)-Fe(2)-S(1)	84.82(11)	C(13)-N(2)-C(10)	112.6(7)
C(4)-Fe(2)-Fe(1)	98.3(4)	C(13)-N(2)-C(12)	106.7(7)
C(5)-Fe(2)-Fe(1)	154.3(4)	C(10)-N(2)-C(12)	110.0(8)
P(1)-Fe(2)-Fe(1)	104.69(10)	C(13)-N(3)-C(11)	111.6(7)
S(2)-Fe(2)-Fe(1)	56.21(8)	C(13)-N(3)-C(14)	107.4(7)
S(1)-Fe(2)-Fe(1)	55.76(8)	C(11)-N(3)-C(14)	109.6(7)
C(10)-P(1)-C(9)	98.0(4)	O(1)-C(1)-Fe(1)	179.1(10)
C(10)-P(1)-C(11)	98.5(5)	O(2)-C(2)-Fe(1)	178.8(10)
C(9)-P(1)-C(11)	97.2(4)	O(3)-C(3)-Fe(1)	177.3(11)
C(10)-P(1)-Fe(2)	116.9(3)	O(4)-C(4)-Fe(2)	178.5(10)
C(9)-P(1)-Fe(2)	122.4(3)	O(5)-C(5)-Fe(2)	179.1(10)
C(11)-P(1)-Fe(2)	118.9(3)	C(7)-C(6)-S(1)	115.0(7)
C(6)-S(1)-Fe(1)	110.9(3)	C(6)-C(7)-C(8)	114.0(8)
C(6)-S(1)-Fe(2)	113.6(3)	C(7)-C(8)-S(2)	114.4(7)
Fe(1)-S(1)-Fe(2)	68.42(9)	N(1)-C(9)-P(1)	111.9(6)
C(8)-S(2)-Fe(2)	113.5(3)	N(2)-C(10)-P(1)	113.4(6)
C(8)-S(2)-Fe(1)	111.5(3)	N(3)-C(11)-P(1)	113.0(6)
Fe(2)-S(2)-Fe(1)	68.15(9)	N(1)-C(12)-N(2)	113.4(7)
C(14)-N(1)-C(9)	110.9(8)	N(2)-C(13)-N(3)	115.9(8)
		N(1)-C(14)-N(3)	114.1(8)

Table A-10. Crystal Data and Structure Refinement for (μ-pdt)[$Fe(CO)_2PTA]_2$

Empirical formula	C19 H30 Fe2 N6 O4 P2 S2	
Formula weight	644.25	
Temperature	110(2) K	
Wavelength	0.71073 Å	
Crystal system	Monoclinic	
Space group	P2(1)/c	
Unit cell dimensions	a = 12.8193(10) Å	α = 90°.
	b = 24.0187(19) Å	β = 105.5690(10)°.
	c = 8.4330(7) Å	γ = 90°.
Volume	2501.3(3) $Å^3$	
Z	4	
Density (calculated)	1.711 Mg/m^3	
Absorption coefficient	1.495 mm^{-1}	
Crystal size	0.4 x 0.1 x 0.1 mm^3	
Theta range for data collection	1.65 to 28.26°.	
Index ranges	-15<=h<=17, -32<=k<=24, -11<=l<=10	
Reflections collected	15572	
Independent reflections	5746 [R(int) = 0.0479]	
Refinement method	Full-matrix least-squares on F^2	
Data / restraints / parameters	5746 / 0 / 316	
Goodness-of-fit on F^2	1.099	
Final R indices [I>2sigma(I)]	R1 = 0.0555, wR2 = 0.1303	
R indices (all data)	R1 = 0.0710, wR2 = 0.1444	
Largest diff. peak and hole	3.015 and -0.575 $e.Å^{-3}$	

Table A-11. Atomic Coordinates (x 10^4) and Equivalent Isotropic Displacement Parameters ($Å^2$x 10^3) for (μ-pdt)[Fe(CO)$_2$PTA]$_2$. U(eq) Is Defined as One Third of the Trace of the Orthogonalized U^{ij} Tensor.

	x	y	z	U(eq)
Fe(1)	3604(1)	3788(1)	7391(1)	20(1)
Fe(2)	2378(1)	4406(1)	5203(1)	19(1)
S(1)	3891(1)	4705(1)	7115(1)	21(1)
C(5)	3585(3)	5101(2)	8795(4)	28(1)
C(6)	2384(3)	5136(2)	8708(4)	29(1)
C(7)	1872(3)	4580(2)	8884(4)	28(1)
S(2)	1910(1)	4044(1)	7372(1)	22(1)
C(1)	4143(3)	3628(1)	9503(4)	27(1)
O(1)	4464(2)	3503(1)	10873(3)	41(1)
C(2)	3153(3)	3112(2)	6687(4)	27(1)
O(2)	2897(2)	2670(1)	6216(4)	37(1)
C(3)	1516(3)	4996(1)	4644(4)	25(1)
O(3)	927(2)	5365(1)	4232(3)	32(1)
C(4)	3092(3)	4445(1)	3698(4)	24(1)
O(4)	3557(2)	4462(1)	2689(3)	34(1)
P(1)	5101(1)	3618(1)	6633(1)	19(1)
C(8)	6260(3)	3363(2)	8294(4)	27(1)
C(9)	5853(3)	4157(1)	5799(5)	29(1)
C(10)	5107(3)	3064(2)	5113(5)	31(1)
N(1)	7219(2)	3229(1)	7706(4)	27(1)
N(2)	6850(2)	3926(1)	5488(4)	27(1)
N(3)	6193(2)	2963(1)	4886(4)	34(1)
C(11)	7611(3)	3724(1)	6996(4)	27(1)
C(12)	6958(3)	2797(2)	6431(5)	36(1)

Table A-11 (continued)

C(13)	6613(3)	3472(2)	4297(4)	33(1)
P(2)	1220(1)	3832(1)	3584(1)	19(1)
C(14)	305(2)	3381(1)	4390(4)	23(1)
C(15)	163(2)	4175(1)	1940(4)	22(1)
C(16)	1659(2)	3308(1)	2285(4)	24(1)
N(4)	-468(2)	3071(1)	3062(3)	23(1)
N(5)	-585(2)	3779(1)	888(3)	22(1)
N(6)	729(2)	3008(1)	1205(4)	25(1)
C(17)	-1159(2)	3451(1)	1866(4)	24(1)
C(18)	123(3)	2708(1)	2181(4)	25(1)
C(19)	-13(3)	3388(1)	76(4)	24(1)

Table A-12. Bond Lengths [Å] and Angles [°] for (μ-pdt)[Fe(CO)$_2$PTA]$_2$

Fe(1)-C(1)	1.771(4)	C(8)-N(1)	1.479(4)
Fe(1)-C(2)	1.773(4)	C(9)-N(2)	1.480(4)
Fe(1)-P(1)	2.2176(9)	C(10)-N(3)	1.475(4)
Fe(1)-S(2)	2.2530(9)	N(1)-C(12)	1.466(5)
Fe(1)-S(1)	2.2536(9)	N(1)-C(11)	1.479(4)
Fe(1)-Fe(2)	2.5535(6)	N(2)-C(13)	1.459(5)
Fe(2)-C(4)	1.755(4)	N(2)-C(11)	1.462(4)
Fe(2)-C(3)	1.782(3)	N(3)-C(12)	1.460(5)
Fe(2)-P(2)	2.2103(9)	N(3)-C(13)	1.474(5)
Fe(2)-S(2)	2.2477(9)	P(2)-C(16)	1.852(3)
Fe(2)-S(1)	2.2793(9)	P(2)-C(15)	1.852(3)
S(1)-C(5)	1.834(3)	P(2)-C(14)	1.853(3)
C(5)-C(6)	1.525(5)	C(14)-N(4)	1.482(4)
C(6)-C(7)	1.511(5)	C(15)-N(5)	1.467(4)
C(7)-S(2)	1.823(3)	C(16)-N(6)	1.479(4)
C(1)-O(1)	1.157(4)	N(4)-C(17)	1.468(4)
C(2)-O(2)	1.150(4)	N(4)-C(18)	1.479(4)
C(3)-O(3)	1.155(4)	N(5)-C(19)	1.470(4)
C(4)-O(4)	1.164(4)	N(5)-C(17)	1.474(4)
P(1)-C(10)	1.849(4)	N(6)-C(18)	1.464(4)
P(1)-C(8)	1.851(3)	N(6)-C(19)	1.469(4)
P(1)-C(9)	1.861(3)		

C(1)-Fe(1)-C(2)	98.13(16)	P(1)-Fe(1)-S(2)	162.82(4)
C(1)-Fe(1)-P(1)	96.64(11)	C(1)-Fe(1)-S(1)	106.60(12)
C(2)-Fe(1)-P(1)	87.97(11)	C(2)-Fe(1)-S(1)	155.26(12)
C(1)-Fe(1)-S(2)	100.47(11)	P(1)-Fe(1)-S(1)	88.43(3)
C(2)-Fe(1)-S(2)	91.15(11)	S(2)-Fe(1)-S(1)	85.21(3)

Table A-12 (continued)

C(1)-Fe(1)-Fe(2)	148.36(11)	Fe(2)-S(2)-Fe(1)	69.13(3)
C(2)-Fe(1)-Fe(2)	102.04(11)	O(1)-C(1)-Fe(1)	176.9(3)
P(1)-Fe(1)-Fe(2)	108.12(3)	O(2)-C(2)-Fe(1)	177.3(3)
S(2)-Fe(1)-Fe(2)	55.34(2)	O(3)-C(3)-Fe(2)	177.1(3)
S(1)-Fe(1)-Fe(2)	56.19(2)	O(4)-C(4)-Fe(2)	178.8(3)
C(4)-Fe(2)-C(3)	99.97(15)	C(10)-P(1)-C(8)	97.76(17)
C(4)-Fe(2)-P(2)	88.91(10)	C(10)-P(1)-C(9)	98.08(17)
C(3)-Fe(2)-P(2)	93.85(11)	C(8)-P(1)-C(9)	97.13(16)
C(4)-Fe(2)-S(2)	156.10(11)	C(10)-P(1)-Fe(1)	119.82(11)
C(3)-Fe(2)-S(2)	103.92(11)	C(8)-P(1)-Fe(1)	115.05(11)
P(2)-Fe(2)-S(2)	88.79(3)	C(9)-P(1)-Fe(1)	123.82(11)
C(4)-Fe(2)-S(1)	89.17(10)	N(1)-C(8)-P(1)	112.9(2)
C(3)-Fe(2)-S(1)	106.65(11)	N(2)-C(9)-P(1)	111.4(2)
P(2)-Fe(2)-S(1)	159.43(4)	N(3)-C(10)-P(1)	112.8(2)
S(2)-Fe(2)-S(1)	84.74(3)	C(12)-N(1)-C(11)	107.9(3)
C(4)-Fe(2)-Fe(1)	102.40(11)	C(12)-N(1)-C(8)	110.7(3)
C(3)-Fe(2)-Fe(1)	150.61(11)	C(11)-N(1)-C(8)	111.3(3)
P(2)-Fe(2)-Fe(1)	105.34(3)	C(13)-N(2)-C(11)	108.5(3)
S(2)-Fe(2)-Fe(1)	55.53(2)	C(13)-N(2)-C(9)	111.9(3)
S(1)-Fe(2)-Fe(1)	55.24(2)	C(11)-N(2)-C(9)	112.1(3)
C(5)-S(1)-Fe(1)	110.64(12)	C(12)-N(3)-C(13)	108.0(3)
C(5)-S(1)-Fe(2)	113.10(11)	C(12)-N(3)-C(10)	111.1(3)
Fe(1)-S(1)-Fe(2)	68.57(3)	C(13)-N(3)-C(10)	110.6(3)
C(6)-C(5)-S(1)	114.4(2)	N(2)-C(11)-N(1)	113.5(3)
C(7)-C(6)-C(5)	114.0(3)	N(3)-C(12)-N(1)	115.3(3)
C(6)-C(7)-S(2)	117.5(2)	N(2)-C(13)-N(3)	114.5(3)
C(7)-S(2)-Fe(2)	111.06(12)	C(16)-P(2)-C(15)	97.86(15)
C(7)-S(2)-Fe(1)	113.23(11)	C(16)-P(2)-C(14)	98.24(15)

Table A-12 (continued)

C(15)-P(2)-C(14)	97.28(15)	C(18)-N(4)-C(14)	110.3(2)
C(16)-P(2)-Fe(2)	121.93(11)	C(15)-N(5)-C(19)	111.7(2)
C(15)-P(2)-Fe(2)	114.79(11)	C(15)-N(5)-C(17)	110.6(3)
C(14)-P(2)-Fe(2)	121.65(11)	C(19)-N(5)-C(17)	107.7(3)
N(4)-C(14)-P(2)	112.2(2)	C(18)-N(6)-C(19)	108.7(2)
N(5)-C(15)-P(2)	113.1(2)	C(18)-N(6)-C(16)	110.8(3)
N(6)-C(16)-P(2)	111.9(2)	C(19)-N(6)-C(16)	111.7(3)
C(17)-N(4)-C(18)	108.5(3)	N(4)-C(17)-N(5)	114.7(2)
C(17)-N(4)-C(14)	111.3(3)	N(6)-C(18)-N(4)	114.5(3)
		N(6)-C(19)-N(5)	114.4(3)

Table A-13. Crystal Data and Structure Refinement for (μ-pdt)[$Fe(CO)_3$] [$Fe(CO)_2$IMes]

Empirical formula	C31 H34 Fe2 N2 O5.50 S2	
Formula weight	698.42	
Temperature	100(2) K	
Wavelength	0.71073 Å	
Crystal system	Monoclinic	
Space group	I2/a	
Unit cell dimensions	a = 19.158(17) Å	α = 90°.
	b = 11.432(10) Å	β = 107.148(17)°.
	c = 30.15(3) Å	γ = 90°.
Volume	6309(10) $Å^3$	
Z	8	
Density (calculated)	1.471 Mg/m^3	
Absorption coefficient	1.096 mm^{-1}	
Crystal size	0.40 x 0.30 x 0.20 mm^3	
Theta range for data collection	2.71 to 23.44°.	
Index ranges	-21<=h<=21, -12<=k<=12, -27<=l<=33	
Reflections collected	13741	
Independent reflections	4490 [R(int) = 0.1922]	
Absorption correction	Semi-empirical from equivalents	
Max. and min. transmission	0.8107 and 0.6684	
Refinement method	Full-matrix least-squares on F^2	
Data / restraints / parameters	4490 / 10 / 388	
Goodness-of-fit on F^2	1.061	
Final R indices [I>2sigma(I)]	R1 = 0.0720, wR2 = 0.1426	
R indices (all data)	R1 = 0.1820, wR2 = 0.1858	
Largest diff. peak and hole	0.630 and -0.512 $e.Å^{-3}$	

Table A-14. Atomic Coordinates ($x\ 10^4$) and Equivalent Isotropic Displacement Parameters ($Å^2 x\ 10^3$) for (μ-pdt)[$Fe(CO)_3$][$Fe(CO)_2$IMes]. U(eq) Is Defined as One Third of the Trace of the Orthogonalized U^{ij} Tensor

	x	y	z	U(eq)
Fe(1)	428(1)	8738(1)	3690(1)	36(1)
Fe(2)	-886(1)	8095(1)	3372(1)	39(1)
S(1)	-206(1)	8750(3)	2920(1)	45(1)
S(2)	-538(1)	9780(2)	3775(1)	41(1)
C(1)	770(5)	7369(11)	3575(4)	44(3)
O(1)	906(4)	6425(7)	3502(2)	47(2)
C(2)	603(5)	8235(10)	4264(4)	45(3)
O(2)	705(4)	7795(7)	4627(3)	53(2)
C(3)	-787(6)	6678(12)	3149(4)	56(3)
O(3)	-723(4)	5802(8)	2987(3)	67(2)
C(4)	-1036(5)	7544(9)	3890(4)	44(3)
O(4)	-1185(4)	7173(6)	4216(3)	53(2)
C(5)	-1826(6)	8377(9)	3031(3)	42(3)
O(5)	-2414(4)	8524(6)	2841(2)	53(2)
C(6)	1314(5)	9767(10)	3793(3)	41(3)
N(1)	1979(4)	9455(8)	3761(3)	40(2)
N(2)	1451(4)	10894(8)	3974(3)	42(2)
C(7)	2500(5)	10336(11)	3911(4)	50(3)
C(8)	2172(5)	11195(11)	4041(4)	53(3)
C(9)	2167(5)	8338(11)	3622(4)	51(3)
C(10)	2012(5)	8040(10)	3144(3)	38(3)
C(11)	2204(5)	6949(10)	3036(3)	43(3)
C(12)	2523(5)	6121(10)	3364(4)	43(3)

Table A-14 (continued)

C(13)	2677(6)	6470(12)	3826(4)	60(3)
C(14)	2532(5)	7536(12)	3959(4)	54(3)
C(15)	2715(6)	7866(13)	4471(3)	83(5)
C(16)	1645(5)	8947(9)	2784(3)	44(3)
C(17)	2683(6)	4917(12)	3229(4)	75(4)
C(18)	927(5)	11757(9)	4053(3)	37(3)
C(19)	719(5)	11723(10)	4443(4)	43(3)
C(20)	256(5)	12589(10)	4525(3)	42(3)
C(21)	58(6)	13520(11)	4224(5)	64(4)
C(22)	335(7)	13552(11)	3828(4)	66(4)
C(23)	792(6)	12687(10)	3747(4)	51(3)
C(24)	933(5)	10754(9)	4803(3)	47(3)
C(25)	1103(7)	12820(12)	3350(4)	82(4)
C(26)	-381(6)	14498(11)	4324(5)	87(5)
C(27)	-548(6)	10111(12)	2668(4)	68(4)
C(28)	-428(7)	11048(12)	2970(4)	72(4)
C(29)	-835(5)	11007(9)	3371(4)	64(4)
O(1S)	6931(10)	5302(18)	4576(6)	111(5)
C(2S)	7578(12)	5810(30)	4521(6)	111(5)
C(3S)	8046(11)	6170(20)	4995(8)	111(5)
C(4S)	7699(11)	5590(30)	5329(6)	111(5)
C(5S)	6904(10)	5470(30)	5040(7)	111(5)

Table A-15. Bond Lengths [Å] and Angles [°] for (μ-pdt)[$Fe(CO)_3$][$Fe(CO)_2$IMes]

Fe(1)-C(2)	1.758(12)	C(9)-C(14)	1.392(15)
Fe(1)-C(1)	1.771(13)	C(9)-C(10)	1.424(13)
Fe(1)-C(6)	2.012(10)	C(10)-C(11)	1.367(14)
Fe(1)-S(2)	2.277(3)	C(10)-C(16)	1.517(13)
Fe(1)-S(1)	2.282(4)	C(11)-C(12)	1.376(13)
Fe(1)-Fe(2)	2.525(3)	C(12)-C(13)	1.394(14)
Fe(2)-C(4)	1.782(13)	C(12)-C(17)	1.492(15)
Fe(2)-C(3)	1.785(14)	C(13)-C(14)	1.338(15)
Fe(2)-C(5)	1.820(12)	C(14)-C(15)	1.527(13)
Fe(2)-S(2)	2.270(3)	C(18)-C(19)	1.347(13)
Fe(2)-S(1)	2.274(3)	C(18)-C(23)	1.382(14)
S(1)-C(27)	1.770(13)	C(19)-C(20)	1.399(13)
S(2)-C(29)	1.834(11)	C(19)-C(24)	1.520(14)
C(1)-O(1)	1.146(12)	C(20)-C(21)	1.376(15)
C(2)-O(2)	1.168(11)	C(21)-C(22)	1.442(17)
C(3)-O(3)	1.138(13)	C(21)-C(26)	1.484(15)
C(4)-O(4)	1.179(11)	C(22)-C(23)	1.390(16)
C(5)-O(5)	1.115(11)	C(23)-C(25)	1.494(15)
C(6)-N(1)	1.355(11)	C(27)-C(28)	1.381(15)
C(6)-N(2)	1.394(13)	C(28)-C(29)	1.621(16)
N(1)-C(7)	1.395(12)	O(1S)-C(5S)	1.430(9)
N(1)-C(9)	1.423(13)	C(2S)-C(3S)	1.502(9)
N(2)-C(8)	1.380(12)	C(3S)-C(4S)	1.512(10)
N(2)-C(18)	1.476(12)	C(4S)-C(5S)	1.522(10)
C(7)-C(8)	1.286(14)	O(1S)-C(2S)	1.419(9)
C(2)-Fe(1)-C(1)	86.0(5)	C(2)-Fe(1)-C(6)	97.6(4)

Table A-15 (continued)

C(1)-Fe(1)-C(6)	101.7(5)	C(27)-S(1)-Fe(2)	110.0(4)
C(2)-Fe(1)-S(2)	89.2(3)	C(27)-S(1)-Fe(1)	117.4(4)
C(1)-Fe(1)-S(2)	147.6(3)	Fe(2)-S(1)-Fe(1)	67.33(11)
C(6)-Fe(1)-S(2)	110.7(3)	C(29)-S(2)-Fe(2)	108.0(4)
C(2)-Fe(1)-S(1)	153.3(3)	C(29)-S(2)-Fe(1)	115.5(4)
C(1)-Fe(1)-S(1)	85.5(3)	Fe(2)-S(2)-Fe(1)	67.46(10)
C(6)-Fe(1)-S(1)	108.9(3)	O(1)-C(1)-Fe(1)	171.1(9)
S(2)-Fe(1)-S(1)	84.53(11)	O(2)-C(2)-Fe(1)	173.5(10)
C(2)-Fe(1)-Fe(2)	99.1(3)	O(3)-C(3)-Fe(2)	176.5(11)
C(1)-Fe(1)-Fe(2)	93.1(3)	O(4)-C(4)-Fe(2)	175.5(9)
C(6)-Fe(1)-Fe(2)	158.4(3)	O(5)-C(5)-Fe(2)	176.1(10)
S(2)-Fe(1)-Fe(2)	56.13(9)	N(1)-C(6)-N(2)	101.4(8)
S(1)-Fe(1)-Fe(2)	56.19(8)	N(1)-C(6)-Fe(1)	127.2(8)
C(4)-Fe(2)-C(3)	94.1(5)	N(2)-C(6)-Fe(1)	130.8(7)
C(4)-Fe(2)-C(5)	99.8(4)	C(6)-N(1)-C(7)	112.6(9)
C(3)-Fe(2)-C(5)	98.3(5)	C(6)-N(1)-C(9)	125.6(9)
C(4)-Fe(2)-S(2)	86.0(3)	C(7)-N(1)-C(9)	121.7(8)
C(3)-Fe(2)-S(2)	157.6(4)	C(8)-N(2)-C(6)	110.7(9)
C(5)-Fe(2)-S(2)	103.8(3)	C(8)-N(2)-C(18)	120.6(9)
C(4)-Fe(2)-S(1)	155.6(3)	C(6)-N(2)-C(18)	128.6(8)
C(3)-Fe(2)-S(1)	85.9(4)	C(8)-C(7)-N(1)	106.5(9)
C(5)-Fe(2)-S(1)	104.4(3)	C(7)-C(8)-N(2)	108.8(10)
S(2)-Fe(2)-S(1)	84.88(12)	C(14)-C(9)-N(1)	119.5(10)
C(4)-Fe(2)-Fe(1)	99.8(3)	C(14)-C(9)-C(10)	119.3(11)
C(3)-Fe(2)-Fe(1)	101.7(3)	N(1)-C(9)-C(10)	121.1(10)
C(5)-Fe(2)-Fe(1)	150.8(3)	C(11)-C(10)-C(9)	118.0(10)
S(2)-Fe(2)-Fe(1)	56.41(7)	C(11)-C(10)-C(16)	123.6(9)
S(1)-Fe(2)-Fe(1)	56.48(10)	C(9)-C(10)-C(16)	118.4(10)

Table A-16 (continued)

C(10)-C(11)-C(12)	123.3(10)	C(20)-C(21)-C(22)	117.9(11)
C(11)-C(12)-C(13)	116.1(11)	C(20)-C(21)-C(26)	120.7(13)
C(11)-C(12)-C(17)	121.5(10)	C(22)-C(21)-C(26)	121.2(13)
C(13)-C(12)-C(17)	122.4(10)	C(23)-C(22)-C(21)	122.2(11)
C(14)-C(13)-C(12)	124.0(11)	C(18)-C(23)-C(22)	115.6(11)
C(13)-C(14)-C(9)	119.1(10)	C(18)-C(23)-C(25)	125.0(12)
C(13)-C(14)-C(15)	121.5(12)	C(22)-C(23)-C(25)	119.3(12)
C(9)-C(14)-C(15)	119.4(11)	C(28)-C(27)-S(1)	115.4(9)
C(19)-C(18)-C(23)	124.1(11)	C(27)-C(28)-C(29)	116.6(11)
C(19)-C(18)-N(2)	120.8(10)	C(28)-C(29)-S(2)	113.1(7)
C(23)-C(18)-N(2)	114.0(9)	C(2S)-O(1S)-C(5S)	110.2(7)
C(18)-C(19)-C(20)	119.9(11)	O(1S)-C(2S)-C(3S)	107.4(6)
C(18)-C(19)-C(24)	123.9(10)	C(2S)-C(3S)-C(4S)	104.9(7)
C(20)-C(19)-C(24)	116.2(9)	C(3S)-C(4S)-C(5S)	102.9(7)
C(21)-C(20)-C(19)	119.8(11)	O(1S)-C(5S)-C(4S)	104.6(8)

VITA

Ma. del Rosario Mejía Rodríguez was born in Querétaro, Querétaro, México on September 25, 1961. She graduated from the Universidad Autónoma (Autonomus University of Queretaro) in September 1986 with a B.S. degree in chemistry. After working for thirteen years, first as a lecturer, and then as tenured professor, in the Chemistry Department of the same university, she came to the United States of America in 1995 to pursue graduate education. She was awarded a Master of Science degree in chemistry from Western Illinois University in July, 1999. She joined the doctorate program at Texas A&M University in August, 1999, and worked under the direction of Professor Marcetta Y. Darensbourg. The author can be contacted through the Chemistry Department of the Autonomus University of Queretaro, at Facultad de Quimica, Universidad Autonoma de Queretaro, Centro Universitario, Queretaro, Qro., Mexico.